Vegard Lundby

Combining Additive Manufacturing and Flexible Tooling for Utilization in Rotary Stretch Bending Processes

Master's thesis in Mechanical Engineering - Manufacturing Technology
Supervisor: Sigmund Arntsønn Tronvoll
July 2023

Vegard Lundby

Combining Additive Manufacturing and Flexible Tooling for Utilization in Rotary Stretch Bending Processes

Master's thesis in Mechanical Engineering - Manufacturing Technology
Supervisor: Sigmund Arntsønn Tronvoll
July 2023

Norwegian University of Science and Technology
Faculty of Engineering
Department of Mechanical and Industrial Engineering

NTNU
Norwegian University of
Science and Technology

O NTNU

Norwegian University of
Science and Technology

DEPARTMENT OF MECHANICAL AND INDUSTRIAL ENGINEERING

TPK 4940 – Manufacturing Technology, Master's Thesis

Combining Additive Manufacturing and Flexible Tooling for Utilization in Rotary Stretch Bending Processes

Author:

Vegard Lundby

Supervisor:

Sigmund Arntsønn Tronvoll

July 21, 2023

Abstract

Metal forming is a manufacturing method that faces high demands from several advanced engineering industries. This master's thesis will investigate the potential for combining tools developed with additive manufacturing and the metal forming process, flexible rotary stretch bending, to produce high quality and cost-effective parts. This work is a continuation of the research conducted in the specialization project in the subject TPK4540 - Manufacturing Technology, Specialization Project.

This thesis presents processes employing 2D stretch bending to bend hollow aluminum profiles into desired shapes. The flexible dies utilized to shape the profiles into the desired geometry are fitted with additive manufactured surface tools to achieve a high-quality surface finish. Conventional tools used in this profile shaping process are typically designed for specific geometries. However, employing additive manufacturing to create adjustable tooling offers a rapid and potentially advantageous method for generating new tools. These AM-based tooling solutions must meet specific mechanical and structural criteria, which will be investigated though experimental analysis.

Given the limited existing research in this area, this project follows a trial-and-error approach, building upon the findings and results from the previous specialization project. The methodology involves utilizing proof-of-concept prototyping using PLA designs and testing them with two different bending radii.

The outcomes of this master's thesis have demonstrated the significant potential of combining additive manufactured tooling with flexible 2D stretch bending. This research aims to bridge the existing research gap within this field, providing valuable insights and contributing to the advancement of metal forming processes.

Sammendrag

Metallforming er en produksjonsmetode som møtes med høye krav fra flere avanserte ingeniørindustrier. Denne masteroppgaven vil undersøke potensialet for å kombinere verktøy utviklet med additiv tilvirkning og metallformingsprosessen, fleksibel strekkbøying, for å kostnadseffektivt produsere deler av høy kvalitet. Dette arbeidet er en videreføring av forskningen gjennomført i prosjektoppgaven tilhørende emnet TPK4540 – Produksjonsteknologi, fordypningsprosjekt.

Denne masteroppgaven vil presenterer prosesser som bruker 2D-strekkbøying for å bøye hule aluminiumsprofiler til ønskede former. De fleksible formene som brukes for å forme profilene til den tiltenkte geometrien, er utstyrt med additivt tilvirkede formingsverktøy for å oppnå en høykvalitets overflatetekstur. Konvensjonelle verktøy som brukes i denne formingsprosessen er vanligvis designet for spesifikke geometrier. Additiv tilvirkning kan potensielt være en rask og fordelaktig metode for produksjon av justerbare verktøy. Disse additivt tilvirkede verktøyene må oppfylle mekaniske og strukturelle krav, som vil bli kartlagt gjennom eksperimentell analyse.

Gitt at forskningen på dette område er begrenset, følger dette prosjektet en prøve-og-feile-metodikk, bygget på resultater og analyser fra prosjektoppgaven. Metoden innebærer proof-of-concept prototyping med design laget med PLA plastikk og vil benytte to bøyeradier til testing av de produserte prototypene.

Resultatene fra denne masteroppgavens har vist at det bor betydelig potensial i å kombinere additivt tilvirket verktøy og strekkbøyingprosesser. Denne forskningen har som formål å fylle forskningsgapet som eksisterer innenfor dette feltet og å gi verdifull innsikt, samt å bidra til fremskritt innenfor metallformingsprosesser.

Preface and Acknowledgements

This master's thesis is submitted to meet the requirements for a MSc degree at the Department of Mechanical and Industrial Engineering (MTP) at the Norwegian University of Science and Technology (NTNU) in Trondheim, Norway, in the spring semester of 2023. The project has been supervised by Sigmund Arntsønn Tronvoll. This master's thesis and its associated subject is worth 30 ECTS points.

I would like to extend a warm thank you to the supervisor of this master's project, Sigmund Arntsønn Tronvoll, for excellent and helpful supervision and for the opportunity to work on this project. I would also like to thank Jun Ma for co-supervising the early parts of the project and the NAPIC team for having me on the team. Further, I would like to thank Knut Sørby for assisting me and letting me make use of his excellent measuring lab in this project. I would also like to thank the amazing people in the MTP workshop for assisting me with tools and services required for this project. Finally, I would like to say thank you to my girlfriend, family, friends, and classmates for supporting me through this master's project. An extra hand of gratitude needs to be extended to my classmates and girlfriend, which have made the time at NTNU an experience for a lifetime.

Contents

List of Figures

List of Tables

List of Abbreviations

Al	Aluminum
AM	Additive Manufacturing
CAD	Computer Aided Design
FDM	Fused Deposition Modeling
FFF	Fused Filament Fabrication
PLA	Polylactic acid
R600	Radius 600 mm
R1200	Radius 1200 mm

1. Introduction

1.1 Background

Technology and products become increasingly more advanced. The capabilities, accessibility, and utilities of modern technologies grow rapidly. A such, the methods of producing these products and machines also need to evolve parallelly. The field of manufacturing technology encounters growing requirements for quality and precision because of this. The market demands aspects such as cost-efficiency, sustainability, and eco-friendliness, which serve as motivating factors for the manufacturing industry to enhance their manufacturing methods.

One of these manufacturing technologies is metal forming. This manufacturing technology is often faced with significant lead times from initial idea and conceptualization to a finished product. This method plays a crucial role in various large industries, including automotive, aerospace, and offshore engineering, where customized and shaped metal components are extensively utilized. Discovering innovative and efficient approaches to improve the metal forming process, while upholding the market's strict demands for accuracy and quality, would bring about substantial advantages.

Additive Manufacturing (AM) is a manufacturing technology that has, in recent years, witnessed a notable increase in both quality and popularity. It is utilized by a wide range of customers, from small, private hobby projects to vast industries. Reasons for this is that it provides a cost-effective and time-efficient manufacturing approach. It is well-suited for rapid prototyping and production of highly customized components. By utilizing this manufacturing method, costs and lead times can be significantly reduced, thereby offering substantial benefits.

The objective of this master's project is to focus on rotary stretch bending, a technique employed to shape and bend metal specimens into diverse geometries. The rotary stretch bending process is essentially a versatile method of generating 3D shapes, often utilizing specifically designed dies for each geometry. Consequently, this approach leads to elevated tool costs and longer lead times, as a unique die tailored for a specific geometry

is required for every differing geometry. To address this issue, this project employs a flexible and adjustable die tool, which bending radius can be adjusted based on the required geometry. This tool is depicted in Figure 1.
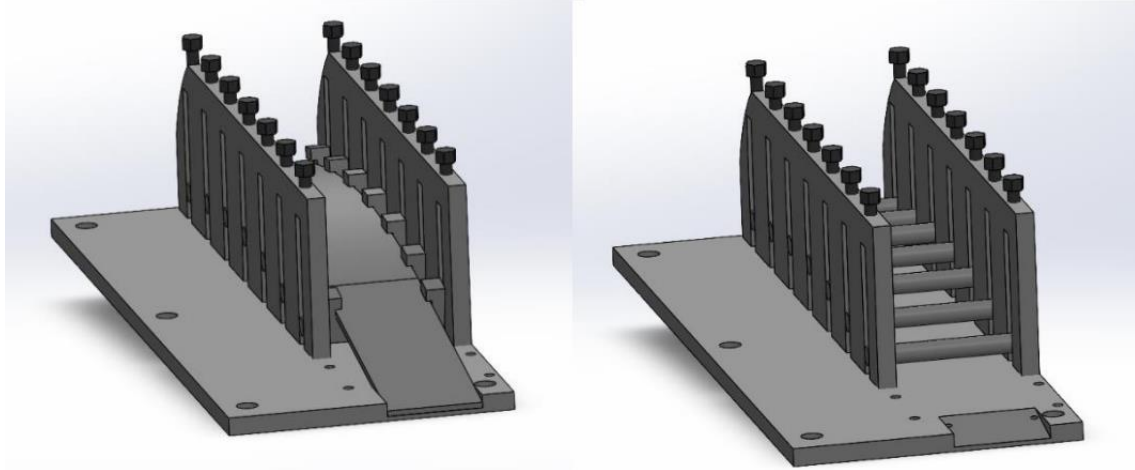
Figure 1: The flexible and adjustable tool with (left) and without (right) the spring steel plate. Taken from the project thesis (Lundby, 2023).

1.2 Problem Description

Due to the spring steel plate's high stiffness, the radius of the plate has proven to be difficult to adjust correctly. Scuffing inflicted at the last point of contact between the spring steel and the specimen has also been an issue when utilizing the spring steel plate. To overcome the challenges associated with these difficulties, a novel solution is required. This solution should be able to be mounted on the steel axles, ensuring accurate forming while minimizing the indentations inflicted on the specimen during the process. This project aims to address this issue by exploring innovative tool concepts and utilizing additive manufacturing for their production. AM offers a significantly faster and cost-effective approach to create customized tools, making it a compelling choice.

1.3 Project scope and limitations

Considering the time constraints, this master's project's scope has been restricted to testing a single revised concept design that addresses the identified problem. Similar to the specialization project, this project has utilized Al-alloy 1900mm long AA6082-T4 hollow profiles with a cross-section of 60x40mm and a thickness of 3 mm as chosen specimens for testing. To streamline the project's goals and to continue iterating based on the specialization project's results, the focus has been limited to performing 2D stretch bending. Additionally, in the absence of time, the experiments conducted in this project

have been confined to investigating the same two bending radii as in the specialization project: 600mm and 1200mm, with 4 experiments conducted utilizing each radius, totaling in 8 aluminum profiles bent. In this project the manufacturing of tools has exclusively employed a single material, namely PLA, which have been produced using the Fused Filament Fabrication (FFF) process.

1.5 Objectives and research questions

The research on this problem was initially conducted as part of the specialization project thesis in the subject TPK4540 - Manufacturing Technology, Specialization Project titled *Concepts Utilizing Additive Manufacturing for Flexible Tooling in Rotary Stretch Bending Processes* (Lundby, 2023). The aim of the specialization project as well as this master's project is to examine whether solutions produced using additive manufacturing possess the essential structural qualities required for this type of manufacturing. It seeks to determine if AM can be a feasible alternative to conventional metal solutions for manufacturing tools for this kind of process. Additionally, the project intends to devise concepts, manufacture them, and conduct experiments with them to evaluate their performance. The objective is to design a solution for the identified problem described in this thesis though comprehensive analysis and investigation. To offer a thorough understanding of the problem and objectives, it is essential to establish research questions. The research questions for this master's thesis will be derived from the research questions established in the specialization project, along with their corresponding results. This approach ensures continuity and builds upon the foundation laid by the previous project. The research questions established in the project thesis were:

I. Does AM tooling have the required structural qualities to be used in a rotary stretch bending process?
II. How does the selected geometry affect the AM tooling and how does the AM tooling affect the surface finish of the bending specimens?
III. What should be studied on further and how should the tools be further developed?

To summarize, the findings revealed that additive manufactured tools made from PLA plastic using FFF have the potential to meet the necessary structural requirements for integration with rotary stretch bending, provided that specific experimental parameters are in place. When utilizing a predetermined infill density, the tools exhibited sufficient

structural strength to withstand the bending process for larger bending radii. However, the structural integrity was compromised when dealing with smaller bending radii. Additionally, it was observed that the printing direction and orientation of the prints were contributing factors in terms of structural integrity of the tools. Moreover, in terms of the surface finish of the bent profile, the use of additive manufactured tooling resulted in a significant improvement in quality, leading to noticeable reduction in indentations compared to the steel axles. Based on these findings, several recommendations for further studies were contrived. One suggestion was to focus on enhancing the design of the additive-manufactured tool by incorporating an exchangeable contact surface tailored specifically to different bending radii. This approach aims to further minimize indentations and marks inflicted during the bending process. Exploring new printing directions based on the fractures observed in the tooling and utilizing higher infill densities were also proposed. To assess the durability and robustness of the manufactured tools more thoroughly, it was suggested to increase the number of cycles per radii in testing and test a third radius, namely 900 mm. As mentioned, this radius will not be tested due to time limitations. Furthermore, developing a more precise method for setting up the adjustable tool and implementing more accurate measurement techniques for evaluating the results were advised. A thorough summary of the project thesis will be presented in chapter 2. Based on these insights, the following new research questions have been formulated for this master's project:

I. Does increasing the infill density of the improve the structural qualities of the AM tooling sufficiently to withstand the rotary stretch bending process across all applicable bending radii?

II. Is the implementation of an exchangeable contact surface on the AM tool effective in reducing the indentations and marks inflicted on the specimens during the bending process and is the improvement significant?

III. How does a build orientation perpendicular to the compressive forces affect both the AM tooling and the surface finish of the specimens?

1.6 Thesis structure

This master's thesis is organized into seven chapters, with this introductory chapter serving as chapter 1. Chapter 2 will encompass a literature review and theory relevant for this master's project. Theory from the specialization project will be incorporated here as it remains highly relevant for the master's project. Additionally, Chapter 2 will be including a comprehensive summary of the specialization project. Furthermore, chapter 3 will provide a thorough description of the methodology employed throughout this project. Chapter 4 will showcase the experimental results, while Chapter 5 will thoroughly discuss and analyze the findings. Chapter 6 contains suggested further work and potential areas for future development. Finally, Chapter 7 will present a conclusion, answering the research questions and provide a conclusive summary of the study in this master's project.

2. Theory: Literature review and project thesis summary

This chapter will delve into the theory and prior research conducted in relevant fields in order to the obtain a thorough and deep understanding of all aspects surrounding the problem at hand and to create a solid theoretical background for the master's project. Prior research containing studies on rotary stretch bending, flexible die tools for stretch bending, and aspects surrounding additive manufacturing will be evaluated and presented. Section 2.1 will present theory regarding the rotary stretch bending process and the machine employed in this project to provide a solid technical understanding of the process and machine utilized in this project. Section 2.2 will contain theory and background on the adjustable tool employed in the project. This will offer a solid technical explanation of the solution utilized to provide flexible geometry, which is vital to develop the best possible products to approach the problem. In Section 2.3 relevant background on additive manufacturing vital to the development will be presented, which will help in providing a solid technical understanding upon which to base choices of printing parameters on. A summary of the specialization project containing all the relevant material and discussions from that research is also a significant part of this chapter and will be presented in Section 2.4. A summary of the conclusions from the project thesis is also presented in Chapter 1 along with the research questions for the project. Sections 2.1 through to 2.3 consists of the theory presented in the specialization project, which is equally relevant for this master's project. Section 2.3 also includes new theory researched for this project. Another overarching goal of this chapter is to locate gaps in existing literature relating to the research on the problem in this project.

2.1 Rotary stretch bending

Stretch bending is a widely employed technique for bending metal specimens, that has proven to be highly effective for shaping hollow profiles in applications demanding strict tolerances and large-scale productions (Tronvoll et al., 2022). This method is extensively utilized in various industries, including automotive, aerospace, and offshore drilling, due to its capacity for manufacturing high-precision shapes (Ma et al., 2022; Welo et al., 2020). Nevertheless, stretch bending does possess limitations. Its applicability is

restricted to bending processes utilizing moderate to large radii due to physical constraints inherent in the stretch bending process.

Compared to conventional bending methods, stretch bending distinguishes itself by applying stretching forces across the profile's cross-section. This is achieved by longitudinally stretching the specimen. This induced tensile strain mitigates buckling by preventing material compression along the side closest to the radial center. Compared with traditional bending processes, stretch bending results in twice the longitudinal strain, causing necking to often occur at an earlier stage (Tronvoll et al., 2022). Another essential advantage of the induced tensile strain is its ability to minimize springback (Welo et al., 2020). However, it is important to note that the springback cannot be eliminated entirely and should still be considered. The stretching process can either be a pre-bending, mid-bending, or post-bending stretch, depending on if the process was applied before, during or after the bending process (Ma et al., 2022). Regardless of the induced stretch, stretching will occur in the specimen during the bending, thanks to the flexible tool design.

Conventional stretch bending typically occurs in 2D, involving translational movement along the x-axis and rotational movement around the y-axis. It relies on rigid geometry dies that cannot be configured, which provides limited to no flexibility for altering the bending shape. However, by replacing these rigid and inflexible geometries with multi-point dies, the flexibility of the desired shape can be significantly enhanced. Multi-point dies allow bending across multiple axes, in addition to the y-axis. Introducing a third degree of freedom enables specimen bending around the z-axis as well (Welo et al., 2020). This approach, utilizing a flexible tooling, facilitates utilization of localized and customized curvatures, which will be explored and discussed further on in this chapter. By employing a rigid geometry die with multiple contact surfaces, a third degree of freedom can also be achieved. One surface is used for horizontal bending while another is used for vertical bending.

To be capable to produce intricate 3D profiles, Welo et al. introduced an innovative concept for a flexible stretch bending machine. This machine is depicted in Figure 2. This machine consists of two bending arms which are symmetric in the x-z plane. These two arms are capable to move freely in five axes. This provides each arm with three degrees of freedom. The first degree of freedom, referred to as Axis 1, enables translational

movement along the x-direction, which is controlled by a hydraulic servo. The second degree of freedom, which is the rotational movement around the y-axis, is governed by Axis 2 and 3 and are controlled by electric servos. Finally, the third degree of freedom, enabling rotational movement around the z-axis, is governed by Axis 4 and 5 and are controlled by hydraulic servos. To secure the specimen, each arm is equipped with a hydraulic-controlled clamp, ensuring proper clamping at each end (Welo et al., 2020).
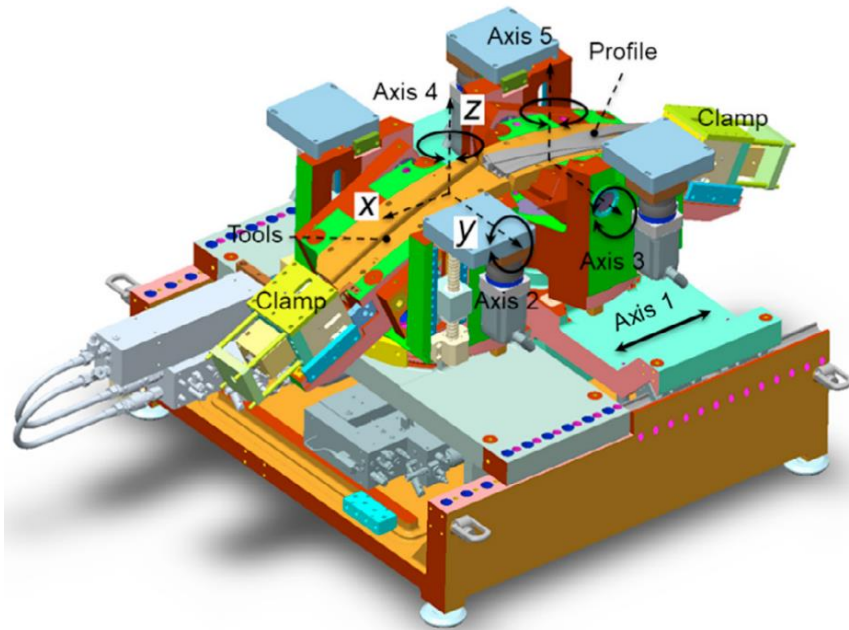
Figure 2: Flexible 3D stretch bender (Welo et al., 2020).

In a study conducted by Ma et al., hollow profiles of AA6082-T4 were subjected to bending with various stretching configuration, including pre-stretching, mid-stretching, post-stretching, and a combination of pre- and post-stretching. The findings revealed that the longitudinal strain along the specimen varied depending on the measurement location. Notably, the highest strain was observed approximately 80% along the specimen, with 0% representing the clamped end and 100% denoting the middle of the specimen at the symmetry plane (Ma et al., 2022). Figure 3 illustrates the strain distributions along the specimen. The study demonstrates a consistent correlation in strain distribution across all specimens, which can have implications for the loads inflicted on the die tools used in the bending process.
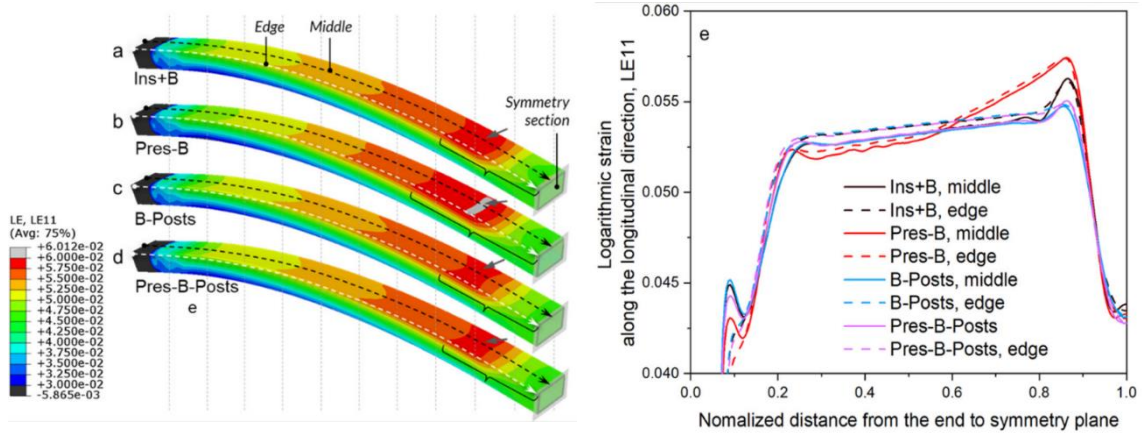
Figure 3: Longitudinal strain distributions from the end to the symmetry plane, where Ins+B denotes mid-stretching, Pres-B denotes pre-stretching, B-Post denotes prost-stretching, while Pres-B-Posts denotes the comination of pre- and post-stretching. Middle denotes the strain at the middle of the face as depicted and edge denotes the strain at the edge of the face as depicted (Ma et al., 2022).

Ma & Welo conducted an additional experiment which corroborates the observed strain distribution. Similar AA6082-T4 specimens were used in this experiment and as well as the same rotary stretch bender. This experiment was done to assess the springback behavior of the bent specimens (Ma & Welo, 2021). Figure 4 provides evidence that supports the previously mentioned findings concerning stress distributions during a 2D stretch bending process. The strain is shown to be most significant near the symmetry plane.
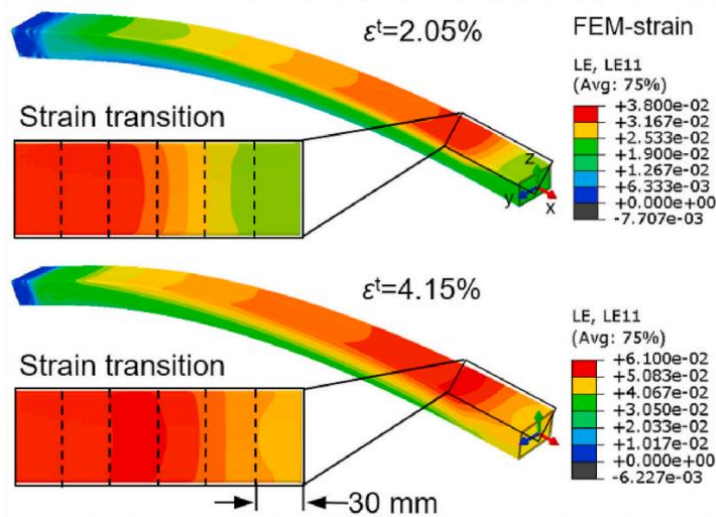
Figure 4: Longitudinal strain distribution from the end to the symmetry plane (Ma & Welo, 2021).

2.2 Flexible tool for rotary stretch bending

Achieving various shapes for specimens necessitates the use of customized tools, as previously mentioned. However, employing multiple die tools where each die tool is specifically tailored for each shape can significantly escalate costs and lead times per part. Consequently, having a flexible and adjustable tool capable of accommodating a diverse range of specimen shapes can prove highly effective in terms of reducing part costs, lead times, and even enabling rapid prototyping (Tronvoll et al., 2022).

In their work, Tronvoll et al. introduced a flexible tool designed for the rotary stretch bending process, meant to be combined with same machine utilized in the experiments mentioned earlier in the chapter. This tool is comprised of seven height-adjustable, hinged brackets mounted on steel axles. These axles are evenly spaced with a 70 mm gap between them and provide support for a spring steel plate. Horizontally, the axles are supported by sidewalls, while vertically, they are supported by threaded rods connected to the sidewalls and a baseplate. By manipulating these brackets, different bending geometries can be achieved using these tools alone, eliminating the need for several customized die tools. This concept is specifically designed to accommodate radii ranging from 500 to 2000 mm. Figure 5 illustrates the tool and its setup in conjunction with the rotary stretch bending machine.

Figure 5: The flexible tool fitted onto the rotary stretch bending machine (Tronvoll et al., 2022).

In Figure 5, a rotation hinge point is depicted, representing the pivot axis around which the specimen is bent. The precise location of this point is crucial for achieving a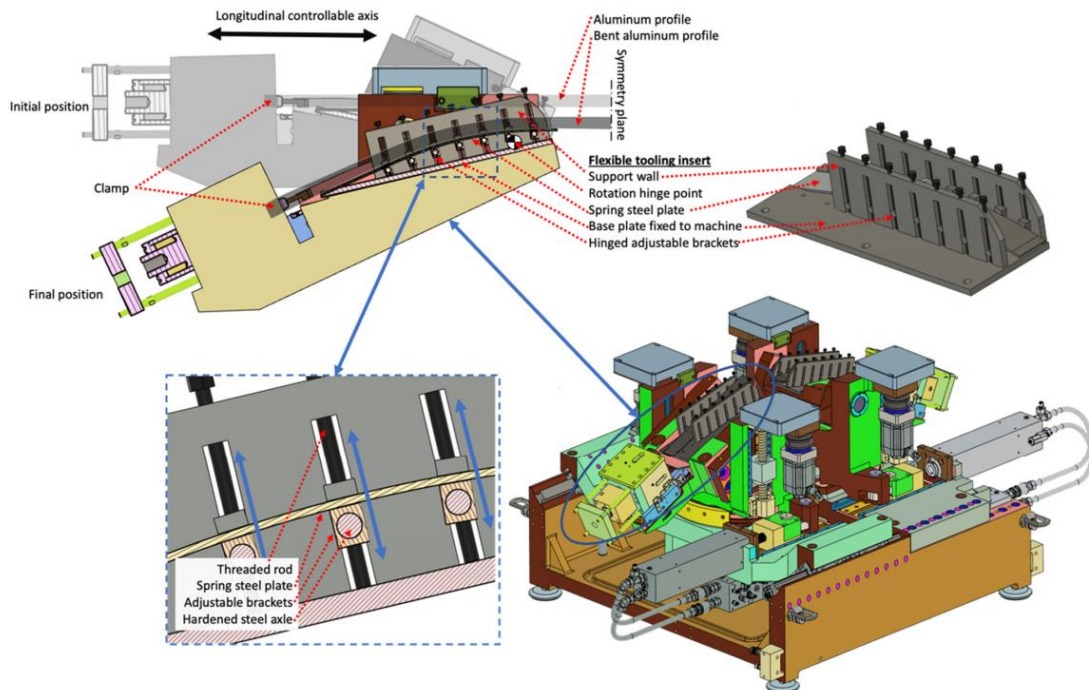 consistent tensile plastic strain throughout the entire specimen, ensuring that no part of the specimen experiences compressive forces. The desired bending radius directly influences the rate of plastic strain, as the pivot point is tailored for a specific tooling setup. Due to this aspect, the strain rate varies with the degree of bending as the contact point between the tool and the specimen, and consequently the bending, moves along the specimen towards the symmetry plane. This movement changes the distance between the pivot point and the bending point. Initially, the radius is at its maximum value, gradually decreasing as the bending point approaches its closest proximity to the pivot point. Subsequently, the radius increases as the bending point moves away towards the symmetry plane. Consequently, the strain rate fluctuates as the bending degree increases. At the bending degree's lowest value, when the pivot point radius is at its largest, the strain rates experienced by the specimen is at its maximum. As the bending process continues and bending degree increases, the strain rate decreases until the pivot point radius reaches its minimum value, after which it begins to increase until the bending process is complete. It is worth noting that if the tool is configured for specific bending radii, the specimen may encounter compressive strain as the pivot point radius approaches its lowest values. Tronvoll et al. conducted two stretch bending experiments utilizing different radii and plotted a graph comparing the bending degree with the strain rate, as presented in Figure 6. These results highlight that the variation in strain rate was more significant for lower bending radii. For instance, the R600 bending radius exhibited a more significant fluctuation in strain rate compared to the R1500 bending radius. Figure 6 also underpins the concept of the strain rate behavior related to the increasing bending degree mentioned earlier in the paragraph (Tronvoll et al., 2022). These radii are comparable to the ones employed in this project, utilizing the same adjustable tool.
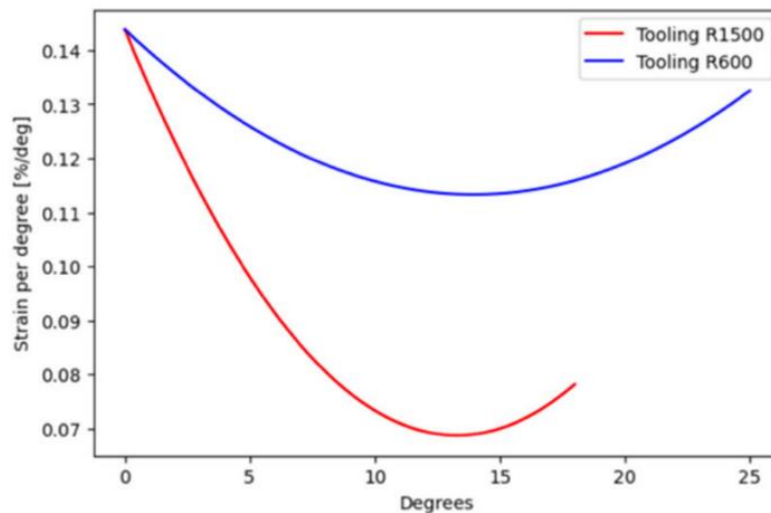
Figure 6: Plot of the strain rate in relation to the bending degrees for R1500 and R600 experiments (Tronvoll et al., 2022).

In a study conducted by Li et al. the focus was on flexible 3D stretch bending using a devise capable of achieving two degrees of freedom simultaneously. The objective of the study was to investigate the impact of the number of roller dies on the forming accuracy of specimens. The specimens examined in this study was also made of AA6082. The findings revealed that the number of roller dies influenced the forming accuracy, as the indentations varied depending on the number of roller dies employed. The research team concluded that increasing the number of roller dies enhanced the forming accuracy by reducing fluctuations in the strain along the thickness direction (Li et al., 2021). This finding is relevant to this project, as the tools utilized incorporate multiple axles that serve as contact points. Reducing the severity of these indentations is among the objectives of this thesis' project.

2.3 Additive manufacturing

As the scope of the project includes manufacturing the tool designs using additive manufacturing, several printing parameters needs to be considered. Therefore, this section will discuss and present theory relevant for the parameters prioritized in this project, namely layer thickness, build orientation and infill density. This section will also present theory regarding additive manufacturing techniques and filaments utilized in this project, for example PLA, which is the chosen filament. Other studies that have researched similar problems will also be discussed.

Additive manufacturing (AM), also known as 3D printing, is a rapidly growing manufacturing technology that revolves around the production of objects designed using computer-aided design (CAD) and an additive manufacturing printer. By incrementally adding material layer by layer, an object is created by the printer. This innovative approach enables designers to create highly customized parts with intricate geometries that may not be easily achievable through traditional manufacturing methods. Moreover, it eliminates the requirements for an extensive array of specialized tools, as the primary essentials are CAD software and an additive manufacturing printer (Gao et al., 2021).

The most common AM technique is known as Fused Filament Fabrication (FFF). This is the technique employed in this project. FFF is similar to the technique called Fused Deposition Modeling (FDM) and both names will be used in this project. FFF involves the utilization of a heated nozzle that selectively deposits a thermoplastic polymer onto a build plate. This polymer is applied layer by layer, with each layer solidifying and bonding to the adjacent layers. One of the notable advantages of FFF is its ability to accommodate a wide range of low-cost feedstock materials, enabling the production of objects in varying sizes, from small-scale to large-scale. Due to its versatility, FFF has gained significant popularity as a preferred manufacturing method in industries such as, automotive, aerospace, and biomedical, where demand for intricate parts and complex geometries is prevalent. (Gao et al., 2021),

Nevertheless, it is important to acknowledge that both AM and FFF possess certain drawbacks that can hinder achieving mechanical properties equivalent to those achieved through conventional means of manufacturing. Elements such as layer thickness, layer bonding, build orientation, and direction are influential factors that can significantly impact the mechanical characteristics of the final product (Gao et al., 2021),

In studies conducted by Rankouhi et al., the influence of layer thickness and orientation on the mechanical properties of 3D printed materials was investigated. Their findings revealed that reducing the layer thickness resulted in increased tensile strength and stiffness of the produced part. However, the study concluded that the failure modes observed in their experiments were predominantly influenced by the raster orientation rather than the layer thickness itself (Rankouhi et al., 2016). Yao et al. came to the same conclusion relating to the importance of layer thickness while conducting studies on the

same subject. In their studies they utilized FFF to produce samples of PLA, upon which they conducted tests. Their findings revealed that decreased layer thickness resulted in increased tensile strength (Yao et al., 2020).

Dwiyati et al. conducted research to explore the impact of build direction on the mechanical properties of 3D printed parts. Their study concluded that aligning the layers in an axial direction, in relation to the applied forces on the part, significantly enhances both the stiffness and the tensile strength compared to printing the layers in the lateral direction. This improvement is attributed to the stronger interlayer bonding in contrast to the intralayer bonding within the part (Dwiyati et al., 2019). The study conducted by Rankouhi et al. and the study conducted by Dwiyati et al. both employed ABS filament as their material of choice.

The infill density is a critical parameter that significantly impacts the mechanical properties of the final 3D printed part. Terekhina et al. conducted experiments focusing on tensile testing of FFF samples manufactured using nylon filament. Their findings revealed that both tensile strength and stiffness experience notable enhancements as the infill density is increased. Particularly, when the infill density surpasses 60%, a significant and drastic improvement in tensile strength and stiffness becomes evident. This increase can be attributed to a substantial increase in contact between the individual strands of the infill material, leading to improved structural integrity (Terekhina et al., 2019). Another research investigating the infill density's impact on the mechanical properties of FFF manufactured samples was conducted by Gunasekaran et al. They conducted tests on samples of PLA to measure the hardness, impact strength, tensile strength, and flexural strength in relation to infill density. All samples were printed with the same printing direction and with infill densities of 25%, 50%, 75%, and 100%. These tests revealed that all the before mentioned properties increased with the infill density, as every value was at its highest with an infill density of 100%. With these findings, the concluded that using FFF manufactured PLA components with a 100% infill density was a viable option in various industries (Gunasekaran et al., 2021). Mishra et al. also conducted experiments of a similar nature they performed impact tests on PLA samples with varying degrees of infill density. When performing Izod impact tests their results revealed that the best infill density in terms of impact strength was 85% in a range of densities from 50% to 100%. They justified this stating that the impact strength strictly

depends on a balance between stress intensity and crack propagation. They argued that gap between the strands of infill at densities up to 85% halted crack propagation. Heavy stress was the dominant factor causing fracture. For higher infill densities, namely 90% and above, the crack propagation increased the rate of fracture (Mishra et al., 2021). Tanveer et al. performed a study where they made a thorough review of the literature available on this topic spotlighting infill density. The study revealed that infill density is a crucial factor for the strength of 3D printed specimens. They emphasized, like the studies earlier in the paragraph, that infill density is directly proportional to strength. The rise of infill density improves the physical behavior of the specimens because of better interlayer bonding as there is more surface for the layers to bond with. They also concluded that lower infill density increases build speed and decrease the amount of material needed. An aspect that needs to be considered is to find an optimum infill density that balances strength, building time and costs (Qamar Tanveer et al., 2022). In terms of compressive strength in relation to infill density for PLA specimens manufactured with FFF, Yadav et al. conducted experiments revealing that infill density increases compressive strength. They found this valid for all considered infill patterns when evaluating the compressive strength in the range from 20% to 80% (Yadav et al., 2021).

In the chapter *Polymer Design Guidelines* in the book *A Practical Guide to Design for Additive Manufacturing* it is mentioned that a characteristic of the additive manufacturing process is a phenomenon called "stair-stepping". This can occur when manufacturing sloped or curved surfaces from the bottom of the slope and up, layer by layer. The layers can then produce a surface comparable to steps of a staircase. Having a thinner layer thickness can combat this problem. Performing post-processing techniques, such as applying chemicals to smoothen the surface, can also diminish this issue. However, this can compromise the part accuracy and mechanical properties. The chapter also suggests that opting for infill densities higher than 50% might offer negative effects on the part's mechanical properties, contrary to the research mentioned earlier (Diegel, 2019).

In the context of employing AM to produce tools utilized in metal forming processes, Schuh et al. conducted a comprehensive study that compared various investigations on sheet metal forming using die tools manufactured through different methods. One research study, highlighted in their paper, employed FFF to manufacture dies for metal deep drawing. When polymer tools manufactured using FFF were utilized in the deep

drawing of thin DC04 steel sheets, the dimensional accuracy of the formed sheet metal was found to be satisfactory. However, concerns arose regarding the longevity of the tools, as the dimensional accuracy appeared to be compromised after producing larger quantities of specimens, particularly when using harder steel materials. Nonetheless, the study emphasized that FFF tools offered advantages such as reduced lead times and lower costs. They concluded that FFF-produced tools for sheet metal deep drawing were suitable for smaller quantities (Schuh et al., 2019).

2.4 Project thesis summary

In this chapter a summary of the project thesis will be presented. As presented in Chapter 1, the aim of the specialization project was to propose an initial solution to the problem at hand, namely, to verify if manufacturing tools using additive manufacturing would be a feasible alternative compared to traditional metal solutions in a rotary stretch bending process. To evaluate the solution in terms of the established research questions for the project thesis was the main objective (Lundby, 2023).

The angle chosen to develop a solution was to establish certain functional requirements that would result in a product able to counteract the indentations on the specimen resulting from the small radius of the steel axles on the die tooling. The specimens processed using these steel axles with said indentations are presented in Figure 7.

Figure 7: Specimen bent using the steel axles (Lundby, 2023).

The seven established functional requirements were (Lundby, 2023):

1. The contact surface of the tool needed to have a radius larger than the radius of the axles, but not so big that it oversteps the bending radius of the specimen.

2. The tool needs to be compatible with the axles of the adjustable tool. The fit must be tight enough to prevent excessive wobbling and travel on the axle, but not too tight preventing the tool to be easily mounted onto the axle.

3. The tool needs to withstand the forces of the bending process by offering adequate structural support.

4. The tool needs to be durable and withstand several cycles of bending.

5. A system for preventing rotation of the tool around the axles must be present.

6. The design needs to leave sufficient room beneath the axle, possibly requiring a specifically tailored tool for the outermost axle.

7. The design needs to be easily manufactured using additive manufacturing.

2.4.1 Tool design

In order to find a feasible solution to these design requirements, two iterations of the additive manufactured tool were designed. The chosen design software for the project was the 3D CAD software SolidWorks. The easiest way to meet the established functional requirements was initially thought to be manufacturing a cylinder that could be mounted on the steel axles, with a center hole corresponding to the diameter of the steel axle and with a length just short of the distance between the sidewalls of the adjustable tool. The measurements chosen for these dimensions were 16.5 mm and 90 mm respectively, with an outer diameter of 65 mm as the distance between each axle was 70 mm. The steel axles had a diameter of the 16 mm and the distance between the side walls was 103.5 mm. To compensate for the decreasing distance from the steel axles to the base plate of the adjustable tool when moving outwards to the outermost axle, cylinders with outer diameters of 44 and 30 mm were designed for the two outermost axles (Lundby, 2023). This design, henceforth called iteration 1, is presented in Figure 8.
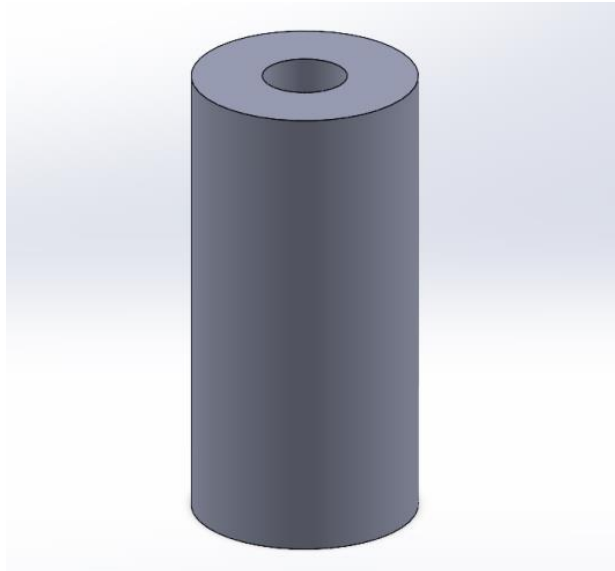
Figure 8: CAD model iteration 1, utilizing a 65 mm
outer diameter (Lundby, 2023).

Without testing iteration 1 it was established that this design utilized the free space around
the axles ineffectively. It occupied similar amounts of space all around the axle when the
space underneath the axles was limited. Having a large radius to counteract the
indentations would result in the tool being unfit due to the excessive space required
underneath the axle. An alternate iteration of the tool was designed that could maximize
the radius of the contact surface while minimizing the occupied space underneath the
axles. This resulted in a shape with a curved contact surface and reduced mass underneath
the axle hole. This shape shared the length of the cylinder, 90 mm, and had a width a bit
smaller than the largest outer diameter of the cylinders, namely 60 mm. The edges of the
contact surface were blended to prevent stress concentrations. The chosen radius of the
contact surface was 300 mm, which is a significant increase compared to the cylinders
32.5 mm radius (Lundby, 2023). This design, henceforth called iteration 2, is shown in
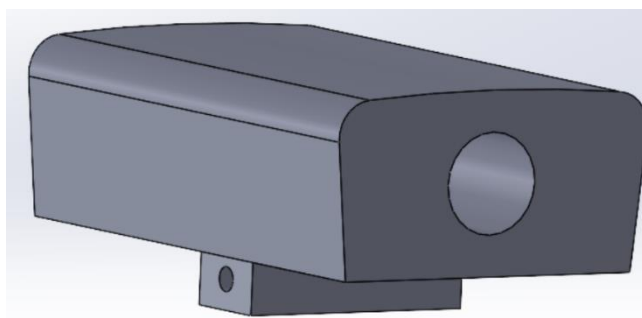Figure 9.

Figure 9: CAD model of iteration 2 (Lundby, 2023).

A customized part needs to be designed in order to compensate for the minimal space available underneath the outermost axle. This tool had a slimmer design to fit the available space and to support a range of bending radii. This tool shared the curvature of the contact surface as the other tools in the second iteration, i.e., 300 mm (Lundby, 2023). Figure 10 presents this design.
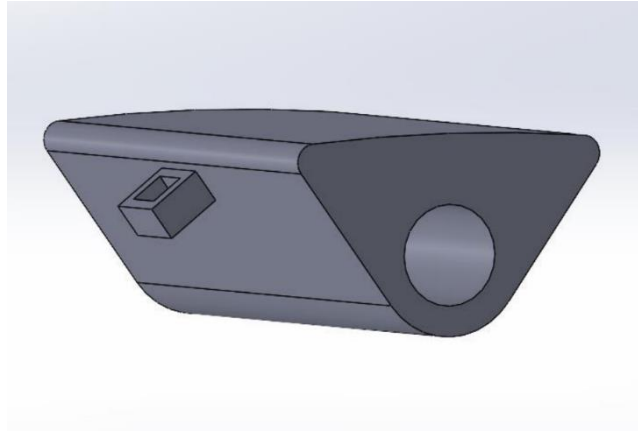

Figure 10: Customized part for the outermost axle (Lundby, 2023).

To adhere to the functional requirement regarding prevention of rotation around the steel axle, a system needed to be developed. This resulted in an extension on the bottom side of the tool designed with a small hole where a steel wire can be threaded through. This extension is visible in Figure 9. As the reduced space under the outermost axle prevented such an extension on the corresponding part, an extension on the on the side was created, with the purpose to mount the steel wire. This mounting point is visible in Figure 10. The steel wire would then connect all the seven tools and prevent rotation (Lundby, 2023).

2.4.2 Tool manufacturing

As the objective of the project was to utilize additive manufacturing to manufacture the tools for the rotary stretch bending process, AM was utilized. The printers utilized in the project were FDM printers, specifically Prusa MK3 and Prusa MK3+. As mentioned in Chapter 2, FDM is very similar to FFF. The printers employed in this project had 0.6 mm nozzles. The infill density was set to 30% and the layer thickness was chosen to be 0.30 mm. The value of 30% was partially arbitrarily chosen, as it was the double of the default value, which was 15%. This would then provide enhanced structural properties and yield a reasonable printing time. 0.30 mm layer thickness was chosen with the same reason regarding printing time, while still being reasonably thin, which also provides stronger

mechanical properties. The filament used to manufacture the tools was PLA (Lundby, 2023).

The tools were printed with print orientation in mind. To make the contact surface as smooth as possible to prevent excessive wear and friction between the specimens and the tools, the orientation was chosen to be as presented in Figure 11. However, this orientation resulted in the layers being parallel to the longitudinal direction of the specimens, which might compromise the structural integrity, as the interlayer bonding would be subjected to large forces, instead of the intralayer bonding. This aspect was sacrificed in order to achieve a smooth contact surface (Lundby, 2023).
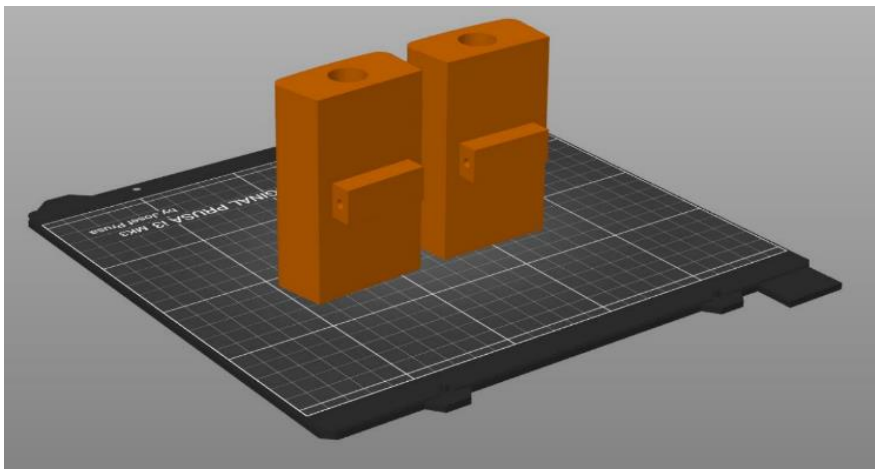

Figure 11: Iteration 2's printing orientation seen in PrusaSlicer (Lundby, 2023).

2.4.3 Adjustable tool set up

As the manufactured tools were to be fitted onto the steel axles, the spring steel along with the clamps were removed. The manufactured tools were then installed. The advanced shapes in iteration 2 were chosen for the tests, as there was no point in testing the cylinders in iteration 1, as they would create deeper and more pronounced indentations in the specimen. The results using iteration 2 would clarify how to proceed with the design development. To immediately get a clear result and to save time printing additional tools, only one adjustable tool was fitted with printed tools. The other adjustable tool made use of the steel axles only. This would quickly present a comparison of the two solutions. To set up the tools and axles with a correct height corresponding to the relevant bending radius, these heights needed to be calculated. The angle of the contact surface of each tool influenced the height of the steel axle. The height would then be calculated by measuring the distance from the baseplate of the adjustable tool up to the highest point on the steel axle. To easily measure this height while considering the angle of the contact surface, a

sketch of the setup made in SolidWorks were drawn. This sketch included all known parameters of the adjustable tool and facilitated easy and rapid measurement of the distance between the center of the cross section of the steel axle and the baseplate. A sketch with the parameters of a 1200 mm bending radius set up was provided and can be viewed in Appendix A. The scope of this project included performing tests on two bending radii, 1200 mm, and 600 mm. The corresponding rotation angles were respectively 20° and 25°. The CAD sketches of the 1200 mm setup and the 600 mm setup can be viewed in Figure 12. It is worth mentioning that the CAD sketch of the 600 mm setup needed to be drawn from the ground up as there was no provided sketch with parameters for this bending radius (Lundby, 2023).
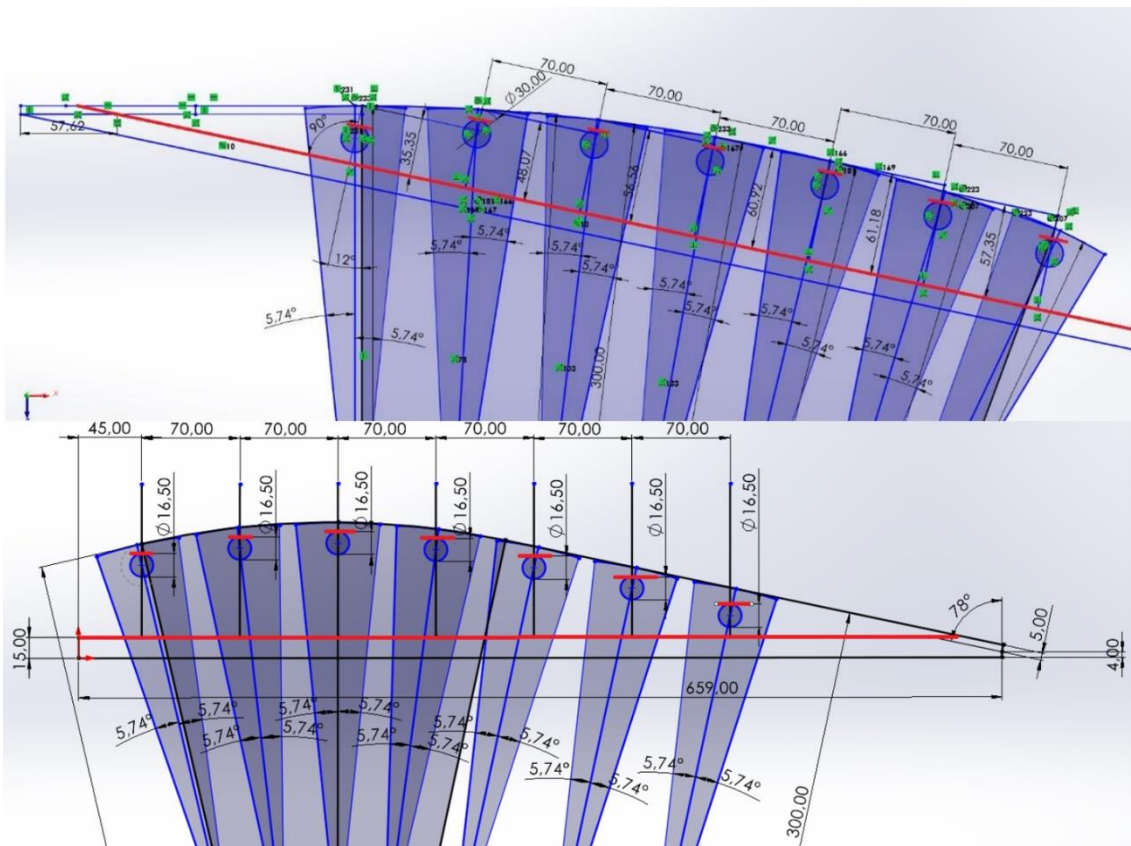

Figure 12: CAD sketches of the 1200 mm setup (top) and the 600 mm setup (bottom). The continuous red line indicates the baseplate height, and the smaller red lines indicate the highest point on the axles (Lundby, 2023).

A technique to adjust the steel axles' height correctly was developed. This technique employed a digital caliper and two metal pieces. To simplify the measurement process, it was determined that measuring the distance from the highest point on the steel axles to the top of the sidewalls was the easiest alternative. The set up was performed by placing one of the two pieces of metal on top of the sidewalls of the adjustable tool and the other on top of the steel axle that was going to be adjusted. This was done to create flat and easily accessible surfaces for the caliper to lean on and to measure. A margin of 0.1 mm was utilized when approving the height. A visual representation of the technique is presented in Figure 13. The thickness and width of these metal pieces needed to be considered when reading the values on the caliper. These values were calculated ahead of the adjustment, based on the CAD sketches (Lundby, 2023). An adjustable tool that has been sufficiently set up can be viewed in Figure 14.
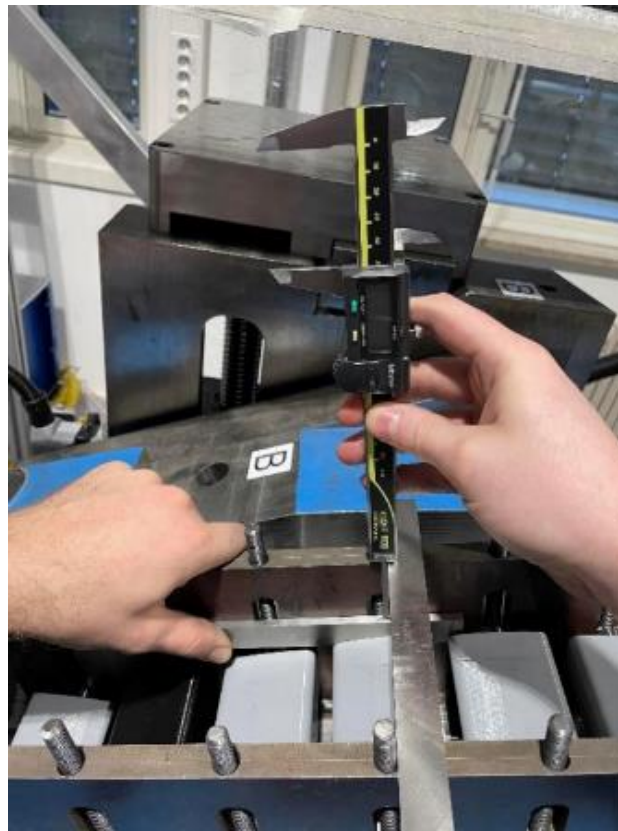

Figure 13: The measuring technique employed when adjusting the height of the steel axles (Lundby, 2023).

Figure 14: Configured adjustable tool with the tools from iteration 2 (Lundby, 2023).

2.4.4 Result verification and measurement

The final measurements of the results were performed by measuring the rotation angle of the specimens and compare them to the desired rotation angle. To make the specimens more manageable to handle, each specimen was cut in half. As three specimens were bent, a total of six parts needed to be measured. A technique was developed to measure the angle of each sample. By aligning the longest straight part of sample along a straight, unbent specimen, and employ two clamps to firmly clamp the two parts together, a digital protractor could be utilized to measure the angle between the bent sample and the unbent specimen. This technique is presented in Figure 15. To verify the measurement, the clamps were loosened and once again tightened a total of three times. For each time the angle was measured. An average angle was then calculated based on these three measurements and used to compare the samples against one another and the desired theoretical rotation angle (Lundby, 2023).

Figure 15: The technique employed to measure the rotation angle (Lundby, 2023).

2.4.5 The project's experimental results

Three aspects were reviewed after the experiments were conducted, namely surface finish and indentations, rotation angle measurements and dimensional accuracy, and the effects on the AM tools. The indentations created on the specimens during the bending process presented a clear difference between the sides of the specimen subjected to bear steel axles and printed tools. For both bending radii it was evident that the printed tool substantially reduced the indentations. Indentations were present on the side subjected to the steel axles, still they were significantly less pronounced (Lundby, 2023). The result is presented in Figure 16.
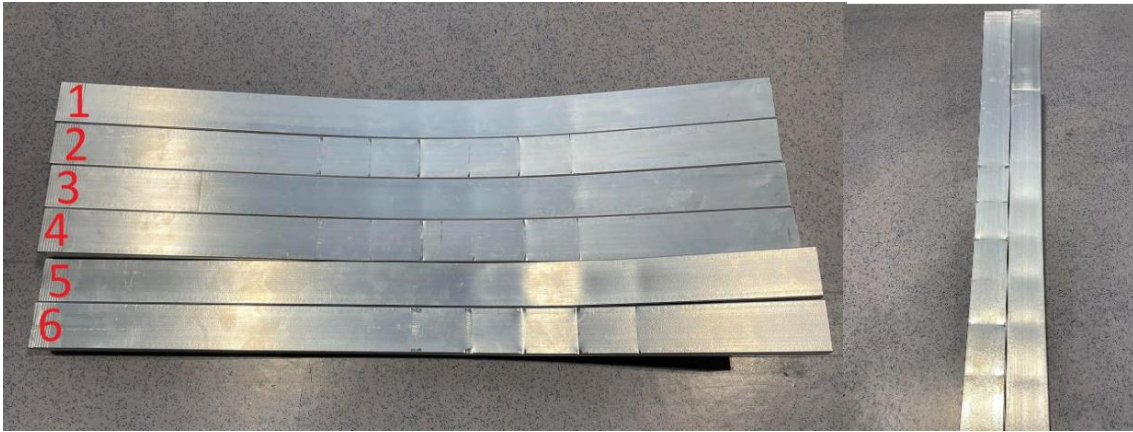
Figure 16: All three specimens after being cut in half. 1 and 2 are the halves of the first specimen bent using a bending radius of 1200 mm, 3 and 4 are the second, while 5 and 6 are the halves of the specimen bent using a 600 mm bending radius. To the right is a closeup of 1 and 2 (Lundby, 2023).

In terms of the measured rotation angles and dimensional accuracy it was revealed that the average rotation angle of each experiment was short of the intended rotation angle. Table 1 presents the results. It was evident that the R1200 experiments deviated from the desired rotation angle by approximately 1° on both sides. The R600 however, showed variation between the sides of the specimen depending on what tools the sides were subjected to. The side subjected to the AM tooling was 0.3° off while the side subjected to the steel axles was approximately 1° off (Lundby, 2023).

Table 1: Average measured rotation angle and corresponding experiments (Lundby, 2023).

Experiment nr.	Experiment parameters	Average angle
1	AM tooling, R1200, 20°, 1. try	18.73°
2	Steel axle, R1200, 20°, 1. try	18.92°
3	AM tooling, R1200, 20°, 2. try	18.98
4	Steel axles, R1200, 20°, 2. try	18.73
5	AM tooling, R600, 25°	24.6
6	Steel axles, R600, 25°	24.02

Regarding the effects the bending process had on the AM tools, the two bending radii exhibited differing outcomes. The experiments employing a 1200 mm radius resulted in minor scuffing on the printed tools, presenting no visual indication of the structural integrity being compromised or any other damage. The experiment using a 600 mm radius however, resulted in clear evidence of structural damage and failure produced by the forces of the bending process. These indentations were approximately 1 mm deep on the

AM tools suffering from the worst damage, and with the same exact width as the specimen. In addition to the visual hints, loud cracking noises could also be heard during the bending process, specifically when the machine began to rotate. This is presented in picture A and B in Figure 17. Closer inspection of the AM tools also revealed that tool number 4, 5 and 6 suffered the worst structural failure during the R600 experiment. Rest of the tools seemed to only suffer from scuffing marks, similar to the R1200 experiments (Lundby, 2023). This is observed in picture C in Figure 17.
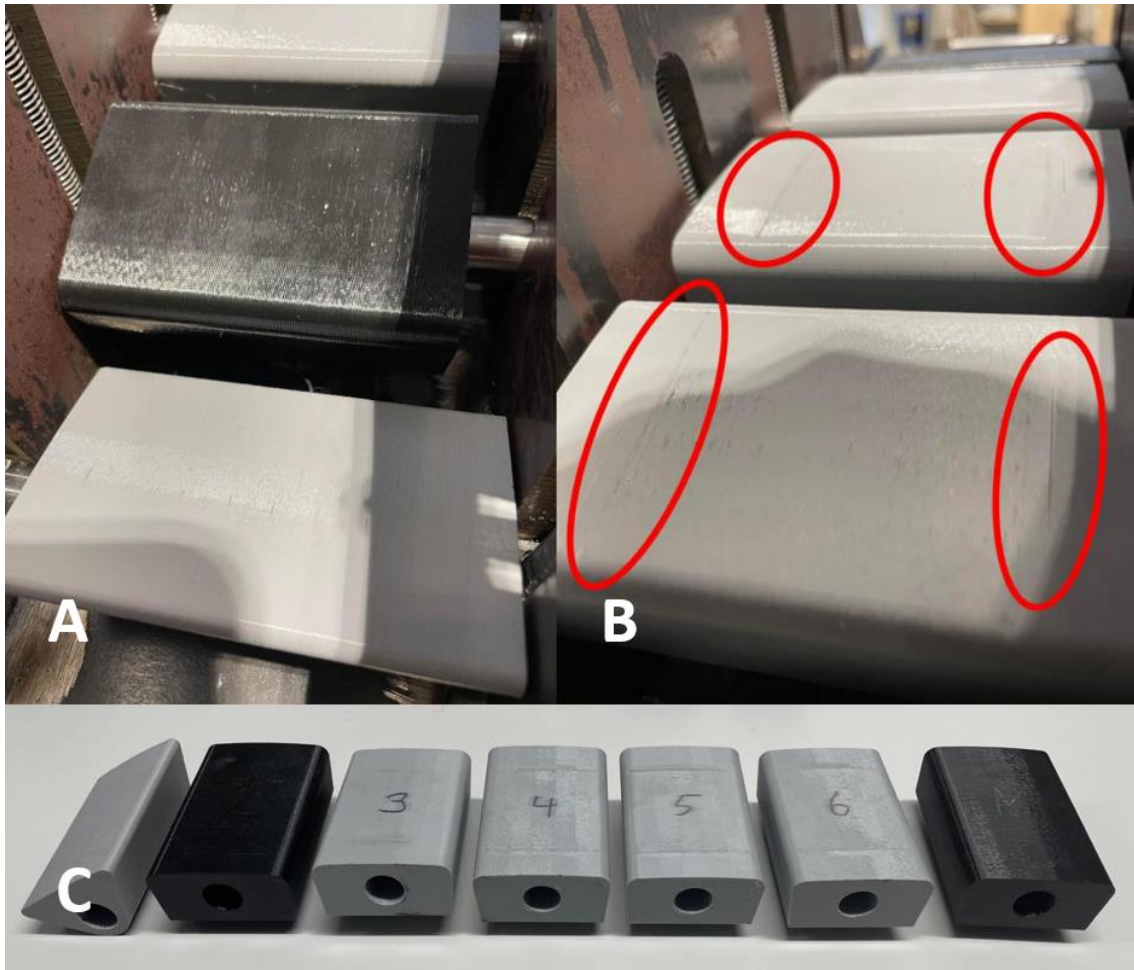
Figure 17: The surfaces of the AM tools after the R1200 experiments (A) and the R600 experiment (B). C showcases the tools with the end tool to left, then tool 2, 3, 4, 5, 6 and M, which signifies the tool closest to the middle of the specimen (Lundby, 2023).

2.4.6 Discussion of the project's results

The project thesis discussed that the results of the experiments indicated that the AM tooling did in fact diminish the indentations caused on the specimen during a 2D rotary stretch bending process and that further developing these AM tools could be sensible (Lundby, 2023).

The data from the measurements of the rotation angle however, showed that the data was inaccurate, with the R1200 experiments deviating with approximately 1° less than the theoretical rotation angle and the R600 experiment deviating with approximately 0.3° and 1° less. This indicated that there may be errors tied to the technique employed to set up the adjustable tools with the correct bending radius, and to the technique employed to measure the rotation angles on the specimens after the bending process. Therefore, it was surmised that finding new techniques to perform these tasks, with a lower margin for error, was logical. The differing rotation angles measured on the specimen subjected to the R600 experiment, could be explained by the malfunction of the AM tooling, therefore altering the bending shape (Lundby, 2023). Aspects the project thesis did not take into account, however, was the springback of the specimen and the inherent inaccuracy of the stretch bending machine itself.

The differing results of the structural integrity of the AM tooling using a bending radius of 1200 mm and 600 mm was explained with the strain rate in the specimens during the bending process. The malfunction of the AM tools during the R600 experiment could be caused by much higher strain rate the specimen was subjected to compared with the R1200 experiments. This can be related to Figure 6 where it is evident that the strain rate is higher during the R600 process compared to the R1500 process, which might explain the success of the R1200 experiments. This aspect was suggested to be countered by compensating the strain rate fluctuations by moving the machine arms longitudinally along the x-axis while the bending process is performed. Regarding the structural damage more severely occurring on tool 4, 5 and 6 could be explained with the strain distribution presented in Figure 3 and Figure 4, Here it is evident that the strain is highest approximately 80% along the specimen from the clamp towards the symmetry plane. This correlated nicely with the position of AM tool 4, 5 and 6. To increase the infill density to for example 60% was suggested to prevent structural malfunction. To experiment with another build orientation and layer thickness to increase the mechanical properties of the AM tools was also proposed (Lundby, 2023).

2.5 Literature Gap

This chapter theory research and literature review clarifies the absence of research literature on technologies revolving stretch bending processes that employs dies permitting flexible geometries and complex shapes. There is also an evident absence of research on solutions that combines said technologies with die solutions manufactured with additive manufacturing. The initial studies conducted in the specialization project revealed several aspects requiring improvement and is as such also part of the literature gap this master's project is trying to fill. These new requirements for the design are established and presented in Chapter 3. Due to this substantial lack of existing literature and research on these fields, this research may prove beneficial for pursuing further studies in these combined fields.

3. Methodology

This chapter will provide a full presentation and description of the complete methodology employed in this project. It will cover various aspects, such as the approach utilized to address the problem, the engineering design process, and the development of the final product. Additionally, this chapter will provide a detailed overview of the specifics of how the end results were achieved and the methods utilized to gather the necessary data. This project employs a proof-of-concept prototyping to assess if the concepts designed possess potential to solve the problem. Similar to the specialization project, the work conducted in this study continued the process adhering to the Value Engineering Method (SAVE International, 2007), which typically involves the following three stages:

1. Pre-Workshop
2. Workshop
3. Post-Workshop

The Pre-Workshop involves performing preparatory work for the project. In the specialization project this included conducting extensive literature review and getting familiar with the rotary stretch bender. Guided tours around the laboratory environment were organized and initial tests to understand the machine's operation were conducted. In this master's project the pre workshop consists of getting a thorough and deep understanding of the results and conclusion of the specialization project and use this knowledge to make logical and well-founded developments of the product. New gaps in the theory and literature review needs to be filled with additional literature searches if needed and testing needed.

The Workshop phase encompasses the execution of a structured job plan which consists of, in this case, six distinct phases. Table 2 provides a comprehensive breakdown of each phase and indicates the relevance of each phase to the master's project, the specialization project, or both. As depicted, all phases are relevant for both projects. Each cell in colored indicating if the task explained was accomplished or needed further work.

- The information gathering phase is relevant for both projects. In the specialization project most of the literature review was performed, however, it was evident that

additional literature reviews were required for developing the designs. Therefore, this phase is marked red for the specialization project and green for the master's project.

- Function analysis is performed in each project. The specialization project established the initial functional requirements for the designs. The results from the test conducted in the specialization project were analyzed to determine new functional requirements for the designs in the master's project. As functional analysis was performed and completed in both projects, the phase is marked green for both.

- The creativity phase was central in each project. In the specialization project this phase encompassed producing initial design, while in the master's project this phase included iterating on the designs based on analysis and previous results. Therefore, this phase is marked green in both projects.

- Evaluating the designs by testing them was a vital part of the both the specialization project and the master's project. Hence, the phase is marked green for both phases.

- Development of the designs based on results and experiences were also performed in each phase. In the specialization project iteration 1 was developed into iteration 2. The new design iteration in the master's project was developed in coherence with the results from the specialization project. This is why the phase is marked green for each project.

- Based on the studies and research conducted both projects' results are presented in a written thesis, with the project thesis and the master's thesis. Therefore, the presentation phase is marked green in both instances.

The Pre-Workshop and Workshop phases can be reduced to a four-step iterative cycle. These steps are:

1. Design
2. Build
3. Run
4. Analyze

The Pre-Workshop phase and the six phases listed in the Workshop phase goes through these steps by creating the designs based on background research and functional analysis. These designs are built and tested and run experiments on. The experimental results are analyzed to establish new design requirements and to further iterate on the design until it reaches a satisfactory result. The master's project is a new cycle based on the results from the specialization project. This cycle is presented in Figure 18 (Thomke, 1998).
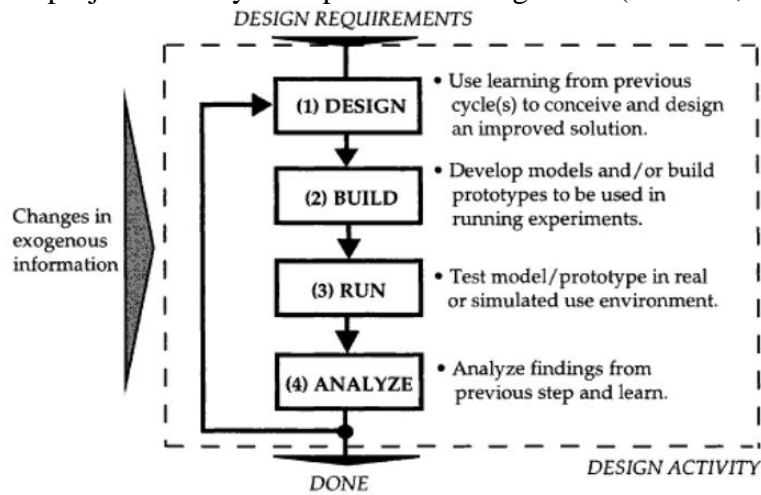

Figure 18: The four-step iterative cycle (Thomke, 1998).

Table 2: An overview of the six phases and relevance to the specialization project and master's project

	Phase	Assignments	Specialization project	Master's project
1	Information	Information gathering, employing literature review, and ascertaining literature gaps and establishing research questions	✓	✓
2	Functional analysis	Determining the products function and establishing the problems the product should solve.	✓	✓
3	Creativity	Designing product concepts and manufacturing	✓	✓
4	Evaluation	Conducting experimental tests with manufactured concepts in the rotary stretch bender.	✓	✓
5	Development	Evaluating test results and mapping the concept's weaknesses. Developing the concept based on revealed weaknesses.	✓	✓
6	Presentation	Writing a report on the study, including data and results.	✓	✓

Finally, the Post-Workshop phase involves documentation. Additionally, implementation of the solution is also included here, however this falls outside the scope of this master's project.

Moreover, this chapter will systematically present the conceptual framework, underlying philosophy and experiences from the specialization project that shaped the rationale behind its development. Subsequent sections will shed a light on the design, manufacturing, and integration processes to get the framework implemented into the machine. Additionally, comprehensive explanations of the methods employed to conduct the tests and detailed analysis of the obtained results will be presented. The designs resulting from the iteration cycles employed in the methodology is depicted in Figure 19.
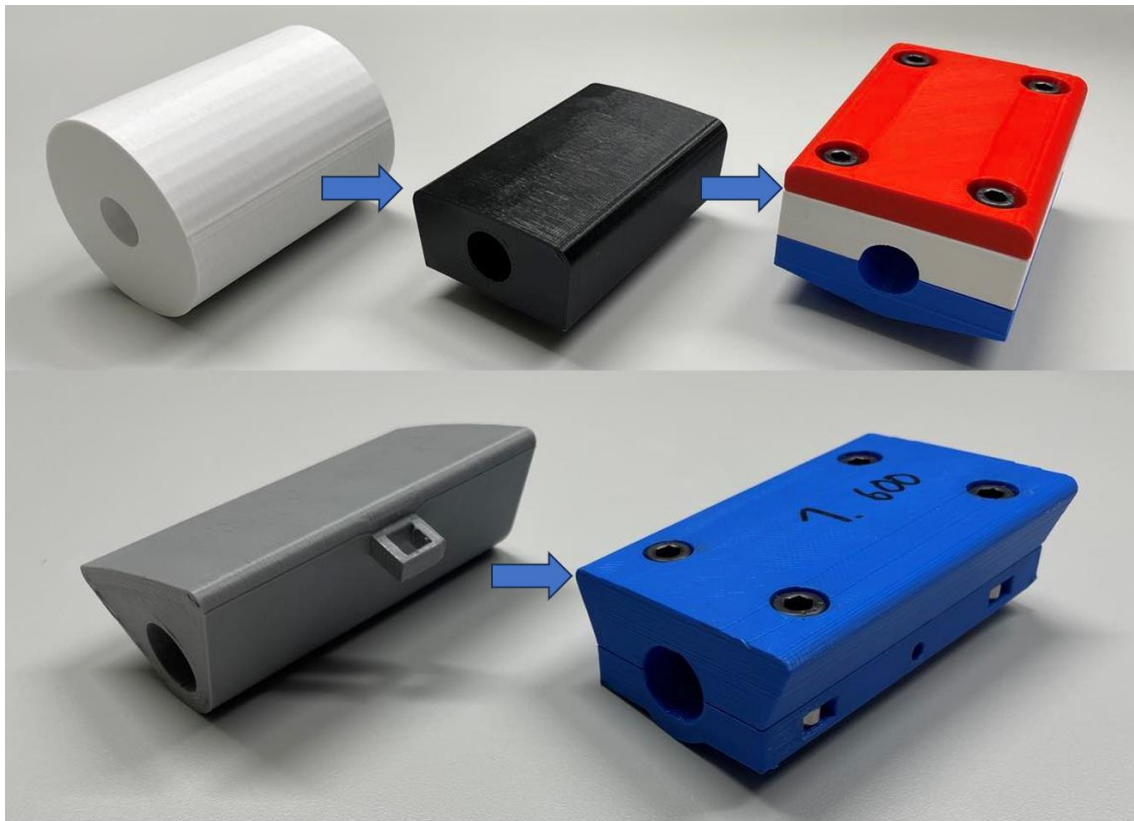

Figure 19: The iterations of the AM tools design, with the first, second, and third iteration of the main AM tool on the top and the first and second iteration of the outermost AM tool on the bottom.

3.1 Design requirements

As this master's project is another iteration cycle based on the research results produced in the specialization, new developments of the AM tools design need to meet the same design requirements as in the specialization project. These design requirements are listed in Chapter 2. As also mentioned in Chapter 1 and 2, the AM tool suffered structural malfunction when preforming a R600 experiment (Figure 17). With this in mind and considering other experiences from the specialization project and novel ideas, these additional design requirements were established for the design development.

1. To further reduce the specimens' surface indentations, a replaceable surface can be employed, where each surface curvature corresponds with the intended bending radius.
2. To simplify the installation of the AM tools, a design that can be installed without removing the threaded rods from the adjustable tool is beneficial.
3. To ensure the specimens placement in the surface of each AM tool is adequately similar, the new design needs to be widened to diminish lateral travel on the steel axle.
4. The AM tool's structural integrity needs to be improved to resist all bending radii and several bending cycles.
5. The mounting point of the steel wire on the outermost AM tool needs to be lowered to facilitate a correct start position of said tool.
6. To ease assembly of all parts of the AM tool, systems must be in place for accessible and manageable installation of fasteners.

3.2 Design development

The advanced shape of the second iteration of the AM tool significantly reduced the indentations inflicted on the specimens and possessed sufficient structural integrity to withstand bending processes employing a bending radius of 1200 mm. The bending processes utilizing a 600 mm bending radius proved to be too forceful for these AM tools. To strengthen the mechanical properties of the AM tool is then logical. This could be done by altering the printing parameters when manufacturing the AM tool. This will be discussed in further detail in Section 3.3 of this chapter. As the structural failure didn't seem to appear due to the overall design of the tool, the same design philosophy

influences this iteration of the tool's design. The aspects that showed potential for improvement in a 3D-modelling environment was the design's manageability in terms of installation on the flexible tool and, as mentioned in the design requirements, providing an opportunity to employ exchangeable contact surfaces utilizing surface curvatures corresponding to the bending radius.

The design presented in Figure 9 remains the foundation of the new design. In order to facilitate exchange of the contact surface the first idea was to split the tool in two horizontally and use fasteners to assemble the lower and upper parts. This suggests that loosening the screws and removing the contact surface followed by placing and fastening another contact surface would accomplish this task. This philosophy could also be utilized to simplify the installation of the AM tool on the adjustable tool. By splitting the lower part of the tool in the horizontal plane correlating with the center of the steel axle hole, installing and uninstalling the tool could be done without necessitating removal of the threaded rods from the adjustable tool. With this in mind, the AM tool can be split into three parts: a lower, mid, and upper part. This became the base idea for the design and the 3D-modelling process. As with the specialization project, SolidWorks is the CAD software of choice for this master's project when 3D-modelling the designs.

This new design utilizes an increased width along the x-axis compared with iteration 2's 60 mm width. As the distance between each steel axle is 70 mm, when measured from the center of the axle, this resulted a 10 mm wide gap between each AM tool. To increase the contact surface and to decrease this gap the new design is designed with a 65 mm width, decreasing the gap to 5 mm, which still yields room for unhindered rotation around the steel axles. As the distance between the supporting walls of the flexible tool is 103.5 mm and the width of the AM tool's second iteration in this direction was 90 mm, 13.5 mm of free space along the steel axle was available. Observing that the AM tool did travel a bit along the steel axle resulting in the specimen not being equally centered on all tools, the new design is 100 mm wide. This leaves less room for travel and centers the specimen more equally on all specimens relatively. The steel axles have a diameter of 16 mm. Like both previous iterations the new design is fitted with a hole with a 16.5 mm diameter, leaving a clearance of 0.5 mm.

The AM tool was split in three parts horizontally to facilitate replacement of the contact surface and simplify the installation onto the steel axles. The lower and mid part together enfolds the steel axle when assembled and the upper part functions as the exchangeable contact surface. The complete design is presented in Figure 20. 20 mm M6 machine screws are used to fasten the lower and mid part together while 30 mm M6 machine screws fasten the contact surface to the assembled lower and mid part. M6 nuts are used in conjunction with the screws. This results in the lower and mid part having eight screw holes, while the upper part has 4 screw holes, meaning that each tool needs four 20 mm M6 screws, four 30 mm M6 screws and eight M6 nuts. The surfaces of the mid part and the upper part are fitted with recesses to accommodate the screw heads to keep the surfaces flush. Figure 20, picture A, D, and E depicts these features. To eliminate the need to hold the nut in place when fastening the screws, the lower part is designed with slots on the sides where the nuts can be inserted. The width and height of said slots corresponds to the smallest width of the nut measured from one flat side to the parallel flat side and the height of the nut. When the nut is inserted, it is simultaneously prevented from rotating, which eliminates the need to manually hold the nut in place while turning the screws. The screw can then be fastened by simply turning the screw. These slots can be seen in picture B of Figure 20.
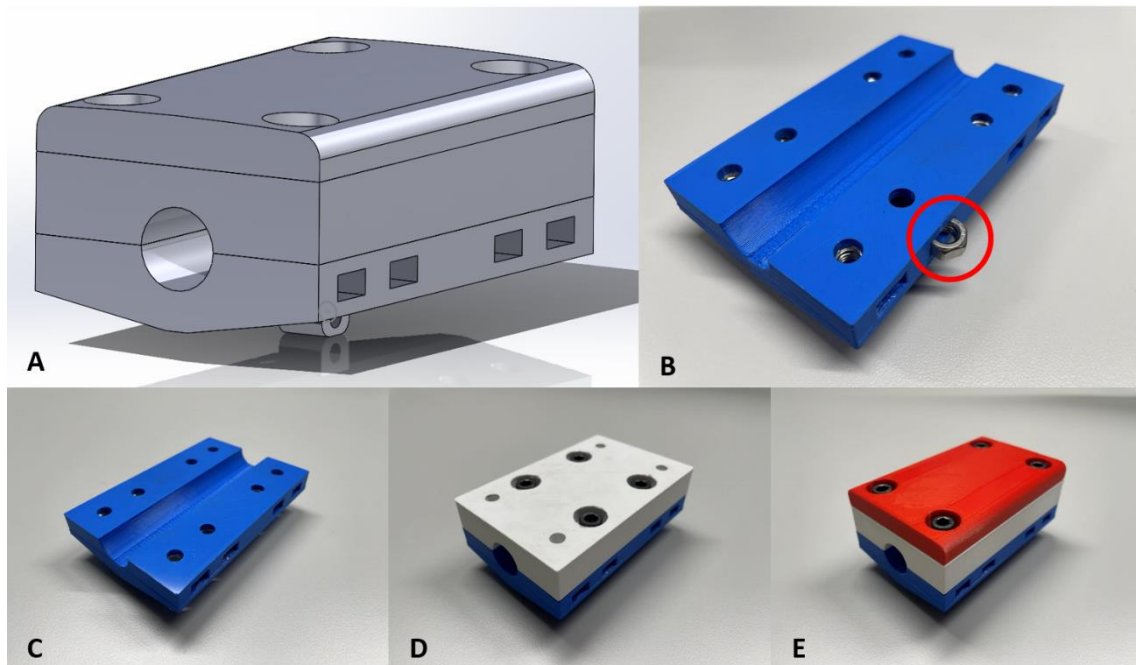

Figure 20: The new design for the AM tool. A depicts a CAD model of the design, B depicts the lower part and its slots for the nuts, and C, D, and E depict the complete design from the ground up adding one part at a time.

As hinted at, the upper part is the part fitted with the contact surface. As the project scope included doing experiments utilizing two different bending radii, 1200 mm, and 600 mm, two variations of the upper part were made, each fitted with one of applicable radii. To minimize the indentations inflicted on the specimen's surface, the edges are blended. This will also minimize damage on the surface edges of the AM tool in contact with the specimen. Due to the reduced space over and underneath the second outermost axle caused by the space between the baseplate and specimen, the upper part's thickness is reduced with 1.5 mm. Figure 21 depicts all three parts individually and their features.
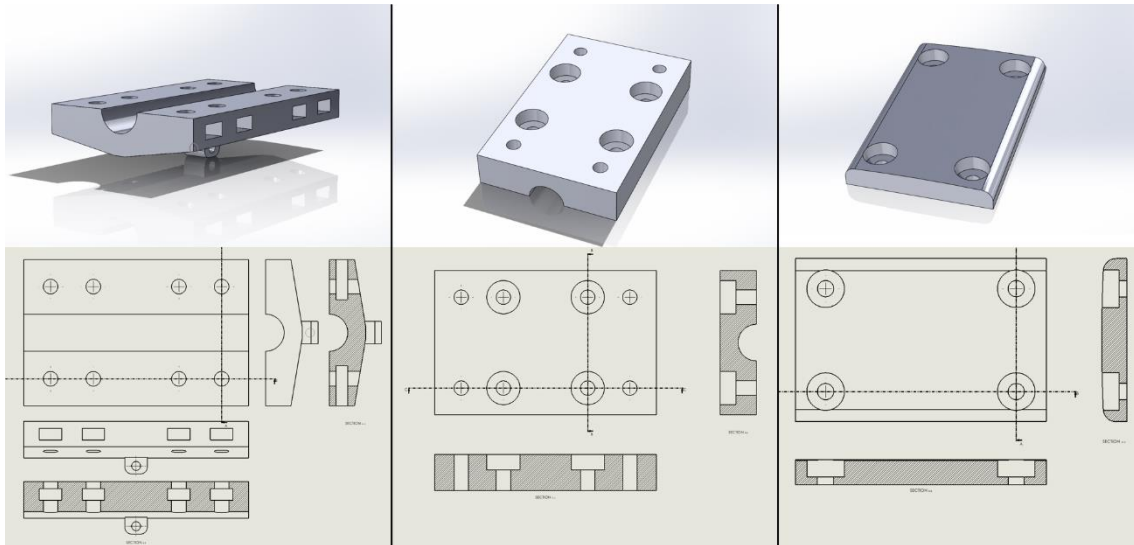

Figure 21: The individual parts of the AM tool, with the lower part to the left, the mid part in the middle, and the upper part to the right.

The new design also includes a system preventing the AM tools from rotating around the steel axles. This system is similar to the system employed in the specialization project. An extension on the bottom side of the lower part is added with a hole piercing through in the x-direction. A steel wire can then be threaded through these extensions and prevent the tools from rotating. This is depicted in Figure 22.
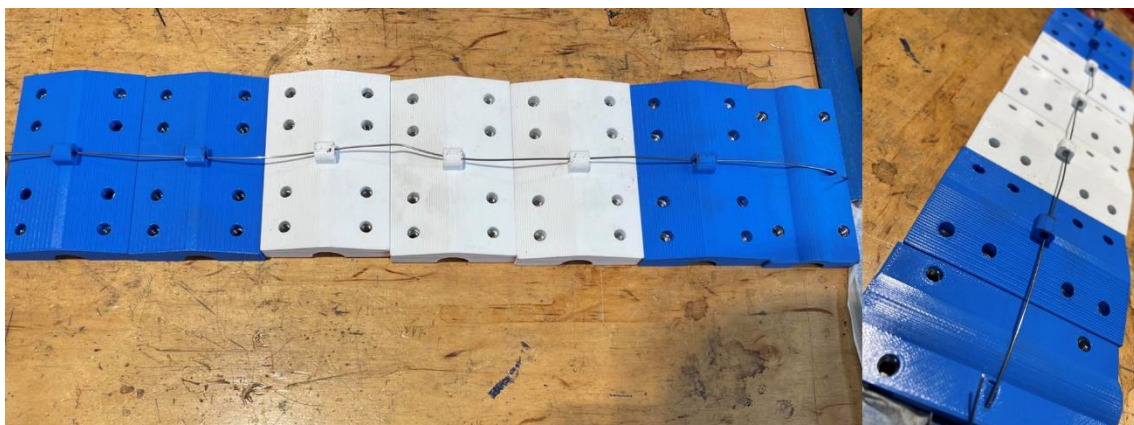

Figure 22: Depiction of the system preventing rotation on the steel axles, consisting of the extensions on the tools and the steel wire.

Because of the reduced available space underneath the outermost axle on the flexible tool, a specially tailored tool needs to be utilized, similar to the specialization project (Figure 23). Because this tool is required to be slimmer due to reduced space between the specimen and the baseplate of the flexible tool, this tool is only split into two parts. The tool is split horizontally at the center of the axle hole, which means it can easily be installed on the steel axle, while also enabling replacement of the contact surface. These two parts are fastened together with four 20 mm M6 screws. The lower part employs the same slots for inserting the M6 nuts, while the upper part employs recesses on the contact surface to accommodate the screw heads, like the other AM tools. Two upper parts are also designed with one of the two applicable curvatures. The upper part also has its edges blended for the same reason. The lower part is also fitted with a mounting point for the steel wire. As listed in the design requirements, this mounting point is placed lower than in the specialization project. Figure 24 depicts the new complete design for the outermost AM tool.
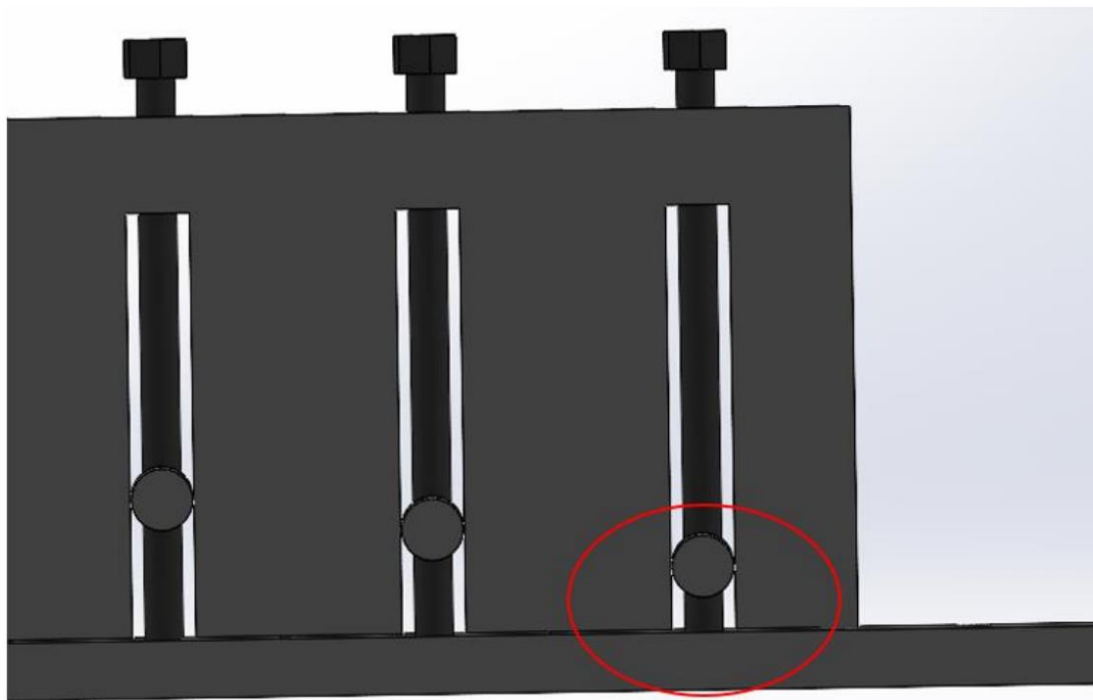

Figure 23: Visualization of the reduced space underneath the outer axles. This figure is taken from the project thesis (Lundby, 2023).
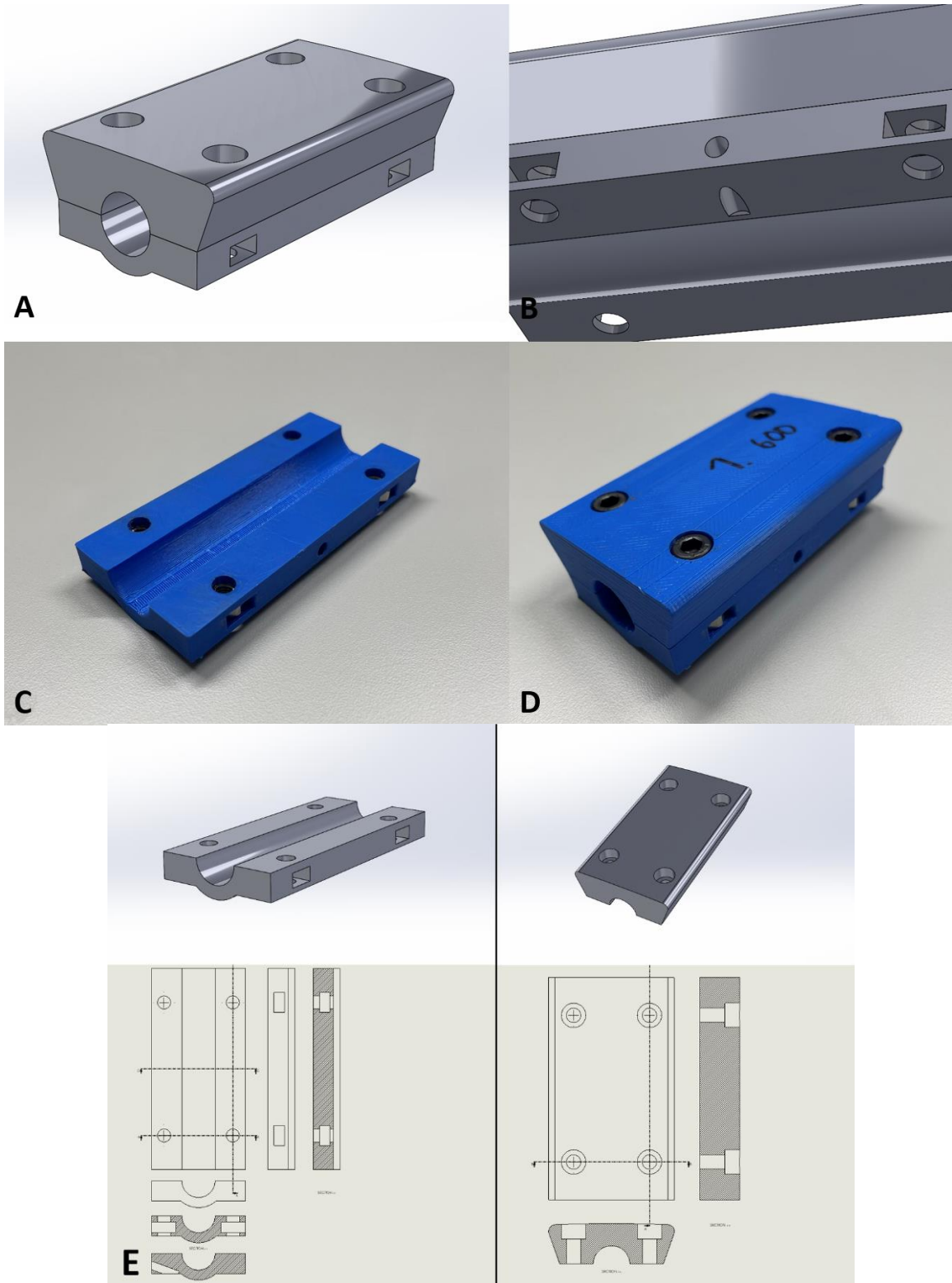
Figure 24: The complete outermost AM tool. A depicts the complete CAD model, B focuses on the steel wire mounting point, while C and D illustrates the assembly of the AM tool, part for part. E contains each individual part.

3.3 Tool manufacturing

To manufacture the CAD designs of the AM tools Prusa MK3 and Prusa MK3+ FDM printers equipped with 0.6 mm nozzles were used. These printers were all set up with PLA filament. The accompanying software used to set print parameters is the software PrusaSlicer. When printing designs with additive manufacturing, several parameters can be customized to receive a part corresponds with the set requirements, such as infill density and layer thickness. The build orientation of the part on the printing board also yields considerable effects on the part, as mentioned in both Chapter 1 and 2.

In the specialization project it was prioritized having a smooth contact surface on the AM tools. This was done instead of adhering to the principles of layer direction and bindings, as this resulted in the layer being parallel to the longitudinal direction of the specimen, exiting pressure on the interlayer bonding instead of the intralayer bonding, as mentioned in Chapter 2. Interlayer delamination may then occur. This orientation was also selected to avoid a layered contact surface suffering from "stair-stepping".

This project employs another orientation to meet the design requirements. It was devised that utilizing an orientation where the forces from the specimen was excited 90° onto the layer surfaces would increase the structural integrity and lessen the chanson of structural failure. This however, results in the beforementioned "stair-stepping" surface. It was determined that the structural enhancements of such an orientation would outshine the disadvantages of the "stair-stepping". Since some of the parts, in particular the contact surfaces, would be so thin that any other orientation could prove difficult to utilize. The orientation employed as well as the "stair-stepping" on the upper parts when manufacturing the AM tools is presented in Figure 25. The "stair-stepping" effect can also be spotted on the red upper part showcased in in picture E in Figure 20.

To neutralize these effects related to "stair-stepping" a lower layer thickness can be used. In this project a layer thickness of 0.20 mm is utilized, which is 33.3% lower than the thickness used in the specialization project. This lowered layer thickness will also help increase the mechanical properties such as tensile strength as Yao et al. concluded in their research.

As described earlier, utilizing a higher infill density can have profound impacts on the tensile strength and toughness, especially when the density supersedes 60% (Terekhina

et al., 2019). The specialization project conclusion therefore suggested using an infill density of 60%. As presented in Chapter 2, the literature review implies that higher infill densities up towards 100%, results in the highest mechanical strengths such as compressive and tensile strength, while sacrificing printing time and costs. Considering this, this project employs an infill density of 80%, as using higher densities yielded unreasonable printing times. The printing parameters is presented in Figure 25.
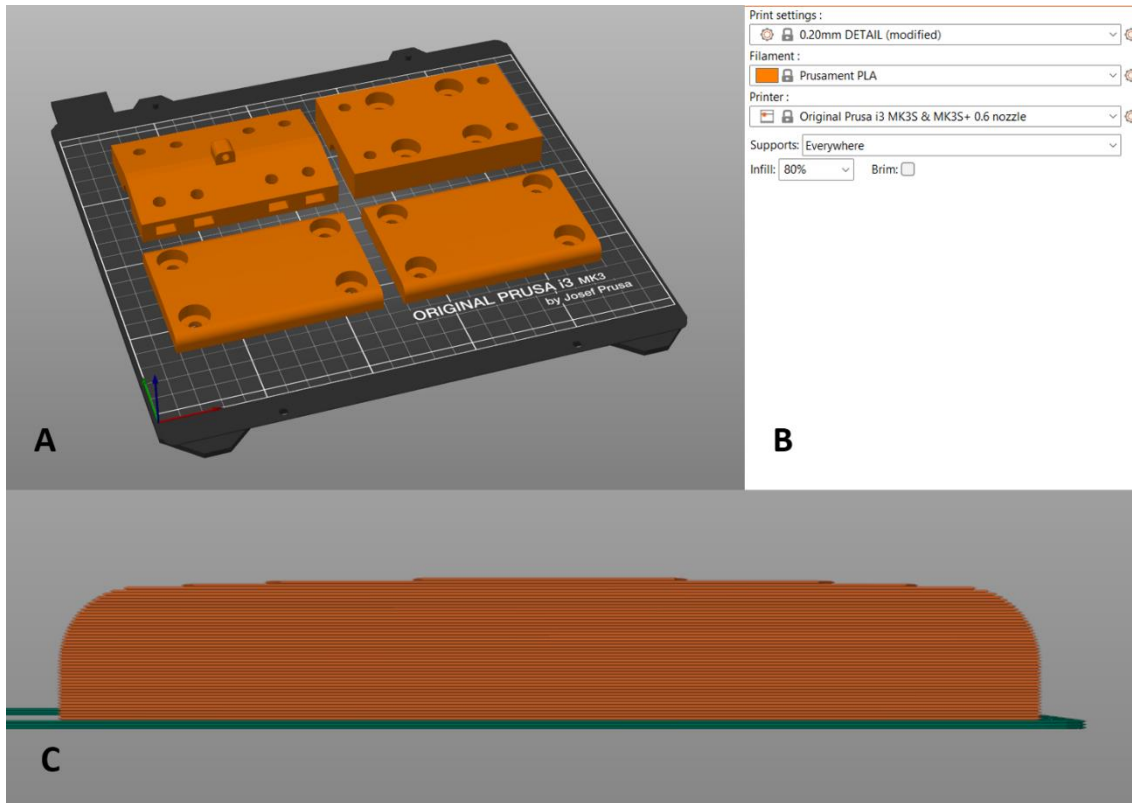

Figure 25: Picture A depicts the printing orientation employed in this master's project, along with the set printing parameters in picture B. Picture C shows the "stair-stepping" effect on the R600 upper part and the layers. These pictures are captured in PrusaSlicer.

3.4 Experiment setup

The experiment preparation consists of two operations, to set up the adjustable tool and to set up the rotary stretch bender.

3.4.1 Setting up the adjustable tool

As with the specialization project, one adjustable tool is fitted with the AM tools, while the other is set up with the bear steel axles, to facilitate easy comparison and to save time. In this project installing the AM tools onto the adjustable toll proved easier than installing the AM tools from the second iteration, thanks to the new design mitigating the need for full removal of the threaded rods which support the steel axles.

To correct bending radius is achieved by setting up the steel axles to the correct height. As with the specialization project, the variation of the angle of the contact surfaces of the AM tools, impacts the height of the point of contact between the tool and the specimen. A quick solution for this, is calculating the heights in CAD software. In the specialization project CAD sketches were made in SolidWorks, based on known parameters of adjustable tool taken from the sketch presented in Appendix A. These two sketches for the bending radii 1200 mm and 600 mm are showed in Figure 12. By altering these sketches based on the dimensions of the new AM tool design and the custom contact surface for each experiment the correct steel axle heights for this project are calculated. Figure 26 portrays the new CAD sketches for the R1200, 20° experiments and the R600, 25° experiments.
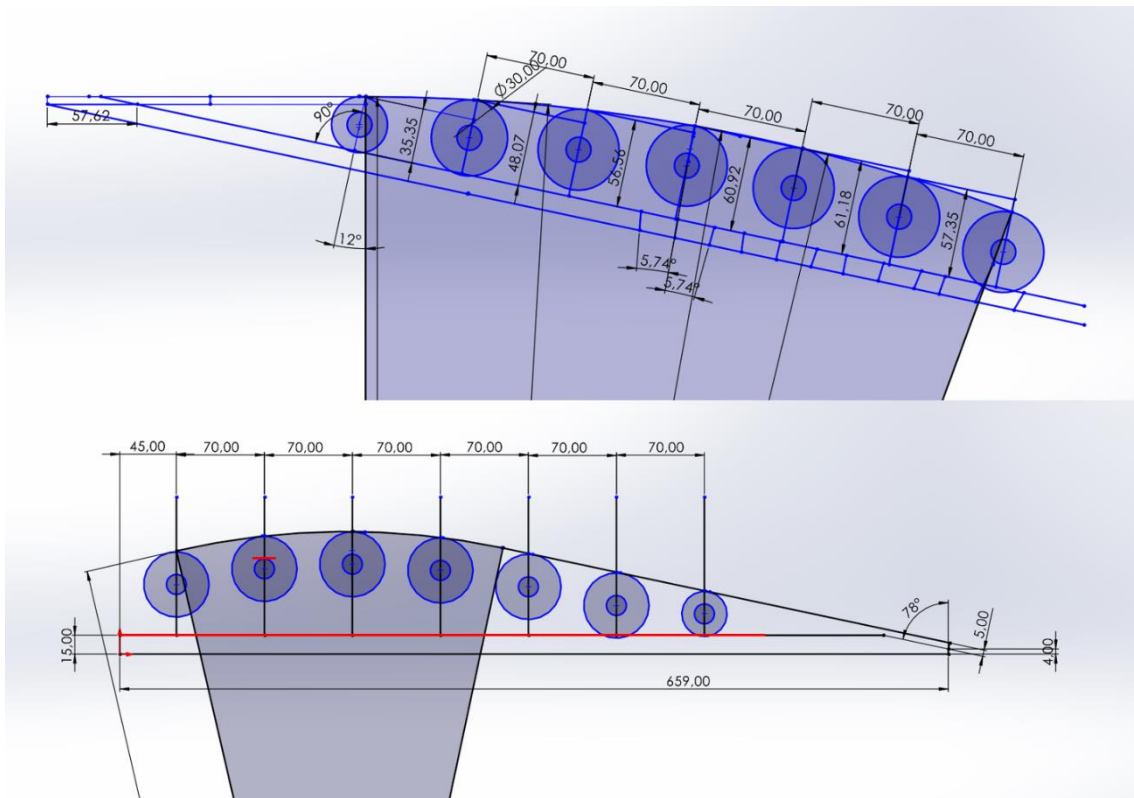

Figure 26: The CAD sketches used for measuring the correct height of each steel axle. The upper sketch portrays the R1200 setup, while the lower sketch portrays the R600 setup. The red lines indicate where the height is measured, from the baseplate (the long red line) to the highest point of the steel axles (the shorter red line).

The specialization project devised a technique to correctly adjust the steel axle heights. As described in Chapter 2, this technique utilizes two metal pieces to produce a stable surface for measuring the height using a digital caliper. One metal piece is placed across the sidewalls to create a base for the caliper, while the other is placed upon the steel axle

to create a flat surface for the caliper to be extended down to. The technique measures the distance from the steel axle up to the top of the supporting sidewall of the adjustable tool. This technique is pictured in Figure 13, as well as in Figure 27. Similar to the specialization project, this project employs an error margin of 0.1 mm to set the correct height.
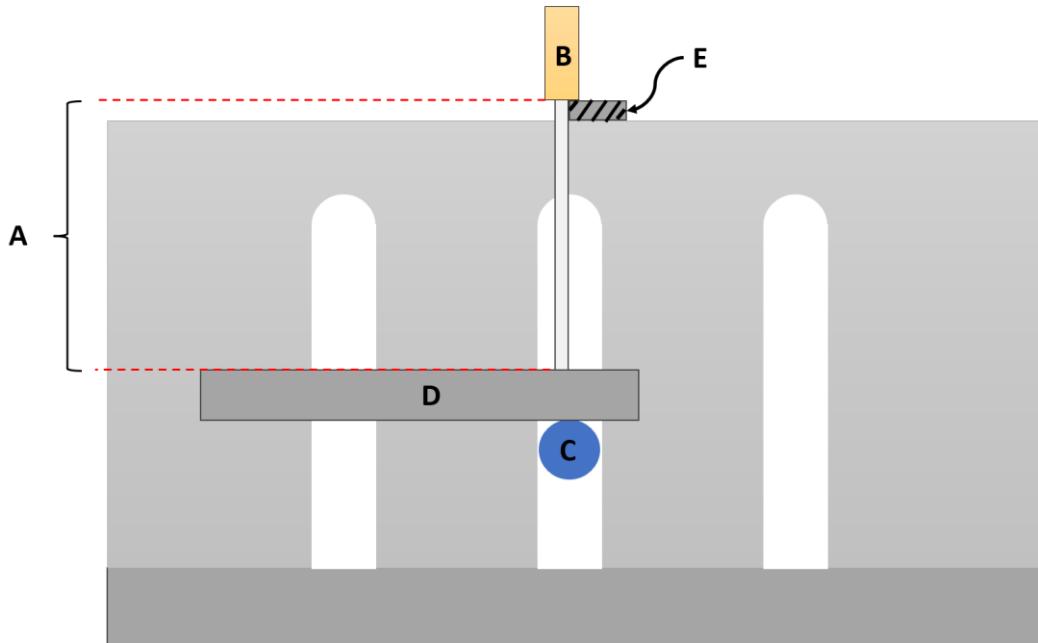

Figure 27: Representation of the measuring technique. A indicates the distance measured by the digital caliper. B depicts the digital caliper. C depicts the steel axle, while D and E represents the two metal pieces.

The correct height for the adjustable tool fitted with the AM tools is calculated by reviewing the CAD sketches depicted in Figure 26 for obtaining the height from the baseplate to the highest point of the steel axles and subtracting this height from the height of the sidewall of the adjustable tool. The same is done for the adjustable tool utilizing bear steel axles, only that the measured distance in the CAD sketches is measured from the baseplate to the contact point between the AM tool and the specimen. The thickness of the metal piece placed across the sidewalls and the width of the metal piece placed on the steel axle needs to be considered to get the correct measurement for the digital caliper. As the new AM tools was widened to diminish the free space between the tool and the sidewalls, a slimmer metal piece needs to be placed on the steel axle. Table 3 depicts the calculated distances for each of the experiment types and tool types. Figure 28 pictures the adjustable tool fitted with the AM tools set up with the correct height.

Table 3: Measurements for the adjustable tools

Experiment	Tool type	Axle number and corresponding measuring distance [mm]						
		End	**2**	**3**	**4**	**5**	**6**	**Mid**
R600, 25°	AM tool	99.54	92.84	77.97	64.89	59.99	63.46	75.86
	Axles	89.14	74.26	59.38	46.67	41.99	45.49	57.35
R1200, 20°	AM tool	99.55	93.1	85,98	81.56	81.33	85.09	93.26
	Axles	89.14	76.42	67.93	63.57	63.31	66.94	74.99

Figure 28: A configured adjustable tool fitted with the new AM tools.

3.4.2 Setting up the rotary stretch bender

Setting up the rotary stretch bender follows the same procedure utilized when setting it up in the specialization project. This procedure was not covered in specialization project summary in Chapter 2, with the reason it being thoroughly described here.

As the experiments in this master's project only encompasses two-dimensional stretch bending, exclusively the machine's pitch and position of the machine's arms in the x-direction requires adjustment. Figure 29 presents an overview of the machine, its servos controlling the bending process and which axis the servos control.
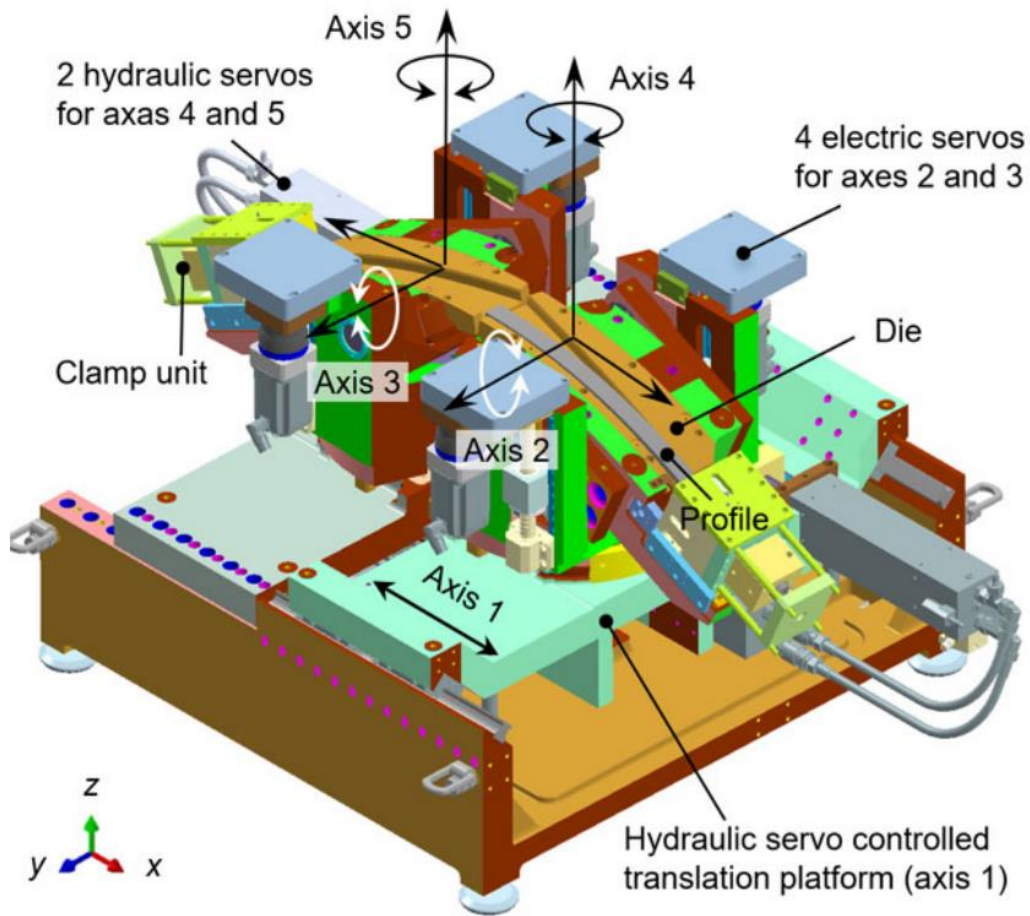
Figure 29: An overview of the rotary stretch bender and its servos and corresponding axis (Ma et al., 2022).

To adjust the described parameters coordinates are adjusted utilizing a user interface for the machine. This user interface, henceforth called the control panel, is depicted in Figure 30. The pitch is adjusted by typing in the coordinates for the servos in charge of pitch control. These coordinates are obtained by reviewing a table containing rotation angles and corresponding coordinates. This table is appended in Appendix B. To adjust the machine arms' position in the x-direction, coordinates must be typed into the control panel, similar to the pitch coordinates. When the specimen is placed in the machine, the gap between the specimen and the tap in front of the clamp, as depicted in Figure 31, is required to be approximately 5 mm. The coordinates must be adjusted incrementally, until this is achieved.
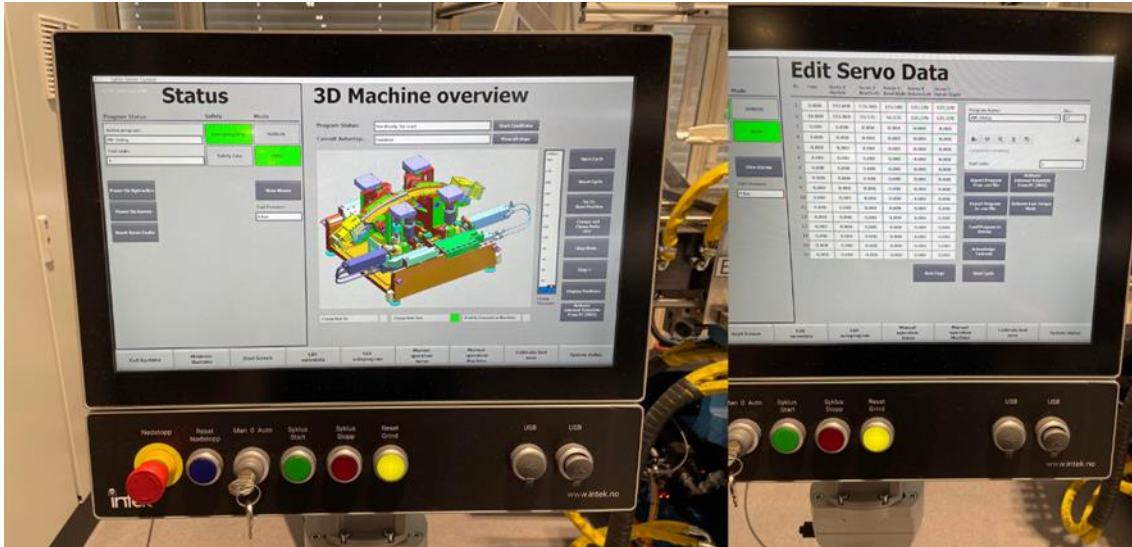
Figure 30: The control panel controlling the rotary stretch bender.

In addition to adjusting machine parameters, the specimen must be placed correctly in the machine. This is done by positioning the specimen in relation to the y-direction. Using the metal square in the middle of the clamp as a reference, the specimen center must be aligned with the center of the metal square. This is done manually. This technique is portrayed in Figure 31. When this is achieved, following the previously mentioned adjustments, all requirements are met for the experiments to commence. The machine in a ready state can be viewed in Figure 32, along with the machine in a finished state after performing the bending process. The bending processes are run and controlled using the described control panel. Process data containing information on forces excited on the servos is also logged, which can be reviewed after the bending process.
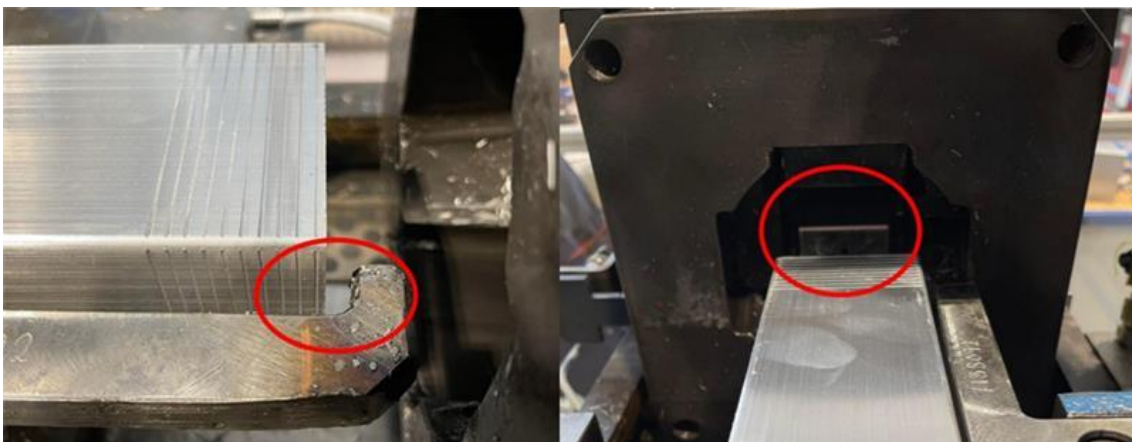

Figure 31: Alignment of the specimen into the machine. The left picture portrays the specimen in relation to the tap of the clamp and the gap used for adjustment. The right picture depicts the specimen in relation to the metal square used to align the specimen. These pictures were taken from the project thesis (Lundby, 2023).
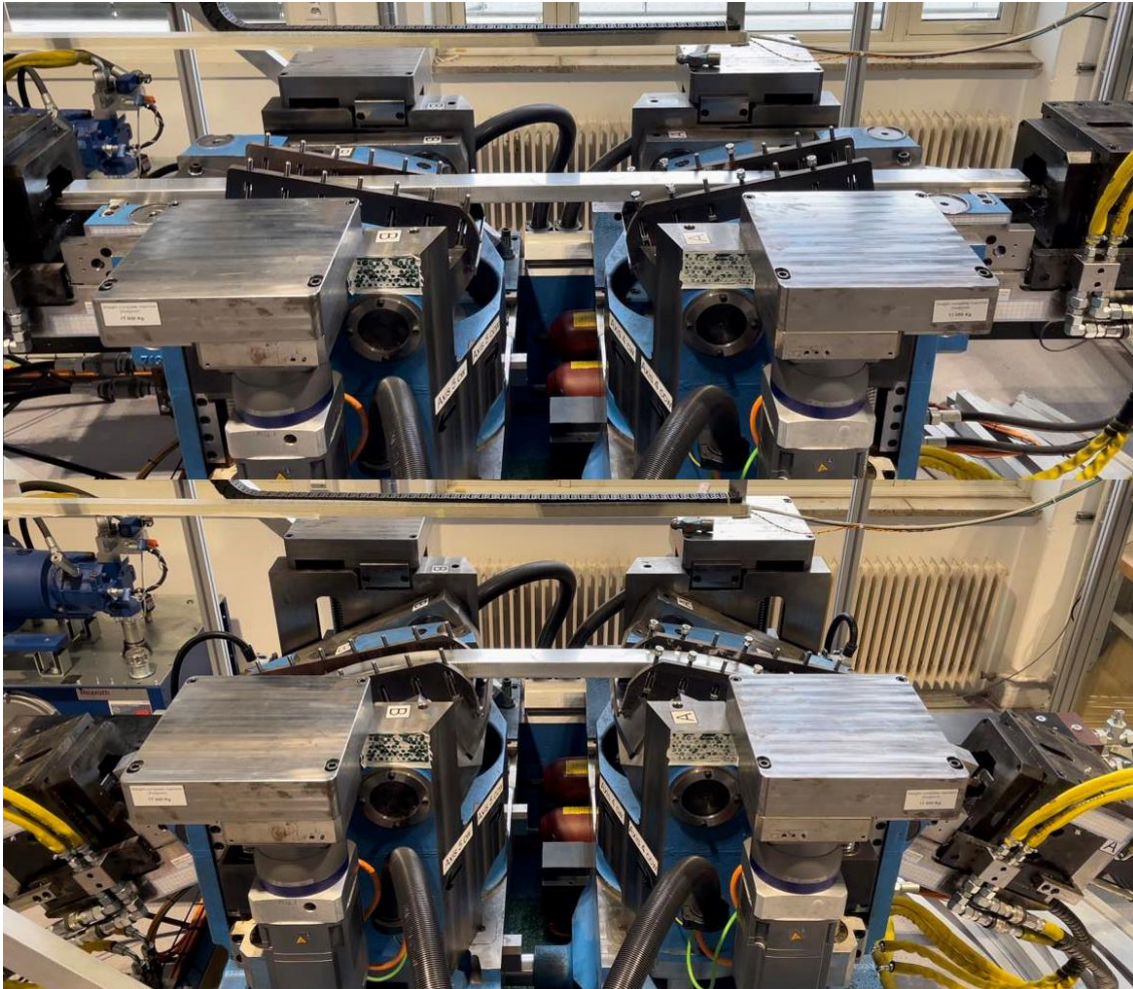
Figure 32: The stretch bending machine with the specimen. The top picture depicts the machine ready for commencing the bending process, while the bottom picture depicts the machine after having bent the specimen. The left adjustable tool is fitted with the AM tool.

3.5 Result verification and measurement

To verify the results the specimens' rotation angle is measured, similar to the specialization project, in addition to the bending radius. As the angles in specialization project were measured by employing a crude technique bearing a significant risk for measurement error, a different technique is utilized in this master's project. This time a highly advanced measuring machine is employed. The machine in question is a Leitz PMM-C 600 coordinate measuring machine. This machine has a maximum permissible error calculated with the following equation:

$$MPE_E = 0.6 + \frac{L}{600}$$

This is measured in micrometers where L represents the length of the measured specimen, which indicates a significant amount of accuracy (Sørby, 2022). The machine is pictured in Figure 33. To be able to fit the specimens into the machine, the specimens are required to be cut in half. This is done by using a bandsaw.
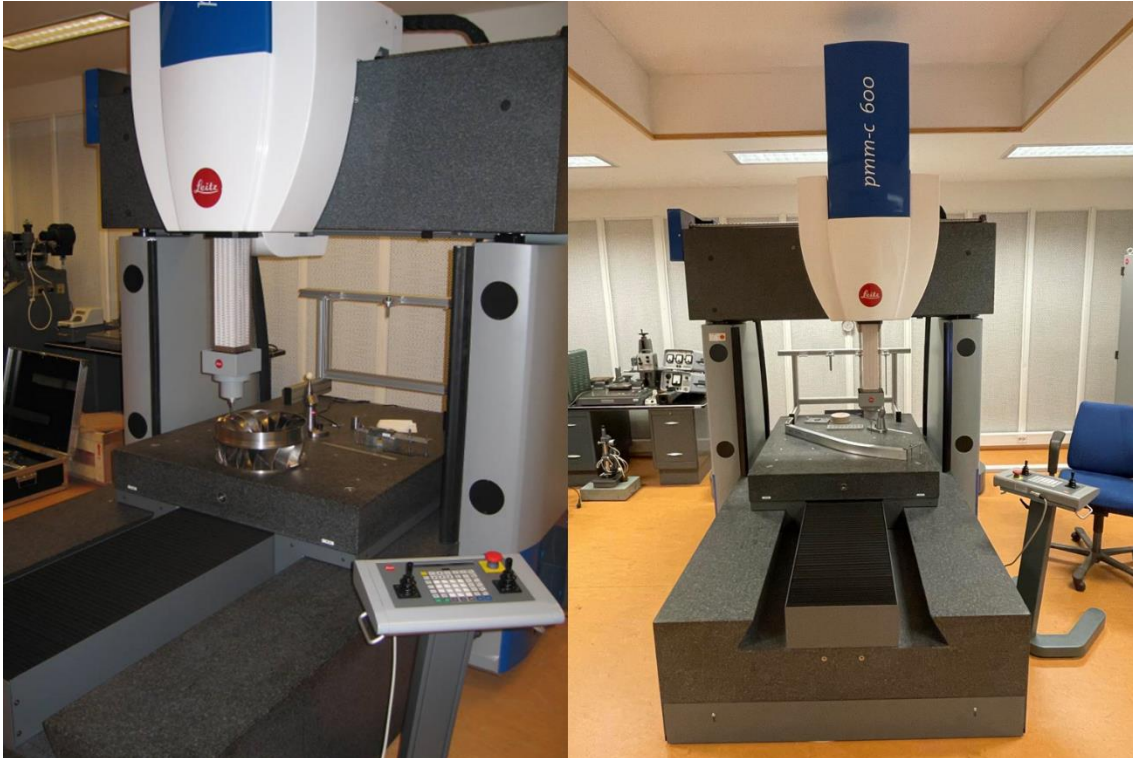
Figure 33: The coordinate measuring machine. The picture to the right depicts the machine with a specimen (Sørby, 2022).

The machine measures points, or coordinates, on the specimen placed in the machine and can utilize these coordinates in several ways. These coordinates can for example be applied to accurately measure the curvature of the line through the coordinates. The machine can also calculate an angle between two mapped lines with significant accuracy. By mapping coordinates in the curvature of the specimen and the straight parts preceding and succeeding the curvature, the rotation angle and the bending radius can be measured. To standardize the measuring spots on each specimen, the same spots are marked on the same place on each specimen. These marks help the operator of the machine to accurately measure each specimen uniformly. These spots are marked with a red marker, as depicted in Figure 34.
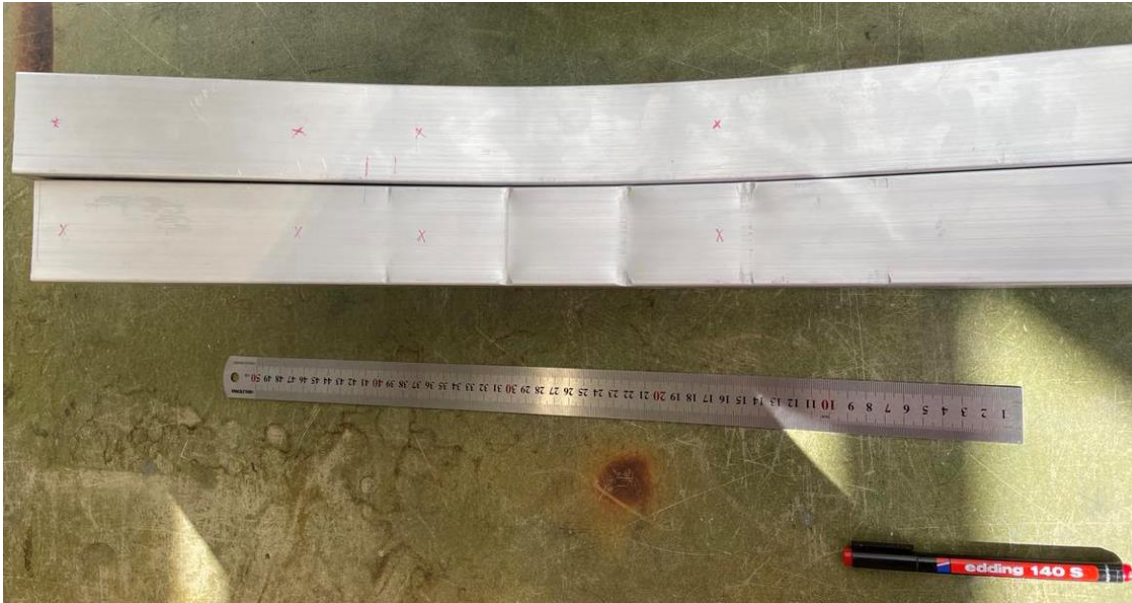
Figure 34: Marking the measuring coordinates on the specimens.

After placing the specimen in the machine, the operator manually maps the red markings as presented in Figure 35. When all coordinates are mapped, the software PC-DMIS is employed to calculate the bending radius and the rotation angle based on the mapped coordinates on the specimens.

Figure 35: Measuring the specimen along the marked coordinates. The left picture showcases the mapping of the curvature, while the right highlights the mapping of the straight parts.

4. Experimental Results

The experimental results are divided into four different categories, which are going to be discussed in this chapter. These four categories are qualitative assessment of the surface finish of the specimens, qualitative assessment of the surface finish and structural integrity of the AM tools, logging data obtained from the bending process, and lastly the angle and bending radius measurements of the specimens bent utilizing the AM tools. These four aspects will help clarify the outcome of employing these AM tools in a 3D rotary stretch bending process.
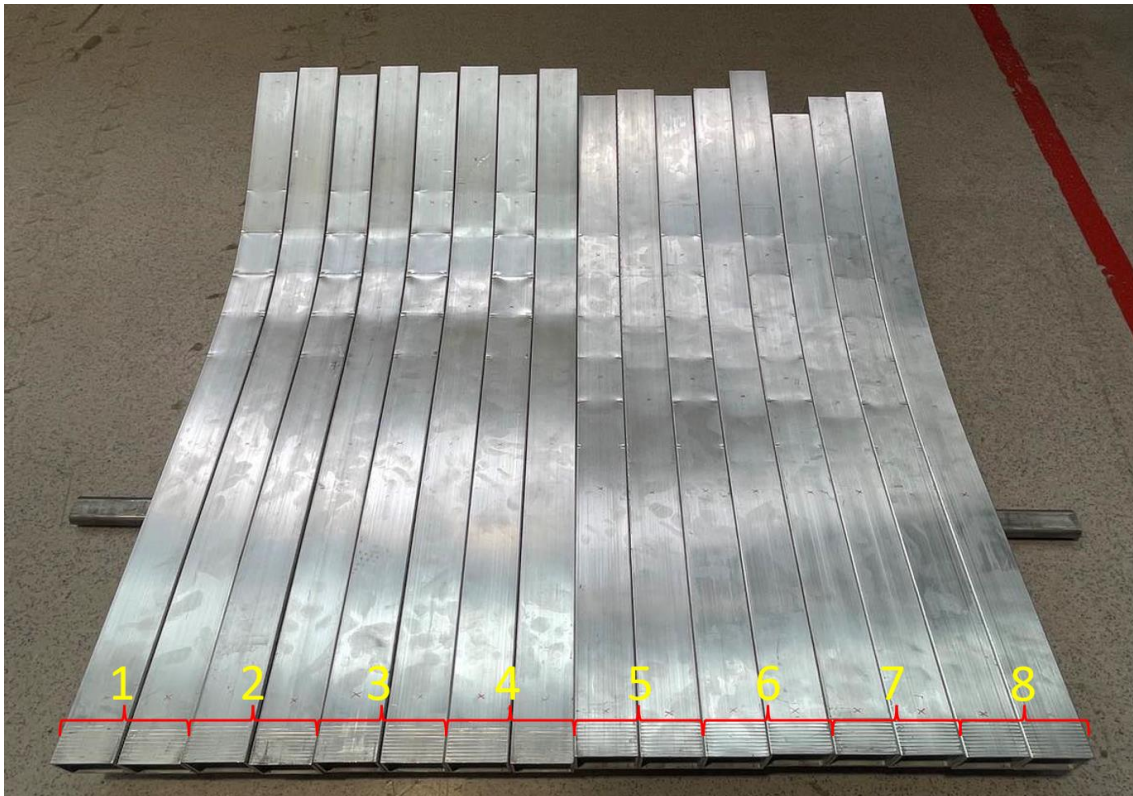
Figure 36: All specimens bent in the project, arranged in the order they were bent. Specimen 1 through 4 is bent using a 600 mm bending radius, and 5 through 8 are bent using the 1200 mm radius. Each specimen consists of one half subjected to the AM tools and one half subjected to the steel axles, as depicted here.

4.1 Qualitative assessment of the specimens' surface finish

As expected, the AM tools exhibits clear improvements on the surface finish of the specimen compared to the steel axles, as pictured in Figure 36. Considering the results from the specialization project, this is expected. As the function of the exchangeable contact surfaces of the AM tools is to utilize a surface curvature identical to the bending

radius to further reduce the indentations on the specimen, comparing the results from the specialization project to these results is relevant. When reviewing Figure 37, it is evident that the indentations caused by the new AM tool designs are less detectable than the indentations caused by the second iteration of the AM tool, especially for the R600 specimens. However, this is valid for both bending radii, yet to a slightly lesser degree for the R1200 specimens. The indentations caused by the new designs are still visible, still there is a clear improvement.
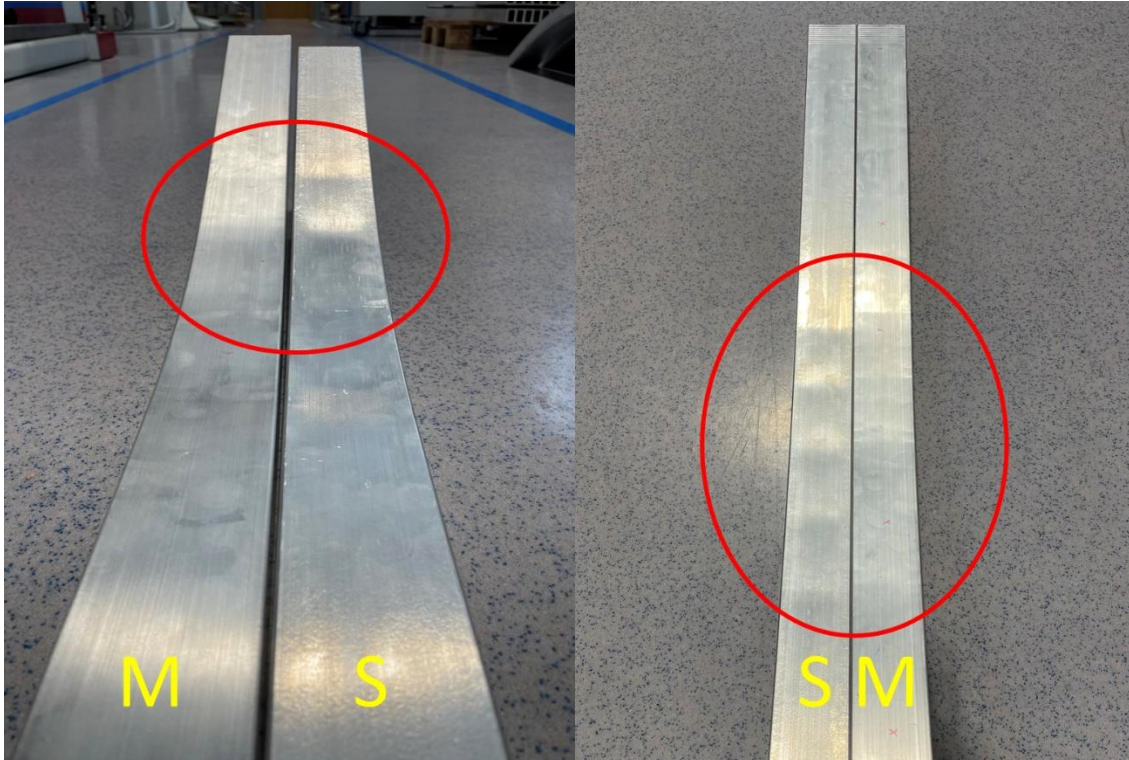
Figure 37: Comparison of the surface finish of the specimens from the specialization project and the master's project. M denotes specimens from the master's project, while S denotes specimens from the specialization project. The specimens to the left are bent using a bending radius of 600 mm, while those on the right are subjected to a bending radius of 1200 mm.

As mentioned earlier in Chapter 3, the disadvantage of the chosen build orientation when printing the tools is the presence of "stair-stepping" caused by the layers. As the specimens are bent over this stepping, it may be a chance that this stepping can impact the surface finish of the bent specimens. When evaluating Figure 38, marks caused by the stepping can be clearly observed. When comparing the stepping marks' positions, relative to the locations of the steel axle indentations, it is evident that this is caused by the stepping. Since the layer thickness used in the AM tools is 0.20 mm, it is remarkable that the stepping is as visible as it is here. Apart from the defects described, no other defects of significance were inflicted on the specimens' surface by the bending process.

Figure 38: Depiction of the marks inflicted on the surface of the specimens due to the "stair-stepping" effect.

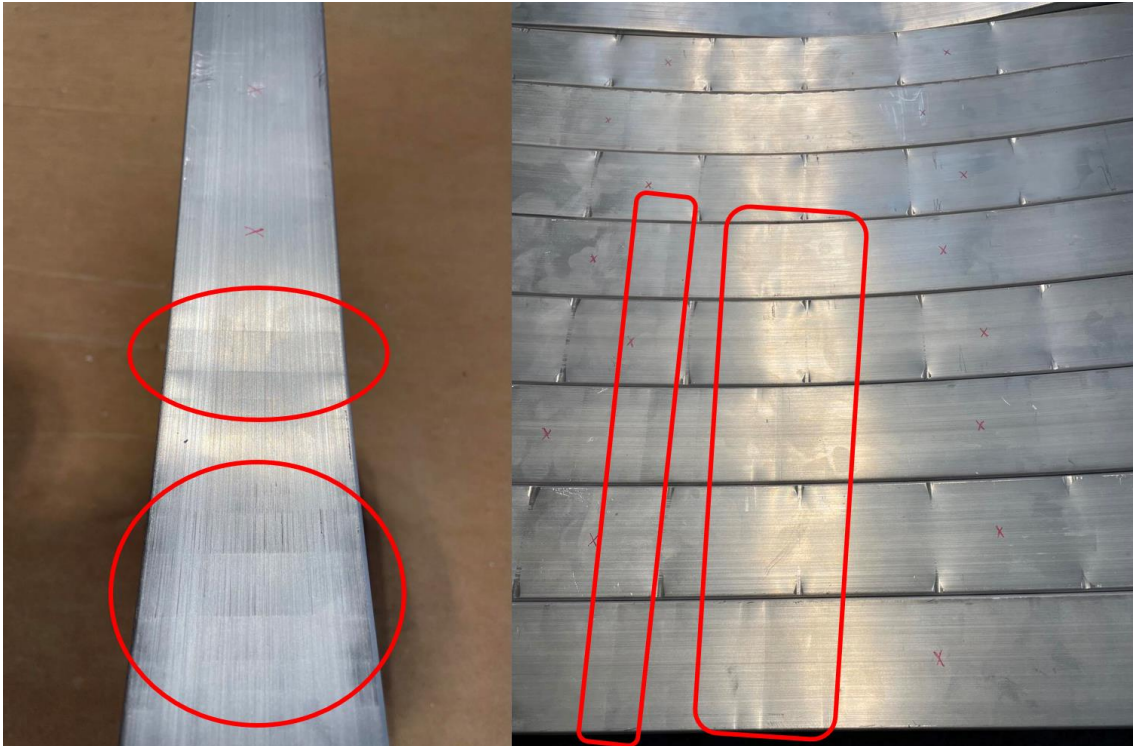## 4.2 Qualitative assessment of the AM tools

The results from after conducting indicates that the AM tools withstood the inflicted forces from the bending process with great success. This is valid for the AM tools applied during both the R600 and R1200 experiments. It seems that the only effect the experiments had on the contact surface of the AM tools was minor scuffing marks where the specimens were placed. These scuffing marks are undetectable when assessing the surfaces with a finger, both on the R600 and the R1200 tools. There are hints of aluminum deposits along the edges of the specimens on several contact surfaces that are detectible by touch. The upper parts of the AM tools, along with the iteration 2 tools, are displayed in Figure 39, depicting the mentioned scuffing marks. The aluminum deposits are visible as small bright particles along the location where the specimen's lower edges scuffed against the AM tools. This applies predominantly for the R1200 AM tools, possibly caused by one rough and scuffed up edge of one of the specimens. As visible in Figure 39, the tool might have been slightly set up with a height difference between each side of the AM tools, as scuffing marks along one edge is more visible than along the other edge. This is evident on AM tool number 2 and 3 of the R600 tools.

Figure 39: The AM tools after the completion of the bending experiments. The tools on the top are the upper parts with a R600 curvature, the tools in the middle are the upper parts with a R1200 curvature, while the tool on the bootom are the tools from the second iteration of the AM tools.

When reviewing the mid and lower parts of the AM tools, no damage of any kind is detectable, save from some dirty spots here and there. This denotes that the structural integrity is completely uncompromised for these parts.

In the specialization project it was evident that tools 4, 5, and 6 was inflicted by the most severe forces, and therefore suffered the worst structural damage. This is also evident after this project's experiments. When reviewing Figure 39, this can be observed. Figure 40 provides a closer look of these three tools, comparing the R600, R1200 and iteration 2 tools. The iteration 2 tools have clear indentations, while the new tools only have dirty scuffing marks.

Figure 40: Upper part of the AM tool number 4, 5, and 6 of the new R600 AM tools (top), the new R1200 AM tools (middle), and tool number 4, 5, and 6 of the tools from iteration 2.

4.3 Logging data from the experiment

As mentioned in Chapter 3, data from the stretch bender's servos was logged. In order to verify that the structural integrity of the AM tools was sustained during the bending processes. By, for example, reviewing the pressure induced on the servo controlling the translational movement along axis 1, it can be ascertained if damage on the contact surface on the tools occurs. If the structural integrity is sustained throughout the experiment, the pressure should continuously increase along with the stretching and

bending of the specimen, with no sudden pressure drops. If a pressure drop occurs, it can mean that the surface of the AM tools succumbs to the pressure induced by the bending process. Figure 41 presents plots depicting the pressure increase on servo 1 during the experiments. These plots are generated by applying the logging data from the experiments in a script that outputs plots based on data from the desired servos. Servo 1 is the servo controlling axis 1 which is the translational stretching movement. The script was provided by the supervisor of this thesis, modified to output plots with clear legends of the accumulated servo 1 pressures for all eight experiments. The script along with the plots can be viewed in Appendix C.
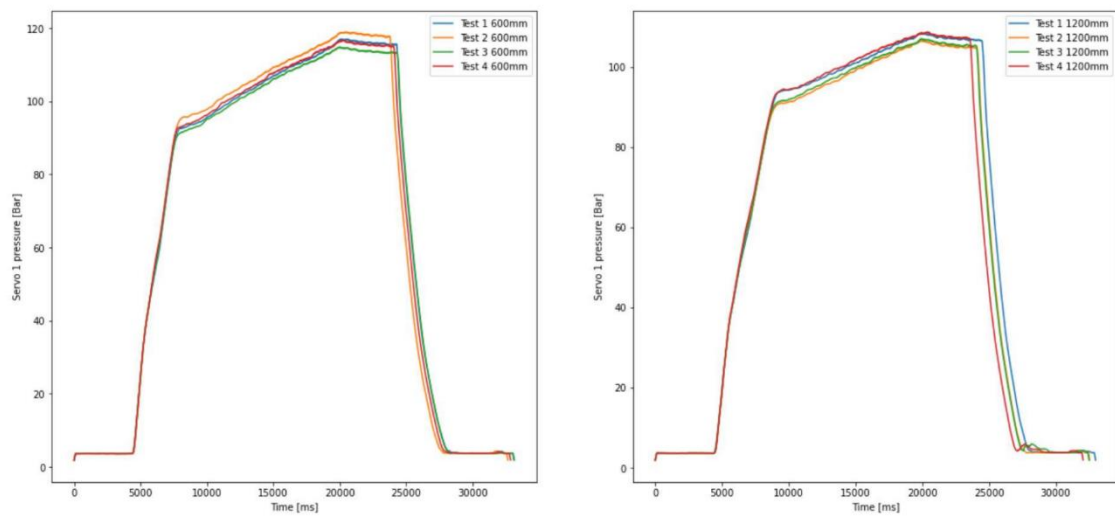
Figure 41: Plots of the servo 1 pressures per unit of time. Pressure is measured in bar while time is measured in microseconds. The plot to the left depicts the pressures accumulated in the R600 experiments, while the plot to the right depicts the pressures accumulated during the R1200 experiments.

Figure 41 shows that the pressures increase continuously without no sudden drops in pressure until the bending pressure dissipates due to the bending being finished. This is valid for both bending radii. The first steep surge in pressure is the initial stretching of the specimen before it is bent, while the slower increase in pressure is the bending process. It is evident that the variation in pressure accumulation between each experiment is very low and with no evident pattern. This is valid for both bending radii. The small variations may be due to material differences in each specimen. This also indicates that the structural integrity of the AM tools is maintained. The plots also indicates that the pressures are higher in the R600 experiments.

4.4 Measurements and dimensional accuracy

The measurements of the rotation angles and curvature radii for each specimen conducted in the coordinate measuring machine is provided in Table 4 and Table 5 respectively.

In terms of the rotation angle, it is evident that each specimen's rotation angle is just short off the nominal rotation angle. In the R600 experiments the rotation angle deviates from the nominal rotation angle with approximately 0.71-0.82° on the AM tooling side, while the steel axle side deviates with approximately 1.33-1.38°. The R1200 experiments' AM side deviates from the nominal rotation angle with approximately 0.66-0.8°. while the steel axle side deviates with approximately 1.33-1.35°.

Table 4: Rotation angle measurements

Bending radius	Tooling	Test no.	Nominal rotation angle	Measured rotation angle	Deviation
600 mm	AM tooling	1	25°	24.234°	-0.766°
		2	25°	24.290°	-0.710°
		3	25°	24.208°	-0.792°
		4	25°	24.181°	-0.819°
	Axles	1	25°	23.621°	-1.379°
		2	25°	23.668°	-1.332°
		3	25°	23.663°	-1.337°
		4	25°	23.643°	-1.357°
1200 mm	AM tooling	1	20°	19.317°	-0.683°
		2	20°	19.199°	-0.801°
		3	20°	19.315°	-0.685°
		4	20°	19.332°	-0.668°
	Axles	1	20°	18.651°	-1.349°
		2	20°	18.670°	-1.330°
		3	20°	18.664°	-1.336°
		4	20°	18.668°	-1.332°

When reviewing the curvature radius measurements, a trend where the measured curvature on the specimen is lower than the nominal curvature is dominant, with an exception. In the R600 experiments the AM tooling side is approximately 5 mm lower than the nominal curvature besides one specimen where the deviation is only approximately -1 mm. For the steel axle side, the approximate deviation is -21 to -23 mm, besides the one and same experiment where the measured curvature radius is deviating from the nominal deviation with around -14 mm. The R1200 experiments follows the

same trend to a degree. The AM tool side is measured lower than the nominal curvature radius with approximately -12 to 40 mm. The steel axle side of the R1200 experiments however, has the only occurrences where the measured curvature radii are larger than the nominal curvature radii. Here the measured data deviates with positive values. The deviations are in this instance between 88 and 96 mm.

Table 5: Curvature measurements

Bending radius	Tooling	Test no.	Nominal curvature radius	Measured curvature radius	Deviation	Circularity ⭘ 0.5
600 mm	AM tooling	1	600 mm	594.950 mm	-5.050 mm	0.276
		2	600 mm	599.028 mm	-0.972 mm	0.272
		3	600 mm	594.692 mm	-5.308 mm	0.278
		4	600 mm	595.296 mm	-4.704 mm	0.284
	Axles	1	600 mm	578.945 mm	-21.055 mm	0.700
		2	600 mm	586.173 mm	-13.827 mm	0.619
		3	600 mm	577.030 mm	-22.970 mm	0.698
		4	600 mm	578.671 mm	-21.329 mm	0.703
1200 mm	AM tooling	1	1200 mm	1166.522 mm	-33.478 mm	0.319
		2	1200 mm	1187.657 mm	-12.343 mm	0.400
		3	1200 mm	1160.810 mm	-39.190 mm	0.336
		4	1200 mm	1170.422 mm	-29.578 mm	0.329
	Axles	1	1200 mm	1295.305 mm	95.305 mm	0.166
		2	1200 mm	1288.264 mm	88.264 mm	0.173
		3	1200 mm	1289.112 mm	89.112 mm	0.178
		4	1200 mm	1290.100 mm	90.100 mm	0.153

Table 5 also contains a column with a measurement of circularity, which indicates how round the curvature is. As observed, the tolerance for the circularity is 0.5 mm. That means the difference between the highest measured diameter and the lowest measured diameter in the same curvature cannot exceed 0.5 mm. The data shows that all the measured circularities are within the set tolerance except the specimens subjected to the steel axles in the R600 experiments, where every specimen is just outside of the tolerance with approximately 0.1 to 0.2 mm. This data is also presented in Figure 42. The outer blue curve of each curvature indicates the boundaries for the maximum diameter tolerated, the inner blue curve indicates the minimum diameter tolerated, while the blue curve in the middle indicates the average diameter measured. Figure 42 explicitly illustrates that the steel axle side of the R600 experiments do not meet the set tolerances.

The fluctuations of the curvatures are caused by the contact areas between the specimen and the AM tools and steel axles.

The complete sets of data obtained from the measurements of each specimen can be viewed in Appendix D.
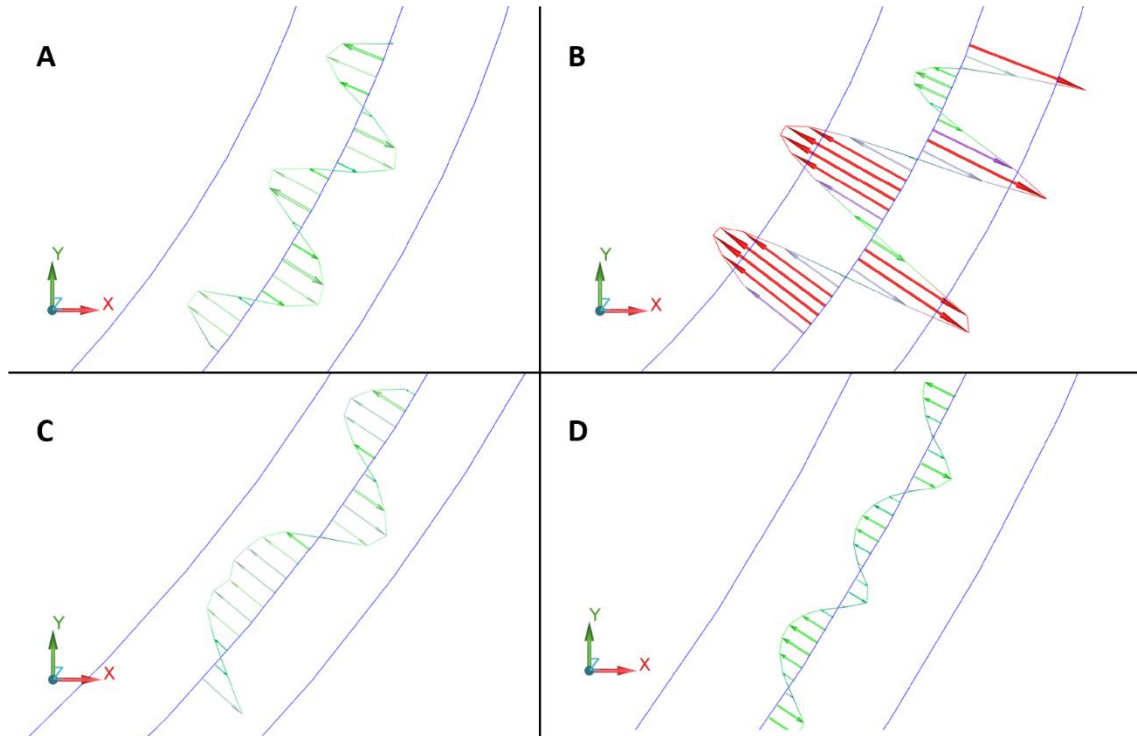

Figure 42: The circularity of the specimens within the permitted tolerances. A depicts the circurlarity of the R600 AM tool specimens, B the R600 steel axle specimens, C the R1200 AM tool specimens, and D the R1200 steel axle specimens.

5. Discussion

This chapter will discuss the experimental results and findings and try to link them up to the project's theory, observations and experiences made during the course of this master's project. The methodology will also be evaluated and addressed in order to obtain a fundamental understanding of what improvements can be applied in further research. This chapter will contain two sections devoted to the results addressing the surface finish of the specimens and the structural integrity and surface finish of the AM tools, as all results obtained from the experiments addresses these two aspects.

5.1 Specimen surface and dimensional accuracy

5.1.1 Specimen surface

As presented in Chapter 4, the surface finish of the specimens bent in this project exhibits less detectable indentations caused by the AM tools, compared to the previous iterations of the AM tools. Figure 37 depicts this. It is also mentioned in Chapter 4 that the improvement is present for both bending radii, however to a slightly lesser degree. This can be related to the higher force inflicted on the tools and the higher strain rate occurring when smaller bending radius is applied (Figure 6). This indicates that the design requirement involving further improvement of the indentations to further even out the specimens' curvature is addressed by this new AM tool design.

5.1.2 Dimensional accuracy and rotation angle

The dimensional accuracy of the rotation angle of each specimen follows a trend where the measured angle is lower than the nominal angle. This is in accordance with the results from the specialization project, where the measured angles also were just short of the nominal angle. The observed deviations for the AM tool sides for both bending radii are nearly similar, as are the deviations for both bending radii on the steel axle side. The cause for these deviations may be tied to inaccuracies inherent to the machine itself and the bending process and differences in the aluminum profiles utilized as the aluminum profiles can come from different manufacturers with extrusion dissimilarities. Two other aspects may be more relevant to discuss, namely the measuring technique and the specimens' springback, as they may more easily measured.

5.1.2.1 Errors tied to the measuring technique for the steel axle heights

A factor contributing to the shorter measured rotation angles, may be the crude and clumsy technique for setting up the adjustable tools with the correct steel axles height and curvature. Small variations in the positions and angles of the metal pieces used for creating flat surfaces for the digital caliper can result in incorrect steel axles heights by parts of a millimeter. It is heavily based on visual estimates and require steady and firm hands. As mentioned in the specialization project, a novel way of measuring the heights of the steel axles may be beneficial and was unfortunately not prioritized in the research's continuation into the master's project.

5.1.2.2 Errors tied to springback

Apart from the errors tied to measuring the steel axle heights, springback can be a factor contributing to the smaller rotation angles. As mentioned in Chapter 2, springback cannot be entirely eliminated, even by inducing strain during the bending process. Based on this, it is logical that springback is a considerable factor for the rotation angle deviation. When reviewing the rotation angle deviations, it is observed that the difference from the nominal angle is not significant. The AM tooling sides for both bending radii, shows the virtually the same deviation of 0.66 to 0.8°. The deviations on the steel axles sides are also nearly identical for both bending radii. This indicates that the error tied to the measuring technique for the steel axle heights may not be severe, implying that springback is the main factor. The difference in the deviations between the AM tooling sides and steel axle sides, can be due to the AM tools. The AM tools offer a more continues and uniform surface for the specimen to be formed by, compared to the steel axles. The bending process propagates almost continuously along the specimen on the side fitted with AM tooling, apart from over the gaps caused by the transition between each AM tool. On the steel axle side, the bending process propagates incrementally along the specimen from one axle to the next, causing the total bending to be distributed over a small number of contact points instead of continuous surfaces. This may influence the springback due to the larger deformations. With the springback in mind, the rotation angle deviations are reasonably accurate.

5.1.3 Dimensional accuracy and curvature radius

The measured curvature radius of the specimens depicts a trend where the measured radius is lower than the nominal radius, with one exception. As mentioned in Chapter 4,

this exception is the specimens subjected to the steel axles during the R1200 experiments. The measured curvature radii deviate in these instances by being larger than the nominal curvature radii. A trend can be observed where the deviations on the steel axle side are larger than the deviations present on the AM tooling side. The deviations also depend on the employed bending radii, as the deviations are larger for the R1200 experiments. This is logical, as a longer radius may amplify the implications of small errors. These deviations may be tied to the setup of the adjustable tools and the steel axle heights, as they are directly responsible for the applied bending radius. This may also explain why the measured curvature radii on the steel axle side during the R1200 experiments are higher. A novel and dependable way of setting up the adjustable tool with correct steel axle heights may mitigate these deviations. The cause of deviations may also be inherent in the CAD sketches produced to calculate the steel axle heights. Due to the exact values and parameters applied when making these sketches, it is illogical. Due to the nature of how the curvature radius is measured, the error may also lie with the marking of the coordinates measured with the coordinate measuring machine. The number of marks applied to the curvature of the specimens, were in some degree arbitrarily chosen on gut feeling. An increase in distributed marks along the curvature may contribute to improving the accuracy of the curvature radius measurements and yield results closer to the nominal values. The roundness of the curvatures is also observed to be rather accurate, apart from the steel axle side in the R600 experiments where the curvatures deviate from a perfect circle with almost twice the value of the other specimens. This may be tied to the setup of the adjustable tool as well, as the other curvatures are well inside the set tolerance.

5.1.4 The build orientation's impact on the specimen surface

The new build orientation of the AM tools has influenced the surface finish, as mentioned in Chapter 4. It is quite remarkable that the "stair-stepping" on the contact surface of the AM tools has inflicted such clear markings on the surface finish of the specimens. The markings are not severe and can be prevented by utilizing post-processing techniques on the contact surface of the AM tool, as presented in Chapter 2. The advantages of the chosen build direction outshine the disadvantages related to the specimens' surface finish.

5.2 The bending process' influence on the AM tooling

As described in Chapter 4, none of the AM tools experienced any significant structural damage in any of the experiments conducted. The only detectable marks on the contact surfaces were scuffing marks and deposits coming from the specimen. This is a significant improvement compared to the previous iterations in the specialization project, where some of the AM tools suffered structural damage during the R600 experiments.

5.2.1 Printing parameters impact on the mechanical properties

It is evident that the new values chosen for layer thickness, infill density, and the new build orientation have had positive impacts on the structural integrity of the AM tools. To summarize, the layer thickness was lowered from 0.30 to 0.20 mm and the infill density was increased from 30 to 80%. As the studies researched in the literature review in Chapter 2 argued, decreasing the layer thickness, and increasing the infill density would increase the stiffness, tensile, and compressive strength of the printed part. As the new AM tool manages to withstand the forces in the bending process, this is evidently true. The plots in Figure 41 also proves this, as no sudden decrease in pressure can be observed. To further increase the infill density further would not be logical, as it will only increase the lead times and part costs. Decreasing the infill density to the lowest value where the mechanical properties are satisfactory, could be a feasible future alternative in order to keep the lead times and costs at low levels. A lower infill density could possibly be applied in this project to save time printing the parts. To utilize a lower infill density and for example use foam or epoxy to fill the empty space can also be a possible alternative to consider instead of using an increased infill density. The build orientation can also have had positive impacts on the AM tools. In the specialization project an orientation where the layers lay parallel to the downforce from the specimen was chosen. The new orientation opted for in the master's project, where the layers are oriented in perpendicular to the compressive forces, may have helped in preventing the same structural failure. The disadvantage is the rougher surface finish of the specimens, discussed in Section 5.1.4.

To split the AM tool into three parts may also have caused the structural integrity to increase. An additive manufactured part is printed with a completely solid top and bottom layer, which provides structural support and a clean surface finish. As there are three parts

which together constitutes one AM tool, there are six surfaces that are printed with a solid layer, increasing the structural integrity of the AM tool.

5.2.2 The bending process' impact on the AM tools surface

As mentioned earlier in this section, the only detectable impacts caused by the bending process on the surface of the AM tools were minor scuffing marks and aluminum and dirt deposits. As these marks were undetectable when sliding a finger across them, it is evident that the structural integrity of the AM tools remained uncompromised. As with the specialization project, AM tool no. 4, 5, and 6 experienced the most severe markings. As argued in the specialization project, this may be linked to Figure 3 and Figure 4 where it is evident that the strain values peak about 80% along the specimen from the clamp towards the symmetry plane. This is approximately where AM tool no. 4, 5, and 6 are located. The markings are slightly more visible on the R600 AM tools, compared with the R1200 tools, which correlates nicely with the experiences from the specialization project where the R600 suffered structural damage. This might be related to Figure 6, where the strain rate for the R600 experiments is always higher than in experiments utilizing a higher bending radius, and therefore might affect the AM tools in the R600 experiments to a larger degree. As mentioned earlier, this effect can be mitigated by instigating a translational movement of the machine arms along the x-axis during while the bend is induced. As depicted in Figure 41, the servo 1 pressures are higher for the R600 process, due to larger distances from the pivot point. This further proves that the forces exhibited in the R600 process are more substantial.

The scuff marks are visibly unsymmetric on both the R600 and R1200 AM tools, as mentioned in Chapter 4. This can also prove that the technique employed to set up the tool is inaccurate, and perhaps should be revised if this research is continued. It may also be caused by small inaccuracies in the machine movements.

6. Suggested Further Work

Based on the results and discussions in this project, further work in this research should experiment with utilizing different infill densities when manufacturing the AM tools. To find a point where a balance between required mechanical properties and printing time would be beneficial. To fill gaps and voids resulting from infill densities and patterns with materials such as foam or epoxy could also be an interesting approach.

There are numerous filaments available for use in FFF and FDM printing, for example nylon filament. To experiment with several filaments combined with the other printing parameters could be potential approaches for further research.

In order to mitigate the build orientation's effects on the specimens' surface, such as the "stair-stepping" effect, post-processing techniques to remove the stepping could be researched.

As evident in the discussions of the results, development of a novel and dependable technique for setting up the adjustable tools can be highly beneficial. A new technique where the same measured result is obtained repeatedly when measuring the same value, would help immensely in understanding the employed techniques effects on the end results.

Lastly, continuing iterating on the AM tooling's design should be done to further streamline the design in terms of easy manufacturing and minimize indentations effectively.

7. Conclusion

The main focus of this master's project was to further iterate on the ideas brought about in the specialization project, regarding using additive manufactured solutions combined with flexible die tooling to minimize indentations inflicted on aluminum specimens during a rotary stretch bending process. In order to facilitate an organized investigation of the problem at hand, research questions were established based on the learnings from the previous project. These research questions were as follows:

I. Does increasing the infill density of the improve the structural qualities of the AM tooling sufficiently to withstand the rotary stretch bending process across all applicable bending radii?

II. Is the implementation of an exchangeable contact surface on the AM tool effective in reducing the indentations and marks inflicted on the specimens during the bending process?

III. How does a build orientation perpendicular to the compressive forces affect both the AM tooling and the surface finish of the specimens?

To approach this problem a thorough literature review was conducted to create a strong theoretical foundation upon which to base the project work on. Much of this background was reused from the specialization project. Combined with the learnings and results from the specialization project, a methodology was established and followed in order to approach the problem in the best way possible. Using a proof-of-concept prototype development approach proved useful in painting a picture of AM tooling's potential in to be combined with flexible rotary stretch bending processes.

The experiment results have revealed that additive manufactured tooling, printed with PLA inhabits sufficient structural strength to withstand forces in a 2D stretch bending process. No signs of structural malfunction were detected, save from minor scuffing marks. By employing adequate values of infill density and layer thickness, the structural qualities of the AM tooling significantly improve, enabling it to be utilized in stretch bending processes that involve both tight and higher bending radii. As additive

manufacturing provides enhanced cost-efficiency compared to traditional metal solutions, utilization of AM tooling in rotary stretch bending shows promise.

In the specialization project, it was demonstrated that the AM tooling enhances the surface quality of the specimens when compared to using steel axles. However, with the incorporation of an exchangeable contact surface, the surface finish is further improved, almost eliminating indentations caused by the tooling during the bending processes.

The newly applied build orientation of the AM tools has demonstrated a significant influence on the outcomes of the experiments. The structural strength gained from the printed layers' new orientation in relation to the direction of the bending forces, likely played a role in preserving the overall structural integrity of the AM tools. However, the orientation has also affected the surface finish of the specimens, leaving visible marks resulting from the layer stepping. Nevertheless, these marks are nearly negligible, and the benefits of the applied build orientation may outweigh the minor shortcomings, making it a favorable approach.

Limitations during the project has prevented testing a planned third bending radius, as well as developing a novel technique for setting up the adjustable tools. Despite this, the project has yielded satisfactory results and proven the potential additive manufactured tooling possesses when combined with metal forming processes.

References

Diegel Olaf and Nordin, A. and M. D. (2019). Polymer Design Guidelines. In *A Practical Guide to Design for Additive Manufacturing* (pp. 103–119). Springer Singapore. https://doi.org/10.1007/978-981-13-8281-9_8

Dwiyati, S. T., Kholil, A., Riyadi, R., & Putra, S. E. (2019). Influence of layer thickness and 3D printing direction on tensile properties of ABS material. *Journal of Physics: Conference Series*, *1402*(6), 066014. https://doi.org/10.1088/1742-6596/1402/6/066014

Gao, X., Qi, S., Kuang, X., Su, Y., Li, J., & Wang, D. (2021). Fused filament fabrication of polymer materials: A review of interlayer bond. *Additive Manufacturing*, *37*, 101658. https://doi.org/10.1016/J.ADDMA.2020.101658

Gunasekaran, K. N., Aravinth, V., Kumaran, C. B. M., Madhankumar, K., & Kumar, S. P. (2021). Investigation of mechanical properties of PLA printed materials under varying infill density. *Materials Today: Proceedings*, *45*, 1849–1856. https://doi.org/10.1016/J.MATPR.2020.09.041

Li, Y., Han, X., Liang, J., Teng, F., & Liang, C. (2021). Effect of multi-point roller dies on the forming accuracy of profile in flexible 3D stretch bending technology. *The International Journal of Advanced Manufacturing Technology*, *112*(3), 897–905. https://doi.org/10.1007/s00170-020-06336-0

Lundby, V. (2023). *Concepts Utilizing Additive Manufacturing for Flexible Tooling in Rotary Stretch Bending Processes* [Project thesis, TPK4540 - Manufacturing Technology, Specialization Project]. NTNU.

Ma, J., Tronvoll, S. A., Welo, T., & Ringen, G. (2022). On Dimensional Control in Rotary Stretch Bending of Aluminum Profiles: Loading-Path Effects. *Manufacturing Letters*, *33*, 242–248. https://doi.org/10.1016/J.MFGLET.2022.07.031

Ma, J., & Welo, T. (2021). Analytical springback assessment in flexible stretch bending of complex shapes. *International Journal of Machine Tools and Manufacture*, *160*, 103653. https://doi.org/10.1016/J.IJMACHTOOLS.2020.103653

Mishra, P. K., Senthil, P., Adarsh, S., & Anoop, M. S. (2021). An investigation to study the combined effect of different infill pattern and infill density on the impact strength of 3D printed polylactic acid parts. *Composites Communications*, *24*, 100605. https://doi.org/10.1016/J.COCO.2020.100605

Qamar Tanveer, M., Mishra, G., Mishra, S., & Sharma, R. (2022). Effect of infill pattern and infill density on mechanical behaviour of FDM 3D printed Parts- a current review. *Materials Today: Proceedings*, *62*, 100–108. https://doi.org/10.1016/J.MATPR.2022.02.310

Rankouhi, B., Javadpour, S., Delfanian, F., & Letcher, T. (2016). Failure Analysis and Mechanical Characterization of 3D Printed ABS With Respect to Layer Thickness and Orientation. *Journal of Failure Analysis and Prevention*, *16*(3), 467–481. https://doi.org/10.1007/s11668-016-0113-2

SAVE International. (2007). *Value Standard and Body of Knowledge*.

Schuh, G., Bergweiler, G., Fiedler, F., Bickendorf, P., & Colag, C. (2019). A Review on Flexible Forming of Sheet Metal Parts. *2019 IEEE International Conference on Industrial Engineering and Engineering Management (IEEM)*, 1221–1225. https://doi.org/10.1109/IEEM44572.2019.8978879

Sørby, K. (2022). *Coordinate Measuring Machines*.

Terekhina, S., Skornyakov, I., Tarasova, T., & Egorov, S. (2019). Effects of the Infill Density on the Mechanical Properties of Nylon Specimens Made by Filament Fused Fabrication. *Technologies*, *7*(3). https://doi.org/10.3390/technologies7030057

Thomke, S. H. (1998). Managing Experimentation in the Design of New Products. *Management Science*, *44*(6), 743–762. http://www.jstor.org/stable/2634644

Tronvoll, S. A., Blindheim, J., Ma, J., & Welo, T. (2022). A new, flexible tool concept for rotary die stretch bending. *Manufacturing Letters*, *33*, 226–231. https://doi.org/10.1016/J.MFGLET.2022.07.029

Welo, T., Ma, J., Blindheim, J., Ha, T., & Ringen, G. (2020). Flexible 3D stretch bending of aluminium alloy profiles: an experimental and numerical study.

Procedia Manufacturing, *50*, 37–44.
https://doi.org/10.1016/J.PROMFG.2020.08.008

Yadav, P., Sahai, A., & Sharma, R. S. (2021). Strength and Surface Characteristics of
FDM-Based 3D Printed PLA Parts for Multiple Infill Design Patterns. *Journal of
The Institution of Engineers (India): Series C*, *102*(1), 197–207.
https://doi.org/10.1007/s40032-020-00625-z

Yao, T., Ye, J., Deng, Z., Zhang, K., Ma, Y., & Ouyang, H. (2020). Tensile failure
strength and separation angle of FDM 3D printing PLA material: Experimental and
theoretical analyses. *Composites Part B: Engineering*, *188*, 107894.
https://doi.org/10.1016/J.COMPOSITESB.2020.107894

Appendix

A

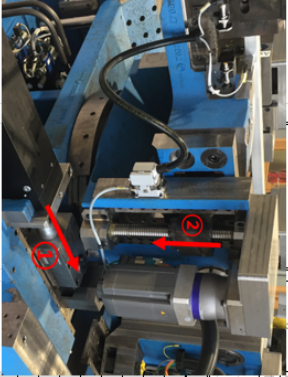Sketch with measurements and parameters for a R1200 setup utilizing the spring steel.
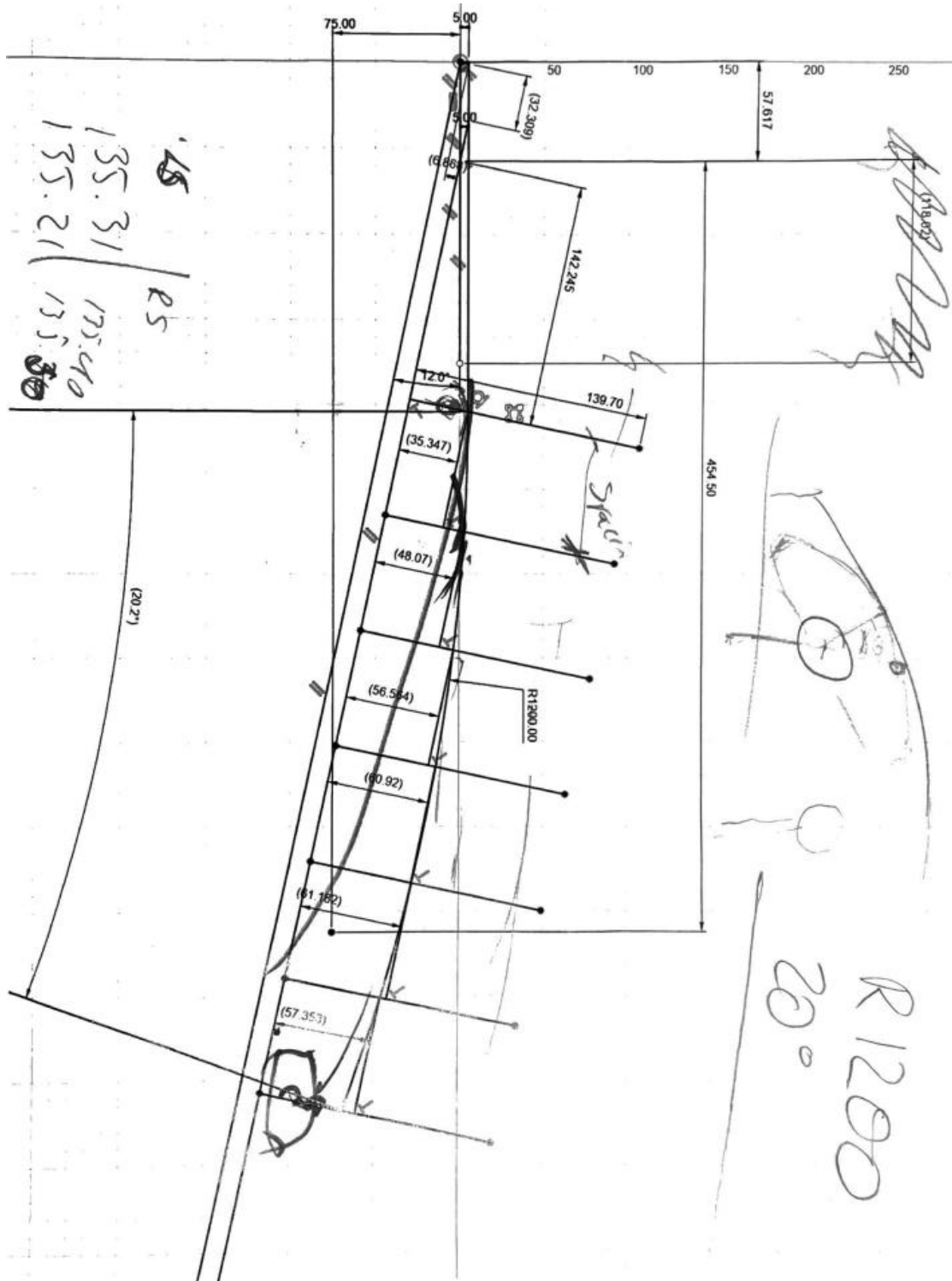
B

Table containing rotation angles and corresponding input coordinates.

Yaw (Servo 4, 5)
Enter the rotation angle you want in the orange-colored cell

my rotation	degree	radian
	0	0

my translation input on the controller: **135,370** mm ①

	initial angle	-2,245742566	-0,0391956
	target	-2,245742566	-0,0391956

Actuator position

				Initial	Final
l	510,39	r	130,5	m	488	-148,6322	-148,6324919

Actuator speed (mm/s)	0,000
time (sec)	5
Rotation speed (rad/s)	0,000

l — the hinge position to rotate the yoke
r — linkage length
m — actuator location from the yoke center

Yaw (Servo 4,5)

degree	input(mm)	degree	input(mm)	degree	input(mm)
1	144,320	11	232,222	21	317,683
2	153,247	12	240,840	22	326,231
3	162,148	13	249,432	23	334,806
4	171,020	14	258,000	24	343,415
5	179,861	15	266,549	25	352,067
6	188,670	16	275,082	26	360,771
7	197,446	17	283,604	27	369,538
8	206,189	18	292,119	28	378,380
9	214,898	19	300,633	29	387,309
10	223,575	20	309,152	30	396,339

Pitch (Servo 2,3)
Enter the rotation angle you want in the orange-colored cell

Homing point (155.500, 135.370)

my rotation	degree	radian
	0	0

my translation input on the controller: **155,500** mm ②

a	262
c	25

Actuator speed (mm/s)	0,000
time (sec)	10
Bending speed (rad/s)	0,000

a — the distance of the ball screw center from the rotating axis
c — the offset distance between centers

degree	input(mm)	degree	input(mm)	degree	input(mm)
1	150,923	11	104,104	21	53,149
2	146,336	12	99,252	22	47,682
3	141,735	13	94,355	23	42,129
4	137,118	14	89,411	24	36,484
5	132,482	15	84,415	25	30,743
6	127,825	16	79,365		
7	123,143	17	74,256		
8	118,433	18	69,084		
9	113,692	19	63,846		
10	108,917	20	58,535		

C

Script utilized for obtaining the pressure curves from the bending process logging data.

```
In [1]: import pandas as pd
        import matplotlib.pyplot as plt
        import numpy as np
        import os
```

71

```
In [2]: fig,ax = plt.subplots(2,2, figsize = (20,20))


        direc = 'vegard/økt1'
        files = os.listdir(direc)


        for file in files:

            fulldirec = direc+'\\'+file

            #display(files)

            file_name = os.path.basename(file)

            df=pd.read_parquet(fulldirec, engine='pyarrow')
            df.columns = df.columns.str.replace(r'Regulator_Data.', '')

            t = df['timestamp']
            t = (t-t[0])/1000
            p = df['servo1_pressure']

            cutoff = 30000
            convolutionarray = np.ones(100)/100
            ax[0,0].plot(df.timestamp[0:cutoff]-df.timestamp[0],np.convolve(df.servo1_
        pressure[0:cutoff],convolutionarray,'same'),label = os.path.splitext(file_nam
        e)[0])
            ax[1,0].plot(df.timestamp[0:cutoff]-df.timestamp[0],df.servo2a_position[0:
        cutoff])
            ax[0,0].legend()
            ax[0,0].set_xlabel('Time [ms]')
            ax[0,0].set_ylabel('Servo 1 pressure [Bar]')
            ax[1,0].set_xlabel('Time [ms]')
            ax[1,0].set_ylabel('Servo 2 position [μm]')

            #ax[0,1].plot(t,df.servo1_pressure)
            #ax[1,0].plot(t,df.servo2a_torque)
            #ax[1,1].plot(t,df.servo5_torque)


        direc = 'vegard/økt2'
        files = os.listdir(direc)

        for file in files:

            fulldirec = direc+'\\'+file

            #display(files)

            file_name = os.path.basename(file)

            df=pd.read_parquet(fulldirec, engine='pyarrow')
            df.columns = df.columns.str.replace(r'Regulator_Data.', '')

            t = df['timestamp']
```

72

```python
    t = (t-t[0])/1000
    p = df['servo1_pressure']

    cutoff = 30000
    convolutionarray = np.ones(100)/100
    ax[0,1].plot(df.timestamp[0:cutoff]-df.timestamp[0],np.convolve(df.servo1_
pressure[0:cutoff],convolutionarray,'same'),label = os.path.splitext(file_nam
e)[0])
    ax[1,1].plot(df.timestamp[0:cutoff]-df.timestamp[0],df.servo2a_position[0:
cutoff])
    ax[0,1].legend()
    ax[0,1].set_xlabel('Time [ms]')
    ax[0,1].set_ylabel('Servo 1 pressure [Bar]')
    ax[1,1].set_xlabel('Time [ms]')
    ax[1,1].set_ylabel('Servo 2 position [µm]')

    #ax[0,1].plot(t,df.servo1_pressure)
    #ax[1,0].plot(t,df.servo2a_torque)
    #ax[1,1].plot(t,df.servo5_torque)
```
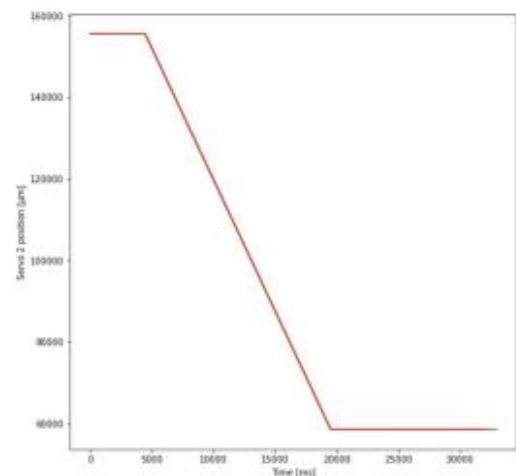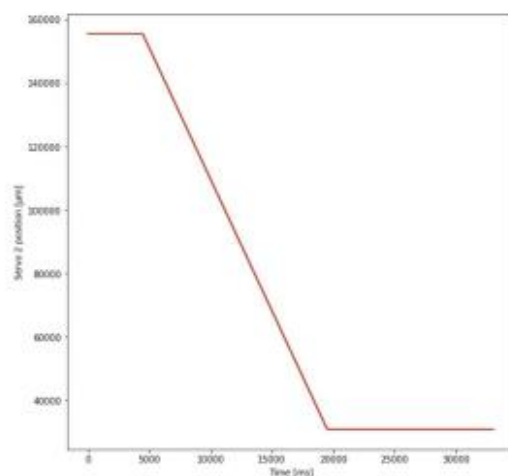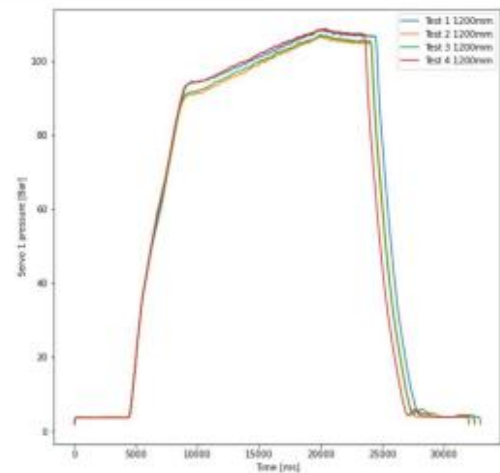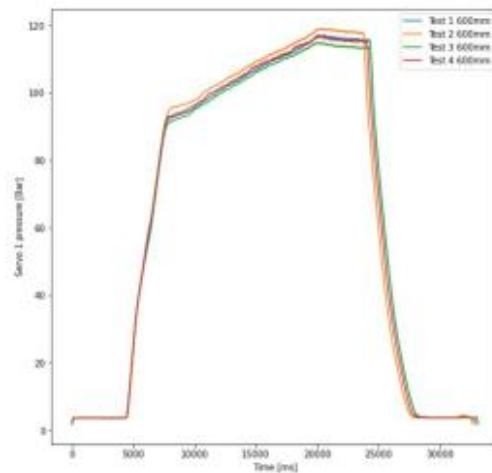
In [22]: `files[0]`

Out[22]: `'test-2023-05-10T130206.817405.parquet'`

In [23]: `files`

Out[23]: `['test-2023-05-10T130206.817405.parquet',`
`'test-2023-05-10T130516.953391.parquet',`
`'test-2023-05-10T130747.610802.parquet',`
`'test-2023-05-10T131048.426634.parquet']`

In [ ]:

74

D

Complete measurements obtained from the coordinate measuring machine.

Pc		PART NAME :	2023-06-23 Profil 600 #1			juni 22, 2023	11:06
		REV NUMBER :		SER NUMBER :		STATS COUNT :	1

∡	DEG	ANGL1 - LIN1 TO LIN2					
AX		NOMINAL	+TOL	-TOL	MEAS	DEV	OUTTOL
A		25.000	1.000	-1.000	24.234	-0.766	0.000

⊕	MM	LOC1 - CIR1					
AX		NOMINAL	+TOL	-TOL	MEAS	DEV	OUTTOL
R		600.000	2.000	-2.000	594.950	-5.050	3.050

FCFCIRTY1 Size		MM		Ø 1195.896 +/- 0.01		DEFAULT	ISO 1101
Feature		NOMINAL	+TOL	-TOL	MEAS	DEV	OUTTOL
CIR1 - MIN		1195.896	0.010	-0.010	1189.797	-6.099	6.089
CIR1 - MAX		1195.896	0.010	-0.010	1190.086	-5.809	5.799

FCFCIRTY1		MM		◯ 0.5		DEFAULT	ISO 1101
Feature		NOMINAL	+TOL	-TOL	MEAS	DEV	OUTTOL
CIR1		0.000	0.500		0.276	0.276	0.000

Pc		PART NAME :	2023-06-23 Profil 600 #2			juni 22, 2023	09:43
		REV NUMBER :		SER NUMBER :		STATS COUNT :	1

∡	DEG	ANGL1 - LIN1 TO LIN2					
AX		NOMINAL	+TOL	-TOL	MEAS	DEV	OUTTOL
A		25.000	1.000	-1.000	24.290	-0.710	0.000

⊕	MM	LOC1 - CIR1					
AX		NOMINAL	+TOL	-TOL	MEAS	DEV	OUTTOL
R		600.000	2.000	-2.000	599.028	-0.972	0.000

FCFCIRTY1 Size		MM		Ø 1208.638 +/- 0.01		DEFAULT	ISO 1101
Feature		NOMINAL	+TOL	-TOL	MEAS	DEV	OUTTOL
CIR1 - MIN		1208.638	0.010	-0.010	1197.964	-10.674	10.664
CIR1 - MAX		1208.638	0.010	-0.010	1198.257	-10.381	10.371

FCFCIRTY1		MM		◯ 0.5		DEFAULT	ISO 1101
Feature		NOMINAL	+TOL	-TOL	MEAS	DEV	OUTTOL
CIR1		0.000	0.500		0.272	0.272	0.000
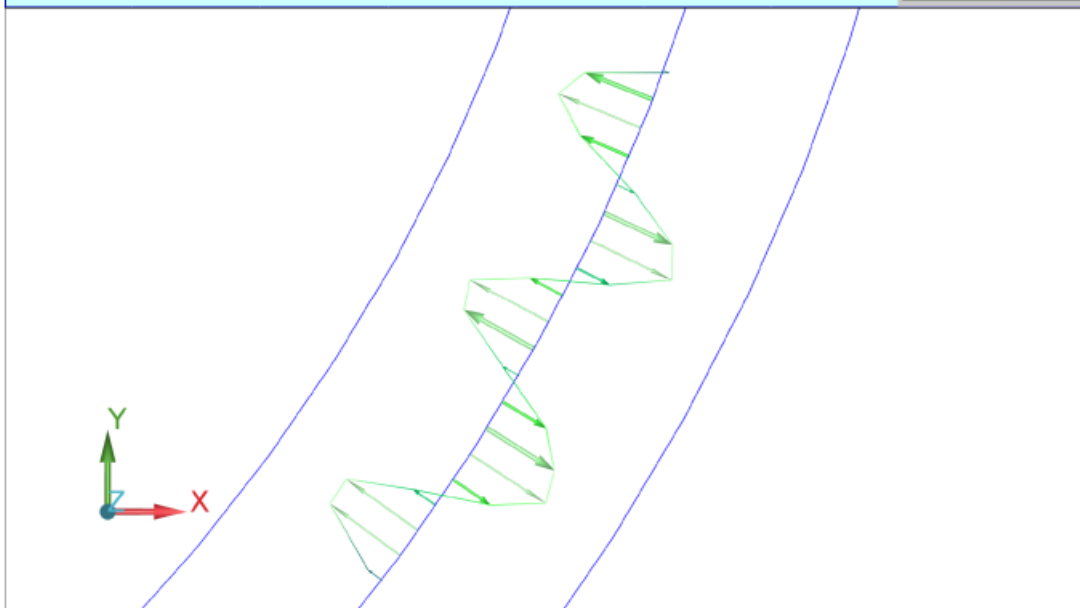
	Pc	PART NAME :	2023-06-23 Profil 600 #3			juni 22, 2023	11:27
		REV NUMBER :		SER NUMBER :		STATS COUNT :	1

⦜	DEG	ANGL1 - LIN1 TO LIN2						
AX		NOMINAL	+TOL	-TOL	MEAS	DEV	OUTTOL	
A		25.000	1.000	-1.000	24.208	-0.792	0.000	

⊕	MM	LOC1 - CIR1						
AX		NOMINAL	+TOL	-TOL	MEAS	DEV	OUTTOL	
R		600.000	2.000	-2.000	594.692	-5.308	3.308	

FCFCIRTY1 Size		MM		∅ 1203.901 +/- 0.01			DEFAULT	ISO 1101
Feature		NOMINAL	+TOL	-TOL	MEAS	DEV	OUTTOL	
CIR1 - MIN		1203.901	0.010	-0.010	1189.273	-14.628	14.618	
CIR1 - MAX		1203.901	0.010	-0.010	1189.574	-14.328	14.318	

FCFCIRTY1		MM		○ 0.5			DEFAULT	ISO 1101
Feature		NOMINAL	+TOL	-TOL	MEAS	DEV	OUTTOL	
CIR1		0.000	0.500		0.278	0.278	0.000	

	Pc	PART NAME :	2023-06-23 Profil 600 #4			juni 22, 2023	10:41
		REV NUMBER :		SER NUMBER :		STATS COUNT :	1

⦜	DEG	ANGL1 - LIN1 TO LIN2						
AX		NOMINAL	+TOL	-TOL	MEAS	DEV	OUTTOL	
A		25.000	1.000	-1.000	24.181	-0.819	0.000	

⊕	MM	LOC1 - CIR1						
AX		NOMINAL	+TOL	-TOL	MEAS	DEV	OUTTOL	
R		600.000	2.000	-2.000	595.296	-4.704	2.704	

FCFCIRTY1 Size		MM		∅ 1196.24 +/- 0.01			DEFAULT	ISO 1101
Feature		NOMINAL	+TOL	-TOL	MEAS	DEV	OUTTOL	
CIR1 - MIN		1196.240	0.010	-0.010	1190.479	-5.762	5.752	
CIR1 - MAX		1196.240	0.010	-0.010	1190.785	-5.455	5.445	

FCFCIRTY1		MM		○ 0.5			DEFAULT	ISO 1101
Feature		NOMINAL	+TOL	-TOL	MEAS	DEV	OUTTOL	
CIR1		0.000	0.500		0.284	0.284	0.000	

	Pc		PART NAME :	2023-06-23 Profil 1200 #1			juni 22, 2023	12:05
			REV NUMBER :		SER NUMBER :		STATS COUNT :	1

⊿	DEG	ANGL1 - LIN1 TO LIN2						
AX		NOMINAL	+TOL	-TOL	MEAS	DEV	OUTTOL	
A		20.000	1.000	-1.000	19.317	-0.683	0.000	

⊕	MM	LOC1 - CIR1						
AX		NOMINAL	+TOL	-TOL	MEAS	DEV	OUTTOL	
R		1200.000	2.000	-2.000	1166.522	-33.478	31.478	

FCFCIRTY1 Size		MM		Ø 2381.469 +/- 0.01			DEFAULT	ISO 1101
Feature		NOMINAL	+TOL	-TOL	MEAS	DEV	OUTTOL	
CIR1 - MIN		2381.469	0.010	-0.010	2333.025	-48.444	48.434	
CIR1 - MAX		2381.469	0.010	-0.010	2333.354	-48.115	48.105	

FCFCIRTY1		MM		○ 0.5			DEFAULT	ISO 1101
Feature		NOMINAL	+TOL	-TOL	MEAS	DEV	OUTTOL	
CIR1		0.000	0.500		0.319	0.319	0.000	

	Pc		PART NAME :	2023-06-23 Profil 1200 #2			juni 22, 2023	11:41
			REV NUMBER :		SER NUMBER :		STATS COUNT :	1

⊿	DEG	ANGL1 - LIN1 TO LIN2						
AX		NOMINAL	+TOL	-TOL	MEAS	DEV	OUTTOL	
A		20.000	1.000	-1.000	19.199	-0.801	0.000	

⊕	MM	LOC1 - CIR1						
AX		NOMINAL	+TOL	-TOL	MEAS	DEV	OUTTOL	
R		1200.000	2.000	-2.000	1187.657	-12.343	10.343	

FCFCIRTY1 Size		MM		Ø 2461.531 +/- 0.01			DEFAULT	ISO 1101
Feature		NOMINAL	+TOL	-TOL	MEAS	DEV	OUTTOL	
CIR1 - MIN		2461.531	0.010	-0.010	2375.283	-86.249	86.239	
CIR1 - MAX		2461.531	0.010	-0.010	2375.721	-85.811	85.801	

FCFCIRTY1		MM		○ 0.5			DEFAULT	ISO 1101
Feature		NOMINAL	+TOL	-TOL	MEAS	DEV	OUTTOL	
CIR1		0.000	0.500		0.400	0.400	0.000	

Pc		PART NAME :	2023-06-23 Profil 1200 #3			juni 22, 2023	11:48
		REV NUMBER :		SER NUMBER :		STATS COUNT :	1

⊿	DEG	ANGL1 - LIN1 TO LIN2					
AX		NOMINAL	+TOL	-TOL	MEAS	DEV	OUTTOL
A		20.000	1.000	-1.000	19.315	-0.685	0.000

⌖	MM	LOC1 - CIR1					
AX		NOMINAL	+TOL	-TOL	MEAS	DEV	OUTTOL
R		1200.000	2.000	-2.000	1160.810	-39.190	37.190

FCFCIRTY1 Size		MM		∅ 2389.229 +/- 0.01		DEFAULT	ISO 1101
Feature		NOMINAL	+TOL	-TOL	MEAS	DEV	OUTTOL
CIR1 - MIN		2389.229	0.010	-0.010	2321.608	-67.620	67.610
CIR1 - MAX		2389.229	0.010	-0.010	2321.978	-67.250	67.240

FCFCIRTY1		MM		◯ 0.5		DEFAULT	ISO 1101
Feature		NOMINAL	+TOL	-TOL	MEAS	DEV	OUTTOL
CIR1		0.000	0.500		0.336	0.336	0.000

Pc		PART NAME :	2023-06-23 Profil 1200 #4			juni 22, 2023	11:53
		REV NUMBER :		SER NUMBER :		STATS COUNT :	1

⊿	DEG	ANGL1 - LIN1 TO LIN2					
AX		NOMINAL	+TOL	-TOL	MEAS	DEV	OUTTOL
A		20.000	1.000	-1.000	19.332	-0.668	0.000

⌖	MM	LOC1 - CIR1					
AX		NOMINAL	+TOL	-TOL	MEAS	DEV	OUTTOL
R		1200.000	2.000	-2.000	1170.422	-29.578	27.578

FCFCIRTY1 Size		MM		∅ 2404.278 +/- 0.01		DEFAULT	ISO 1101
Feature		NOMINAL	+TOL	-TOL	MEAS	DEV	OUTTOL
CIR1 - MIN		2404.278	0.010	-0.010	2340.836	-63.442	63.432
CIR1 - MAX		2404.278	0.010	-0.010	2341.193	-63.085	63.075

FCFCIRTY1		MM		◯ 0.5		DEFAULT	ISO 1101
Feature		NOMINAL	+TOL	-TOL	MEAS	DEV	OUTTOL
CIR1		0.000	0.500		0.329	0.329	0.000

	PC	PART NAME :	2023-06-23 Profil knekk 600 #1		juni 22, 2023	12:03
		REV NUMBER :		SER NUMBER :	STATS COUNT :	1

⊿	DEG	ANGL1 - LIN1 TO LIN2					
AX		NOMINAL	+TOL	-TOL	MEAS	DEV	OUTTOL
A		25.000	1.000	-1.000	23.621	-1.379	0.379

⊕	MM	LOC1 - CIR1					
AX		NOMINAL	+TOL	-TOL	MEAS	DEV	OUTTOL
R		600.000	2.000	-2.000	578.945	-21.055	19.055

FCFCIRTY1 Size		MM		∅ 1193.944 +/- 0.01		DEFAULT	ISO 1101
Feature		NOMINAL	+TOL	-TOL	MEAS	DEV	OUTTOL
CIR1 - MIN		1193.944	0.010	-0.010	1157.702	-36.242	36.232
CIR1 - MAX		1193.944	0.010	-0.010	1158.480	-35.464	35.454

FCFCIRTY1		MM		◯ 0.5		DEFAULT	ISO 1101
Feature		NOMINAL	+TOL	-TOL	MEAS	DEV	OUTTOL
CIR1		0.000	0.500		0.700	0.700	0.200

	PC	PART NAME :	2023-06-23 Profil knekk 600 #2		juni 22, 2023	12:33
		REV NUMBER :		SER NUMBER :	STATS COUNT :	1

⊿	DEG	ANGL1 - LIN1 TO LIN2					
AX		NOMINAL	+TOL	-TOL	MEAS	DEV	OUTTOL
A		25.000	1.000	-1.000	23.668	-1.332	0.332

⊕	MM	LOC1 - CIR1					
AX		NOMINAL	+TOL	-TOL	MEAS	DEV	OUTTOL
R		600.000	2.000	-2.000	586.173	-13.827	11.827

FCFCIRTY1 Size		MM		∅ 1190.804 +/- 0.01		DEFAULT	ISO 1101
Feature		NOMINAL	+TOL	-TOL	MEAS	DEV	OUTTOL
CIR1 - MIN		1190.804	0.010	-0.010	1172.168	-18.636	18.626
CIR1 - MAX		1190.804	0.010	-0.010	1172.851	-17.953	17.943

FCFCIRTY1		MM		◯ 0.5		DEFAULT	ISO 1101
Feature		NOMINAL	+TOL	-TOL	MEAS	DEV	OUTTOL
CIR1		0.000	0.500		0.619	0.619	0.119

		PART NAME :	2023-06-23 Profil knekk 600 #3		juni 22, 2023	12:17

Pc

		REV NUMBER :		SER NUMBER :		STATS COUNT :	1

⦜	DEG	ANGL1 - LIN1 TO LIN2					
AX		NOMINAL	+TOL	-TOL	MEAS	DEV	OUTTOL
A		23.651	1.000	-1.000	23.663	0.012	0.000

⌖	MM	LOC1 - CIR1					
AX		NOMINAL	+TOL	-TOL	MEAS	DEV	OUTTOL
R		580.388	2.000	-2.000	577.030	-3.358	1.358

FCFCIRTY1 Size		MM	⌀ 1160.776 +/- 0.01			DEFAULT	ISO 1101
Feature		NOMINAL	+TOL	-TOL	MEAS	DEV	OUTTOL
CIR1 - MIN		1160.776	0.010	-0.010	1153.859	-6.917	6.907
CIR1 - MAX		1160.776	0.010	-0.010	1154.620	-6.156	6.146

FCFCIRTY1		MM	◯ 0.5			DEFAULT	ISO 1101
Feature		NOMINAL	+TOL	-TOL	MEAS	DEV	OUTTOL
CIR1		0.000	0.500		0.698	0.698	0.198

		PART NAME :	2023-06-23 Profil knekk 600 #4		juni 22, 2023	12:55

Pc

		REV NUMBER :		SER NUMBER :		STATS COUNT :	1

⦜	DEG	ANGL1 - LIN1 TO LIN2					
AX		NOMINAL	+TOL	-TOL	MEAS	DEV	OUTTOL
A		25.000	1.000	-1.000	23.643	-1.357	0.357

⌖	MM	LOC1 - CIR1					
AX		NOMINAL	+TOL	-TOL	MEAS	DEV	OUTTOL
R		600.000	2.000	-2.000	578.671	-21.329	19.329

FCFCIRTY1 Size		MM	⌀ 1175.796 +/- 0.01			DEFAULT	ISO 1101
Feature		NOMINAL	+TOL	-TOL	MEAS	DEV	OUTTOL
CIR1 - MIN		1175.796	0.010	-0.010	1157.113	-18.683	18.673
CIR1 - MAX		1175.796	0.010	-0.010	1157.896	-17.900	17.890

FCFCIRTY1		MM	◯ 0.5			DEFAULT	ISO 1101
Feature		NOMINAL	+TOL	-TOL	MEAS	DEV	OUTTOL
CIR1		0.000	0.500		0.703	0.703	0.203

PART NAME :	2023-06-23 Profil knekk 1200 #1		juni 22, 2023	12:31
REV NUMBER :		SER NUMBER :	STATS COUNT :	1

∡	DEG	ANGL1 - LIN1 TO LIN2					
AX		NOMINAL	+TOL	-TOL	MEAS	DEV	OUTTOL
A		20.000	1.000	-1.000	18.651	-1.349	0.349

⌖	MM	LOC1 - CIR1					
AX		NOMINAL	+TOL	-TOL	MEAS	DEV	OUTTOL
R		1200.000	2.000	-2.000	1295.305	95.305	93.305

FCFCIRTY1 Size		MM	⌀ 2586.648 +/- 0.01			DEFAULT	ISO 1101
Feature		NOMINAL	+TOL	-TOL	MEAS	DEV	OUTTOL
CIR1 - MIN		2586.648	0.010	-0.010	2590.490	3.842	3.832
CIR1 - MAX		2586.648	0.010	-0.010	2590.666	4.018	4.008

FCFCIRTY1		MM	○ 0.5			DEFAULT	ISO 1101
Feature		NOMINAL	+TOL	-TOL	MEAS	DEV	OUTTOL
CIR1		0.000	0.500		0.166	0.166	0.000

PART NAME :	2023-06-23 Profil knekk 1200 #2		juni 22, 2023	12:39
REV NUMBER :		SER NUMBER :	STATS COUNT :	1

∡	DEG	ANGL1 - LIN1 TO LIN2					
AX		NOMINAL	+TOL	-TOL	MEAS	DEV	OUTTOL
A		20.000	1.000	-1.000	18.670	-1.330	0.330

⌖	MM	LOC1 - CIR1					
AX		NOMINAL	+TOL	-TOL	MEAS	DEV	OUTTOL
R		1200.000	2.000	-2.000	1288.264	88.264	86.264

FCFCIRTY1 Size		MM	⌀ 2569.681 +/- 0.01			DEFAULT	ISO 1101
Feature		NOMINAL	+TOL	-TOL	MEAS	DEV	OUTTOL
CIR1 - MIN		2569.681	0.010	-0.010	2576.408	6.726	6.716
CIR1 - MAX		2569.681	0.010	-0.010	2576.588	6.906	6.896

FCFCIRTY1		MM	○ 0.5			DEFAULT	ISO 1101
Feature		NOMINAL	+TOL	-TOL	MEAS	DEV	OUTTOL
CIR1		0.000	0.500		0.173	0.173	0.000

81

	Pc	PART NAME :	2023-06-23 Profil knekk 1200 #3			juni 22, 2023	12:46
		REV NUMBER :		SER NUMBER :		STATS COUNT :	1

∡	DEG	ANGL1 - LIN1 TO LIN2					
AX		NOMINAL	+TOL	-TOL	MEAS	DEV	OUTTOL
A		20.000	1.000	-1.000	18.664	-1.336	0.336

⌖	MM	LOC1 - CIR1					
AX		NOMINAL	+TOL	-TOL	MEAS	DEV	OUTTOL
R		1200.000	2.000	-2.000	1289.112	89.112	87.112

FCFCIRTY1 Size		MM		∅ 2538.191 +/- 0.01		DEFAULT	ISO 1101
Feature		NOMINAL	+TOL	-TOL	MEAS	DEV	OUTTOL
CIR1 - MIN		2538.191	0.010	-0.010	2578.090	39.899	39.889
CIR1 - MAX		2538.191	0.010	-0.010	2578.277	40.086	40.076

FCFCIRTY1		MM		○ 0.5		DEFAULT	ISO 1101
Feature		NOMINAL	+TOL	-TOL	MEAS	DEV	OUTTOL
CIR1		0.000	0.500		0.178	0.178	0.000

	Pc	PART NAME :	2023-06-23 Profil knekk 1200 #4			juni 22, 2023	12:53
		REV NUMBER :		SER NUMBER :		STATS COUNT :	1

∡	DEG	ANGL1 - LIN1 TO LIN2					
AX		NOMINAL	+TOL	-TOL	MEAS	DEV	OUTTOL
A		20.000	1.000	-1.000	18.668	-1.332	0.332

⌖	MM	LOC1 - CIR1					
AX		NOMINAL	+TOL	-TOL	MEAS	DEV	OUTTOL
R		1200.000	2.000	-2.000	1290.100	90.100	88.100

FCFCIRTY1 Size		MM		∅ 2562.547 +/- 0.01		DEFAULT	ISO 1101
Feature		NOMINAL	+TOL	-TOL	MEAS	DEV	OUTTOL
CIR1 - MIN		2562.547	0.010	-0.010	2580.085	17.538	17.528
CIR1 - MAX		2562.547	0.010	-0.010	2580.245	17.699	17.689

FCFCIRTY1		MM		○ 0.5		DEFAULT	ISO 1101
Feature		NOMINAL	+TOL	-TOL	MEAS	DEV	OUTTOL
CIR1		0.000	0.500		0.153	0.153	0.000

E
Project Risk Analysis

NTNU

Date created | Last Revision
19.12.2022 | 03.02.2023

Faculty of Engineering (IV)
Department of Mechanical and Industrial Engineering (MTP)

ONLY VALID FOR DETAILED ACTIVITIES LISTED IN SECTION 5

1. Identification

Laboratory name: MANULAB	Room number:
User's name: Vegard Lundby	☒Master ☐PhD ☐Post-Doc ☐SINTEF ☐Other:
User's e-mail: vegalund@stud.ntnu.no	User's Phone: 98074088
Supervisor: Sigmund Arntsønn Tronvoll	Supervisor's phone:
Project number: 90690400	
Period: Spring 2023	

Description of the project and needs:
The project includes use of the rotary stretch bender in relation to my master thesis. Using this machine sheet metal profiles will be bent.

2. Signatures

The user and the supervisor are aware of all the risks involved in the lab activities that are going to be performed. Additionally, the user confirms that they will follow the preventive measures described in this form to minimize all the risks that have been identified.

User's signature	Supervisor's signature
Signature: *Vegard Lundby*	Signature: *Sigmund A. Tronvoll*
Name: Vegard Lundby	Name: Sigmund A. Tronvoll
Date: 07.02.2023	Date: 07.02.2023

NTNU

Approved by:

	Signature:	Name:	Date:
Room responsible:			
Lab manager:			

Note: a pdf copy with all signatures shall be sent to everyone who has signed above.

3. Team (write "NR" if not relevant)

Project manager and organization (Student)	Vegard Lundby	Responsible for instrumentation	NR
Laboratory responsible	Håvard Vestad	Operator	Vegard Lundby
Auditor for safety check	Jun Ma	Responsible for running the experiment	Vegard Lundby
Responsible for experimental and scientific content (Advisor)	Sigmund Arntsønn Tronvoll	Responsible for logging and storing experimental data	Vegard Lundby
Responsible for dimensioning load bearing and pressurized components	Vegard Lundby	Responsible for building the rig	NR

4. Administration

Answer: Yes, No or NR (Not relevant)

Is the work order signed? (only for external work)	NR
Has the operator the required courses/training on the equipment?	Yes
Has the operator followed the safety courses? **(Mandatory)**	Yes
Can the work be done alone?	No
- If not, the work may have to be done under special conditions (evaluated in section **5**)	
Does an expert have to check the start of the experiment?	Yes
- If yes, who?	Sigmund Arntsønn Tronvoll

5. Description of the Activity

NTNU

Faculty of Engineering (IV)

Department of Mechanical and Industrial Engineering (MTP)

For each activity performed in the lab, health risks affecting the user or others need to be identified. For each risk identified, a preventive measure must be performed, and the final risk value calculated with the "risk matrix". Explanation of the "risk matrix" can be found in the last page of this form.

This page must be replicated for each different activity performed in the lab. Activities involving the use of chemicals must be filled out in the page titled "Chemical Risk Assessment" in section 5.2.

Activity: Using the stretch bender

Risk overview: (mark with X the risk that applies for the activity)

Big loads	X	Danger of fire	
Heavy lifting	X	Working at heights	
Hanging load		Hydraulic pressure	X
Gas pressure		Water pressure	
High temperature		Low temperature	
Parts at high velocity		Chemicals, if yes; fill in sect. 5.2	
Sudden acceleration at fracture/failure		Pre-tensioned components	
Dangerous dust		Severe noise	
Danger of pinching	X	Rotating parts	X

Detailed risk evaluation:

Risks
1. Machine parts falling off machine and hit foot
2. Cutting/bruising yourself on the machine and material
3. Eye damage from material hitting eyes
4. Getting stuck in the machine
5. Get hit by the machine during bending
6. Get hit in the eyes by a hydraulic fluid leakage
7. Get hit by the bounce-back of the bent material
8. Hit someone else in the lab with the material

Risk	Probability (P) (1-5)	Consequence (C)				Risk value (P x C)
		Health (1-5)	Material values (1-5)	Environment (1-5)	Reputation (1-5)	

NTNU

Faculty of Engineering (IV)
Department of Mechanical and Industrial Engineering (MTP)

1	3	2	2	2	3	9
2	3	2	1	1	2	6
3	3	3	1	1	3	9
4	2	4	2	1	3	8
5	1	3	1	1	3	3
6	1	3	3	3	3	3
7	2	4	1	1	3	8
8	3	2	1	1	3	9

Risk matrix of the activity <u>before</u> any safety measures has been applied (Include corresponding color):

Required safety equipment (mark with X the risk that applies for the activity):

Glasses	X	Safety shoes	X
Helmet		Gloves	X
Screen		Lifting equipment	
Ear protection		Hazard suit	
Harness ropes, other measures to prevent falling		Fume hood	
Lab coat	X		

Description of other safety measurements: Eg. Safety cap on the instrument prevents the risk of… and/ or the probability of…

Risk after preventative and corrective measures:

Risks	Preventative and corrective measures
1. Machine parts falling off machine and hit foot	Use safety boots and beware of the parts that are loose and always be careful and aware of your movements.
2. Cutting/bruising yourself on the machine and material	Use safety gloves when placing material into the machine and be careful when handling the material and handle yourself with caution when using the machine.

86

NTNU

Faculty of Engineering (IV)
Department of Mechanical and Industrial Engineering (MTP)

3. Eye damage from material hitting eyes	Safety glasses available in workshop and before start-up: Carry out documented HSE training with the students (use of hand tools and required protective equipment).
4. Getting stuck in the machine	No gloves when operating the machine and roll up sleeves. No loose clothing and use common sense and be aware of the way you are dressed when operating the machine
5. Get hit by the machine during bending	Movement sensor monitoring the work area around the machine, preventing the machine from performing operations when people are located within the critical zone and keep outside the area designated with tape on the floor.
6. Get hit in the eyes by a hydraulic fluid leakage	Safety glasses available in workshop and keep outside the area designated with tape on the floor.
7. Get hit by the bounce-back of the bent material	A security cage is mounted around the machine preventing the material to bounce and hit the workers and keep outside the area designated with tape on the floor.
8. Hit someone else in the lab with the material	Make sure everybody in the lab is wearing proper PPE and be aware of the other people surrounding you and handle and transport the material when there is no one in the way.

Risk matrix of the activity <u>after</u> safety measures has been applied:

Risk	Probability (P) (1-5)	Consequence (C)				Risk value (P x C)
		Health (1-5)	Material values (1-5)	Environment (1-5)	Reputation (1-5)	
1	1	2	1	1	3	3
2	1	2	1	1	2	2
3	1	3	1	1	3	3
4	1	4	2	1	3	4
5	1	3	1	1	3	3
6	1	3	3	3	3	3
7	1	4	1	1	3	4
8	1	2	1	1	3	3

NTNU

Faculty of Engineering (IV)

Department of Mechanical and Industrial Engineering (MTP)

5.2. Chemical Risk Assessment:

Only for activities involving the use of chemicals (except ethanol and acetone for cleaning).

This page **must be replicated** for each different chemical activity performed in the lab. Include all H-sentence and numbers for chemicals used. This can be found in the Safety Data Sheet og the specific chemical(SDS).

Activity: Include specification of **your** work, name of chemicals, composition of alloy, concentration, max volume etc.

Chemicals used:	Full name – Include concentration etc.
Mixture:	If yes, include amount and/or concentration – if known. Otherwise, state roughly max amount
Will the mixture be stored in the cabinet for several uses?	

Risk	Prevention Measures
1.	
2.	
3.	
4.	

Note: All H-sentences must be included as a risk, together with "general" risks when using the specific chemical.

Chemical disposal procedure:
Dangerous waste or not? If not, why? Etc. How are you going to store the waste?

NTNU

Faculty of Engineering (IV)
Department of Mechanical and Industrial Engineering (MTP)

Risk matrix of the chemical activity before safety measures:

Risk	Probability (P) (1-5)	Consequence (C)				Risk value (P x C)
		Health (1-5)	Material values (1-5)	Environment (1-5)	Reputation (1-5)	
1						
2						
3						

Required safety equipment: (mark with X the risk that applies for the activity)

Glasses		Safety shoes	
Helmet		Gloves	
Screen		Lifting equipment	
Ear protection		Hazard suit	
Harness ropes, other measures to prevent falling		Fume hood	
Lab coat			

Description of other safety measurements: Eg. Safety cap on the instrument prevents the risk of…
and/ or the probability of…

Risk after preventative and corrective measures:

Risks	Preventative and corrective measures
1.	
2.	
3.	

89

NTNU

Faculty of Engineering (IV)
Department of Mechanical and Industrial Engineering (MTP)

Risk matrix of the activity <u>after</u> safety measures has been applied:

Risk	Probability (P) (1-5)	Consequence (C)				Risk value (P x C)
		Health (1-5)	Material values (1-5)	Environment (1-5)	Reputation (1-5)	
1						
2						
3						

Comments: Supplementary comments regarding the risk matrixes

6. Sources for mistakes/errors

Is the following considered? Answer: Yes, No or NR (Not relevant)

Loss of electricity	Yes	Voltage surge	Yes
Electrical earth failure	Yes	Insufficient power of the machine	Yes
Climate control in the room (temperature, humidity, etc…)	Yes	Water jet	NR
Unstable pressure or hydraulic force	Yes	Unintended interruption of power supply	Yes
Are load and displacement limits established?	Yes	Leakage of pipes, hoses, joints, etc…	Yes
Possible interference from other activities	Yes	Possible interference towards other activities	Yes
Troubles in acquisition and storage	Yes	Fire in the laboratory	Yes

NTNU

Faculty of Engineering (IV)
Department of Mechanical and Industrial Engineering (MTP)

9 of 10

Date created | Last Revision
19.12.2022 | 03.02.2023

7. Calibration of equipment

If a calibration of the equipment is performed during the activity, please indicate the date:

Equipment	Date (dd.mm.yy)

8. Traceability

Answer: Yes, No or NR (Not relevant)

Are all experimental materials known and traceable?	Yes
Is there a plan for marking all specimens?	Yes
Is the data acquisition equipment identified?	Yes
Are the original data stored safely without modification?	Yes
Is there a back-up procedure for the data (hard disk crash)?	NR
Is there a plan for storing samples after testing?	Yes
Is there a plan for disposing of old samples?	Yes

9. Conclusion

The project is a part of Vegard Lundby's master project with Sigmund Arntsønn Tronvoll as advisor. The machine used in the project is the rotary stretch bender. The specimens are made of steel sheets which will be bent in the machine.

NTNU

Faculty of Engineering (IV)

Department of Mechanical and Industrial Engineering (MTP)

Risk matrix explanation

		Health	Material values	Reputation	Environment
Grade	1	Minor injury/strain that requires simple treatment. Reversible injury. Short recovery time.	Operational shutdown, or shutdown of activities <1 day.	Little effect on credibility and respect.	Negligible injury and short recovery time.
	2	Injury/strain that requires medical treatment. Reversible injury/strain. Short recovery time.	Operational shutdown, or shutdown of activities <1 week.	Negative effect on credibility and respect.	Minor injury and short recovery time.
	3	Serious injury/strain that requires medical treatment. Lengthy recovery time.	Operational shutdown, or shutdown of activities <1 month.	Reduced credibility and respect.	Minor injury and lengthy recovery time.
	4	Serious injury/strain that requires medical treatment. Possible disability /permanent disability.	Operational shutdown > 1/2 year. Shutdown of activities up to 1 year.	Credibility and respect considerably reduced.	Long-lasting injury. Lengthy recovery time.
	5	Death or disability / permanent disability.	Operational shutdown, or shutdown of activities >1 year.	Credibility and respect considerably and permanently reduced.	Very long-lasting and irreversible injury.

Consequence (C)	Very serious	5	10	15	20	25
	Serious	4	8	12	16	20
	Moderate	3	6	9	12	15
	Little	2	4	6	8	10
	Very little	1	2	3	4	5
		Very little	Little	Medium	Big	Very big
		Probability (P)				

Red	Unacceptable risk. Measures need to be implemented.
Yellow	Medium risk. Measures need to be considered.
Green	Acceptable risk. Measures can be considered.

Add the color of the risk matrix that corresponds with the value you have placed in your personal risk matrix.

92